Element Substituted Aluminophosphates

by

Maria del Consuelo Montes de Correa

Dissertation submitted to the Faculty of the

Virginia Polytechnic Institute and State University

in partial fulfillment of the requirements for the degree of

Doctor of Philosophy

in

Chemical Engineering

APPROVED:

Dr. Mark E. Davis, Committee Chairman

Dr. Gerald V. Gibbs

Dr. David F. Cox

Dr. George B. Wills

Dr. William L. Conger

April 13, 1989

Blacksburg, Virginia

Element Substituted Aluminophosphates

by

Maria del Consuelo Montes de Correa

Dr. Mark E. Davis, Committee Chairman

Chemical Engineering

(ABSTRACT)

This dissertation reports the findings of an investigation aiming to the incorporation of the transition elements: cobalt, vanadium, and molybdenum into $AlPO_4$-5 molecular sieves, to the study of the redox properties of the resulting materials and to the potential application of these compounds in the partial oxidation of methane to methanol and formaldehyde.

$AlPO_4$-5 molecular sieves containing Co, V, and Mo were synthesized by hydrothermal crystallization of typical aluminophosphate gels with the adequate metal substrates at temperatures of 200°C, 150°C, and 150°C respectively. Samples of each material were calcined in oxidant, reducing and inert atmospheres and the properties of the treated solids studied by different characterization techniques.

The significant feature of the Co and V containing $AlPO_4$-5, CoAPO-5 and VAPO-5, is that they exhibit different colors depending on the treatment atmosphere. Evidence for cobalt contained in framework positions of CoAPO-5 is obtained by the change in its unit cell volume relative to $AlPO_4$-5, and by diffuse reflectance spectroscopy. CoAPO-5 also contains an appreciable quantity of extra-framework cobalt occluded in the pores, and/or as balancing cations. Evidence for this was obtained from ion exchange, and from oxygen and argon adsorption.

Pentavalent vanadium incorporation is inferred from the change in the unit cell volume of VAPO-5 relative to $AlPO_4$-5, from pH measurements of the reaction vessel

contents before and after heating, from oxygen and argon adsorption, chemical analysis, SEM, XPS, NMR, and diffuse reflectance spectroscopy. A scheme for the substitution of V into $AlPO_4$-5 is postulated based on the acidity observed in VAPO-5 by ion exchange, and potentiometric titration.

Only a very small amount of Mo was found in the molybdenum containing $AlPO_4$-5. Evidence for Mo incorporation into the framework was not obtained.

The use of CoAPO-5 and VAPO-5 as redox catalysts for the partial oxidation of methane to methanol and formaldehyde lead mostly to oxides of carbon.

Dedication

I dedicate this dissertation to my beloved family

Acknowledgements

I am deeply indebted to my advisor Professor Mark E. Davis for giving me the opportunity to work in his group, for his fruitful guidance and for his support and patience during the time I have been here at Virginia Tech. By generous personal example as well as by specific thoughtful tutorage, he has contributed to broadening my scientific perspectives. All his labor on my behalf is most sincerely appreciated.

I also acknowledge with gratitude the time, efforts and suggestions put forth by the other members of my supervisory committee Dr. D.F. Cox, Dr. G.V. Gibbs, Dr. G. B. Wills and Dr. W. L. Conger.

The support given me by the entire Chemical Engineering faculty and staff, as well as fellow graduate students, is truly appreciated. A special note of thanks to

for their enthusiastic help. I also extend my thanks to

from the Chemistry department for the time and effort spent on running XPS, to from Shell for running NMR on CoAPO-5, and to

from The Dow Chemical Co. for running NMR on VAPO-5. Grateful acknowledgement goes to from the Writing Center, whose generous assistance was invaluable during the time of writing this dissertation.

The financial support provided by the National Science Foundation and The Dow Chemical Company under the Presidential Young Investigator Award to

as well as the financial support provided by the American Chemical Society are gratefully aknowledged. I also express my gratitude to the Universidad de Antioquia, for sponsoring my studies through a paid leave of absence.

Finally, I am specially indebted to my beloved family. To my husband, who agreed to change his normal course of life and gave me steady support, encouragement and help to concentrate on my research work. To and my children, for just being so charming, and even without knowing, so emotionally supportive. To my mother, for supporting me through her prayers. Most of all, *I am thankful to the Lord, in Whom all things are possible.*

Table of Contents

1.0 INTRODUCTION **1**

2.0 OBJECTIVES **14**

3.0 EQUIPMENT AND PROCEDURE **16**

3.1 Synthesis of $AlPO_4$-5 and ElAPO-5 16

3.1.1 $AlPO_4$-5 using Tripropylamine 17

3.1.2 $AlPO_4$-5 using Triethylamine 18

3.1.3 CoAPO-5 18

3.1.4 VAPO-5 19

3.1.5 MoAPO-5 20

3.2 Crystallization of $AlPO_4$-5 and ElAPO-5 21

3.3 Thermal Treatment 21

3.4 X-Ray Powder Diffraction 21

3.5 Thermal Analyses 22

3.6 Pore Volume Analyses 22

3.7 Scanning Electron Microscopy 26

3.8 Chemical Analysis 26

3.9 X-Ray Photoelectron Spectroscopy 27

3.10 Ion Exchange and Potentiometric Titration 28

3.11 Magic Angle Spinning NMR 28

3.12 Diffuse UV-VIS Reflectance Spectroscopy 29

3.13 Reactor System 29

3.13.1 Reactor and reactant flow delivery 29

3.13.2 Analytical system 31

4.0 RESULTS 35

4.1 $AlPO_4$-5 Synthesis and Characterization 35

4.2 CoAPO-5 Synthesis and Characterization 50

4.3 VAPO-5 Synthesis and Characterization 72

4.4 MoAPO-5 Synthesis 91

4.5 Catalytic Activity 93

5.0 DISCUSSION 96

5.1 $AlPO_4$-5 Synthesis and Characterization 96

5.2 CoAPO-5 Synthesis and Characterization 98

5.3 VAPO-5 Synthesis and characterization 103

5.4 Catalytic Activity 108

6.0 CONCLUSIONS 109

7.0 RECOMENDATIONS 110

8.0 REFERENCES CITED 111

Vita 118

List of Illustrations

Figure 1. Framework of $AlPO_4$-5 viewed along [001] 4

Figure 2. Schematic Diagram of Vacuum Manifold 24

Figure 3. Schematic Diagram of Chemical Reactor System 30

Figure 4. Diagram of Automatic Sample valve 33

Figure 5. XRD of $AlPO_4$-5 synthesized using tripropylamine 36

Figure 6. XRD of $AlPO_4$-5 synthesized using triethylamine 38

Figure 7. pH during crystallization of $AlPO_4$-5 40

Figure 8. SEM of $AlPO_4$-5 synthesized using tripropylamine 42

Figure 9. SEM of $AlPO_4$-5 synthesized using triethylamine 43

Figure 10. TGA and DTA of $AlPO_4$-5 synthesized using tripropylamine 44

Figure 11. TGA and DTA of $AlPO_4$-5 synthesized using triethylamine 45

Figure 12. ^{27}Al NMR spectra of (A) as-synthesized and (B) calcined $AlPO_4$-5 using tripropylamine 47

Figure 13. ^{31}P NMR spectrum in (A) as-synthesized and (B) calcined $AlPO_4$-5 using tripropylamine 48

Figure 14. XRD patterns during crystallization of CoAPO-5 51

Figure 15. pH profile of + CoAPO-5 and □ $AlPO_4$-5 synthesized with triethylamine . . . 54

Figure 16. Argon Adsorption Isotherm of (A) CoAPO-5, (B) $AlPO_4$-5 55

Figure 17. Argon Adsorption Isotherm of (A) CoAPO-5, (B) $AlPO_4$-5 56

Figure 18. SEM of CoAPO-5 57

Figure 19. TGA and DTA curves for CoAPO-5. 58

Figure 20. ESCA spectra of Co in CoAPO-5 61

Figure 21. Titration curves for calcined exchanged CoAPO-5 after different treatments . . 63

Figure 22. Visible diffuse reflectance spectra of CoAPO-5(TEAOH) 67

Figure 23. Visible diffuse reflectance spectra of as synthesized and calcined samples of CoAPO-5(Et_3N) 68

Figure 24. Visible diffuse reflectance spectra of calcined samples of CoAPO-5(Et_3N) . . . 69

Figure 25. Visible diffuse reflectance spectra of O_2 calc. CoAPO-5 (TEA) (A) before, (yellow-green) (B) after, (blue) methanol exposure 70

Figure 26. Solid-state ^{31}P NMR spectrum of CoAPO-5 71

Figure 27. XRD patterns during crystallization of VAPO-5 73

Figure 28. pH during crystallization of □ VAPO-5 and + $AlPO_4$-5 synthesized with tripropylamine 75

Figure 29. Argon adsorption isotherm of (A) VAPO-5 (B) $AlPO_4$-5 76

Figure 30. Argon adsorption isotherm of (A) VAPO-5 (B) $AlPO_4$-5 77

Figure 31. SEM of VAPO-5 78

Figure 32. TGA and DTA curves for VAPO-5 80

Figure 33. ESCA spectra of V (2p) core level of VAPO-5 82

Figure 34. Titration curves for □ Ar/He, ▲ O_2, △ O_2/H_2 calcined-exchanged VAPO-5. . 85

Figure 35. Solid-state ^{27}Al NMR spectrum of VAPO-5 88

Figure 36. Solid-state ^{31}P NMR spectrum of VAPO-5 89

Figure 37. UV difference spectra of VAPO-5 90

List of Tables

Table 1. Aluminophosphate Based Molecular Sieves 2

Table 2. Radius ratio† and T-O Distances for Substituted Elements in $AlPO_4$ Molecular Sieves 8

Table 3. Examples of Industrial Heterogeneous Catalytic Oxidation Processes 10

Table 4. The Most Important Results in the Oxidation of Methane to Methanol and Formaldehyde 12

Table 5. FID and TCD Gas Chromatograph Operating Conditions 34

Table 6. d-Spacings, 2θ, and Relative Intensities for $AlPO_4$-5 Synthesized with PR_3N (24 hours) 37

Table 7. d-Spacings, 2θ, and Relative Intensities for $AlPO_4$-5 Synthesized with Et_3N (4 hours) 39

Table 8. Binding Energies, XPS and Chemical Analysis of Elements in $AlPO_4$-5 46

Table 9. d-Spacings, 2θ, and Relative Intensities for CoAPO-5 (4 hours) 52

Table 10. Binding Energies of elements in CoAPO-5 60

Table 11. XPS and Chemical Analysis of Elements in CoAPO-5 62

Table 12. Elemental Concentration of Na, Co, P, and Al in CoAPO-5 after NaCl exchange 65

Table 13. Elemental Concentration of Filtrate Solution (µmol/ml) after NaCl Exchange of CoAPO-5 66

Table 14. d-Spacings 2θ, and Relative Intensities for VAPO-5 (24 hours) 74

Table 15. Binding Energies of Elements in VAPO-5 † 81

Table 16. XPS and Chemical Analysis of Elements in VAPO-5 † 83

Table 17. Elemental Concentration of Na, V, Al, and P in VAPO-5 after NaCl exchange . . 86

Table 18. Elemental Concentration of Filtrate Solution (µmol/ml) after NaCl Exchange of VAPO-5 † 87

Table 19. Elemental Concentration of Na, Mo, P, and Al in MoAPO-5 92

Table 20. Oxidation of CH_4 by Nitrous Oxide over CoAPO-5 (TEA) 94

Table 21. Oxidation of CH_4 by Nitrous Oxide over VAPO-5 95

1.0 INTRODUCTION

Aluminophosphate molecular sieves, first reported by Wilson et al.[1] in 1982, represent the first family of molecular sieves free of silica. The original patent listed 15 new structures to which the acronym $AlPO_4$-n was applied, where n, denoted a particular structure type. To date, about 20 three-dimensional, thermally stable, microporous framework structures have been synthesized. A number of these materials are structural analogues of zeolites, but several novel structures have been formed also. Table 1 shows a list of some of these microporous aluminophosphate materials, their structure type, and the largest ring occurring within the structure.

The novel microporous materials are synthesized by hydrothermal crystallization of reactive gels containing aluminum, phosphorus and organic bases, at temperatures between 125 and 200° C. A series of these aluminophosphates has been prepared by using a wide variety of organic amines and quaternary ammonium cations.[1] However, by changing the reaction conditions, several different structures can be produced from only one organic species. Unlike the zeolite molecular sieves, the presence of organic additives appears necessary to promote crystallization in aluminophosphate molecular sieves. Besides, in contrast to zeolites which are synthesized under highly caustic conditions, the $AlPO_4$ gel exhibit an initial pH between 3 and 8 depending on which and how much organic is added. Except for VPI-5,[2] each crystalline product, as synthesized, contains the organic entrapped, or clathrated, within the structural voids. These organic species can be removed by heating in air to 500-600°C. After thermal decomposition of the organic, the $AlPO_4$-n molecular sieves have the general composition of $Al/P = 1.0$, which is in direct

Table 1. Aluminophosphate Based Molecular Sieves

(from ref.3)

Name	Structure Type	Ring Size	Pore Size,A
VPI-5	Novel	18	12
$AlPO_4$-5	Novel	12	8
-36	Novel	12	8
-37	Faujasite	12	8
-40	Novel	12	7
-46	Novel	12	7
-11	Novel	10	6
-31	Novel	10	6.5
-41	Novel	10	6
-14	Novel	8	4
-17	Erionite	8	4.3
-18	Novel	8	4.3
-26	Novel	8	8.3
-33	Novel	8	4
-34	Chabazite	8	4.3
-35	Levynite	8	4.3
-39	Novel	8	4
-42	Type A	8	4.3
-43	Gismondine	8	4.3
-44	Chabazite-like	8	4.3
-47	Chabazite-like	8	4.3
-16	Novel	6	3
-20	Sodalite	6	3
-25	Novel	6	3
-28	Novel	6	3

contrast with the variable compositions of Si/Al found in zeolite structures.

Not all structures are thermally stable since some collapse to a condensed phase upon heating. From the structures of some of the thermally unstable species, it has been determined that they contain 5 coordinated Al, an unusual state for Al.[4,5] Other structures have long basal spacing indicative of a sheet like structure, and it has been shown that some of them can be intercalated.[6]

Structurally, aluminophosphate molecular sieves contain alternating aluminum and phosphorus, each tetrahedrally coordinated by oxygen and corner linked to give neutral frameworks. Countercations are therefore not required and Brönsted acidity does not occur. However, a small amount of weak acidity possibly arising from the difference in electronegativities between Al and P, and/or from structural defects, is exhibited by these materials.

Adsorption of permanent gases and hydrocarbons into aluminophosphate molecular sieves follows a micropore volume-filling mechanism resulting in type I isotherms.[7] The adsorption of water gives varying isotherm shapes.[7]

The first aluminophosphate molecular sieve reported[8] was $AlPO_4$-5. It is of special interest because of its large pore size which is comparable to zeolites of the X-type. Figure 1 shows a structural representation of $AlPO_4$-5.

$AlPO_4$-5 has a novel tridimensional structure with hexagonal symmetry (cell constant : a = 1.373 nm, c = 0.848 nm and γ = 120°). It contains one dimensional channels (pore diameter = 0.8 nm) oriented parallel to the c axis and bounded by 12 membered rings composed of alternating AlO_4 and PO_4 tetrahedra.[9] $AlPO_4$-5 can be synthesized with at least twenty-three organic bases.[8] The most commonly used are tripropylamine and tetrapropylammonium hydroxide.

The saturation capacity of $AlPO_4$-5 for adsorption of hydrocarbons[8] is about 0.13 - 0.16 cm^3/g. The capacity for water is significantly higher (0.27 cm^3/g.). Several

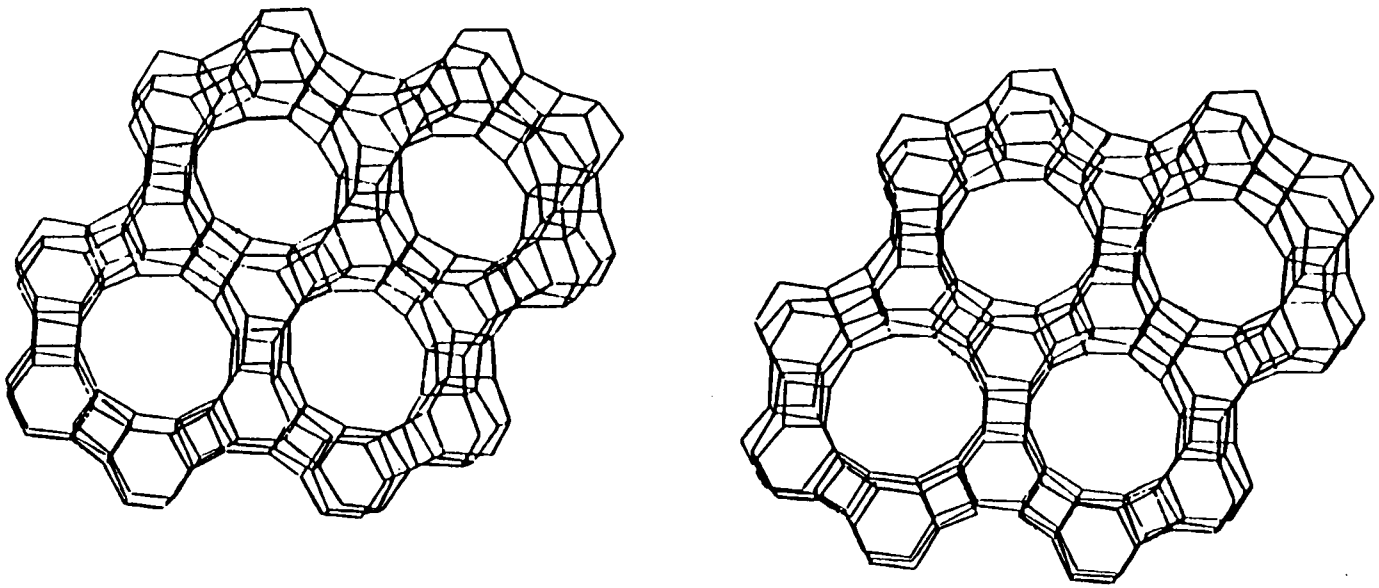

Figure 1. Framework of $AlPO_4$-5 viewed along [001]

reasons have been given to explain this behavior.

- Water has a small kinetic diameter (2.65 Å) and is accessible to all the voids of $AlPO_4$-5.[10]
- There exists the possibility of the formation of a "crystal hydrate" between the crystal and adsorbed water.[12]

$AlPO_4$-5 is thermally stable[13] at temperatures of about 973 K. A very small decrease in its crystallinity and transformation to tridymite has been observed at higher temperatures. However, its channel structure is stable even at 1433 K. Although dehydration of methanol to dimethyl ether has been observed in aluminophosphates[20], it has been claimed that $AlPO_4$-5 contains both Lewis and protonic acid sites and possesses considerable catalytic activity in hydrocarbon cracking, isomerization, and disproportionation reactions, and also in conversion of methanol and ethanol to aromatics.[14,15] However, this is highly unlikely and maybe due to amorphous impurities present in the preparation.

Since the lattice in aluminophosphate molecular sieves is neutral, they do not possess ion exchange ability and thus probably will not be as widely used as zeolites. However, isomorphous substitution of elements like silicon, cobalt, and magnesium in aluminophosphate molecular sieves can be achieved more readily than in the case of zeolites and silica molecular sieves.[7,16] The fewer number of framework elements in zeolites and silica molecular sieves may be due to the prevalent basic pH during synthesis. The high pH favors the precipitation of many of the substitutional elements as extraneous oxides or hydroxides. The solution conditions in microporous $AlPO_4$s can change from acid to alkaline during synthesis, thus permitting the desired substituted species to be more readily presented in an

ionic form suitable for incorporation in the growing crystal.[16]

The first element reported to be substituted in the aluminophosphate system was Si.[17] This new family of molecular sieves was called SAPO. Their adsorption properties, pores sizes, and thermal and hydrothermal stability resemble those of the $AlPO_4$ molecular sieves.

The SAPOs exhibit a range of moderate to high hydrophilic surface selectivity. Their catalytic properties are mildly to strongly acidic depending on silicon concentration and structure type. It has been claimed that the predominant substitution mechanism is silicon for phosphorus, with some substitution of two silicons for an aluminum and phosphorus pair.[7,18] Substitution of SiO_2 for a PO_2 unit creates a negatively charged site within the framework which must be balanced by a cation. If this is a proton then an acid site is created. However the acid strength in SAPO's is generally less than that obtained by Al substitution in a silicate framework.[19,20]

Since the initial patent[1], Flanigen et al.[21] reported the substitution of 15 elements into $AlPO_4$ structures. Several other elements have also been reported to be incorporated.[22,16] The framework siting of some incorporated elements is consistent with their known crystal chemistry and Pauling's radius ratio concepts.[24] Incorporation of other elements, having radius ratios with oxygen and T-O distances outside the accepted crystal chemistry concepts, have been reported also.[21] Radius ratios and T-O distances based on Shannon's crystal radii are listed in Table 2, for the elements reported to be incorporated into aluminophosphate molecular sieves.[25] Several acronyms have been created at Union Carbide to describe the various substituted $AlPO_4$'s.[7] In this work the acronym ELAPO will be used to indicate the substitution of any element different from Si, into the aluminophosphate framework.

The range of structures into which any ion will substitute is not well determined,

Table 2. Radius ratio† and T-O Distances for Substituted Elements in $AlPO_4$ Molecular Sieves

(From ref. 21, 25)

T	Radius Ratio	T-O
B^{+3}	0.20	1.47
P^{+5}	0.25	1.53
Si^{+4}	0.33	1.62
Be^{+2}	0.34	1.63
As^{+5}	0.40	1.70
Al^{+3}	0.43	1.75
Ge^{+4}	0.43	1.75
Ti^{+4}	0.46	1.78
V^{+5}	0.495	1.82
Ga^{+4}	0.50	1.83
Fe^{+3}	0.50	1.85
Mg^{+2}	0.58	1.93
Co^{+2}	0.59	1.94
Li^{+1}	0.60	1.95
Zn^{+2}	0.60	1.96
Fe^{+2}	0.63	1.99
Mn^{+2}	0.66	2.02

†Radius Ratio = $R(T)/R(O^{2-})$ $R(O^{2-}) = 1.22A$
According to Pauling [24],
radius ratio between 0.225-0.414 are
ideal for tetrahedral coordination

but most will substitute into the $AlPO_4$-5 structure[27] and into the sodalite analogue, $AlPO_4$-20. The chabazite analogue, structure type 34, also appears to be able to accomodate different atoms. Some structures have been reported only if substitution is effected, for example MeAPO-36 and MeAPO-47. Substitution is not limited to only one element at a time. Two-, three- and four-element substituted structures have been synthesized.[7] Some of the substituting elements such a Li appear to require the presence of other substituting ions before they will enter the framework.

Several techniques have been used to provide supporting evidence of framework siting of the elements.[7] However, except for few cases,[26] the actual amount of substitution has not been independently characterized.[27] Furthermore, no reports have appeared concerning the thermal and hydrothermal stability of the substituted elements or their possible contribution to the bulk catalytic activity of the material.[3]

Substituted aluminophosphates offer an exciting opportunity to synthesize new microporous crystalline materials with specific physical and catalytic properties. By selecting the appropiate substituting ion the acid strength of the catalyst can be tailored over a wide range. On the other hand, transition metal containing aluminophosphates could potentially catalize oxidation-reduction reactions. The purpose of this study is to synthesize $AlPO_4$-5 molecular sieves containing elements which should potentially change oxidation state and remain in the structure.

Selective oxidations were among the first catalytic processes known.[28] Even before 1835 when J. Berzelius proposed the concept of "catalysis", many processes had been discovered.[28] Examples are:

- The oxidation of hydrogen, carbon monoxide, ether, alcohol and some hydrocarbons on platinum wire by H. Davy in 1817.
- The oxidation of hydrogen by the oxygen of air in the presence of spongy

platinum at room temperature and the oxidation of alcohol over metals (Pt, Ni, Co) and over oxides of manganese, cobalt, nickel, uranium and tin by J. Döbereiner in 1823.

- The oxidation of ethylene, hydrogen chloride and ammonia on platinum by W.Henry in 1825.
- The oxidation of sulfur dioxide into sulfur trioxide on platinum by P. Philips in 1831.

In the early studies many varieties of oxides and supported oxides, based principally in transition metal ions, were found which are widely used today. The catalytic activity of these species is defined as their ability to transfer e^- from the reducing agent to the oxidizer. On the other hand ions and transition metal complexes ensure the possibility of multielectron oxidation reactions, thereby providing new means for the catalysis of these reactions. Table 3 shows several examples of modern industrial catalytic processes involving heterogeneous catalytic oxidation. In these processes, a low price oxidizing agent such as pure oxygen, oxygen from air or their mixtures, is used. Oxidized substrates are natural gases, hydrocarbons from petroleum or coal, or the products obtained from simple gases such as ammonia and methanol.

Selective oxidation of hydrocarbons in general represents a very important field in heterogeneous catalysis. In particular, the activation of alkanes for oxidation reactions to selectively obtain products such as alcohols and aldehydes is of considerable interest for the chemical industry and in fundamental catalysis.

Methane, the main constituent of natural gas, is the simplest hydrocarbon which gives methanol and formaldehyde as partial oxidation products. The direct partial oxidation of methane by air has been extensively studied in the past.[29] Conversions

Table 3. Examples of Industrial Heterogeneous Catalytic Oxidation Processes

(From ref. 28)

Oxidized Substance	Product	Catalyst
Sulfur dioxide	Sulfur trioxide	V-K-S-oxide; V-Ba-Al-oxide; V-K-Si-oxide; Pt on asbestos
Ammonia	Nitric oxide	Pt - Rh gauzes
Hydrogen Chloride	Chlorine	($CuCl_2$ on Al_2O_3)
Hydrogen Sulfide	Sulfur Sulfur dioxide	Bauxite (Containing iron oxide)
Ethylene	Ethylene oxide	Ag on SiC with promoters
Propylene	Acrolein	Cu_2O;Bi-Mo-oxide
Butene	Metacrolein	Bi-Mo-oxide
Butene	Maleic anhydride	V-Mo-oxide
Benzene	Maleic anhydride	V-Mo-oxide
o-Xylene	Phthalic anhydride	V-K-S-Si-oxide
Naphtalene	Phthalic anhydride	V-K-S-Si-oxide
Methanol	Formaldehyde	Ag on Al_2O_3; Fe-Mo-0xide
Dimethylether	Formaldehyde	$WO_3 + H_3PO_4$ on SiC or Al_2O_3
Methane + ammonia	Hydrogen cyanide	Pt-Rh-gauzes
Propylene + ammonia	Acrylonitrile	Bi-Mo-oxide
Ethylene + Hydrogen Chloride	Dicholoroethane	$CuCl_2$ on Al_2O_3
Benzene + Hydrogen chloride	Chlorobenzene	$CuCl_2 + FeCl_3$ on kieselguhr

and selectivities were always very low. Industrially, methane is converted to formaldehyde by the following process.[30]

1. High temperature steam reforming

$$CH_4 + H_2O \xrightarrow[K_2O \text{ promoter, } 800^\circ C]{NiO/\alpha - Al_2O_3} CO + 3H_2$$

2. Low pressure methanol synthesis

$$CO + H_2 \xrightarrow[250^\circ C,\ 50 \text{ atm}]{Cu/ZnO/Al_2O_3} CH_3OH$$

3. Oxidative dehydrogenation of methanol to formaldehyde

$$CH_3OH + O_2 \xrightarrow[Fe_2(MoO_4)_3,\ 425^\circ C]{Ag,\ 600^\circ C \text{ or}} HCHO + H_2O$$

However, one-step conversion by direct partial oxidation using solid catalysts has received considerable attention during the last few years as the best way to utilize the huge amounts of natural gas available. The most important reported results are listed in Table 4.

As can be observed in Table 3 and Table 4, vanadium- and molybdenum-containing catalysts are very useful for catalytic partial oxidation of hydrocarbons. MoO_3 and V_2O_5 supported on silica are the most selective catalysts for the partial oxidation of methane to methanol and formaldehyde.

One important advantage of having active metals or metal oxides on a support is that the active phase can be highly dispersed, perhaps as small crystallites throughout the pore system of the support.[32] As a result, a large active metal or metal oxide surface is produced relative to the weight of metal or metal oxide used. The support can also improve dissipation of reaction heat, retard sintering of metal or metal oxide crystallites, and increase poison resistance. The support may also change the catalytic behaviour because of active phase support interactions.

Table 4. The Most Important Results in the Oxidation of Methane to Methanol and Formaldehyde

(From ref. 31)

Catalyst Feed	T°C P(Mpa)	Selectivity (%)	Conv. CH_4(%)
V_2O_5/SiO_2 $CH_4 : N_2O : H_2O : He$ 1 : 2 : 4.7 :2.3	550 0.1	CH_3OH:85.6 CH_2O:12.7	11.2
MoO_3/SiO_2 $CH_4 : N_2O : H_2O : He$ 1 : 2 : 1.7 :5.3	550 0.1	CH_3OH:79.6 CH_2O:19.3	26.7
MoO_3/SiO_2 $CH_4 : N_2O : H_2O : He$ 1 : 3 : 2 : 3	540 0.1	CH_2O:75 CH_2O:30	5 60

The regular structure of aluminophosphate molecular sieves, as well as zeolites, is particularly suitable for the introduction of catalytically active components. Reports of oxidative dehydrogenation of methane to ethane and ethylene by transition metals Pt, Ag, Pb, Cu, Co, and V supported on $AlPO_4$-5, using incipient wetness, indicate some activity for this reaction.[33] However, a more uniform dispersion may be achieved by direct substitution of a catalytic active component in the aluminophosphate framework. In this case a highly dispersed material having low possibilities of sintering would be obtained since isolated atoms would be located in fixed positions within the framework.

Among the substituted aluminophosphates, CoAPO is of special interest. The acid sites created by substitution of Co by Al promote typical hydrocarbon conversion reactions such as alkylation, aromatization and isomerization.[22] Additionaly, shape selective catalysis has been observed by substituting Co in the different $AlPO_4$ structures.[22] Redox activity due to the change in oxidation state from Co^{+2} to Co^{+3} and conversely has not yet been explored in these materials. Substitution of V into aluminophosphate molecular sieves has been claimed but, a detailed characterization and redox behavior for the resulting materials have not yet been reported.[18,21] So far no claims for substitution of Mo in aluminophosphate frameworks have appeared.

This research will concentrate in the synthesis and characterization of cobalt, vanadium and molybdenum substituted aluminophosphates with the $AlPO_4$-5 structure as potential catalysts for selective oxidations. In particular, the catalysts will be tested for the partial oxidation of methane to methanol and formaldehyde.

2.0 OBJECTIVES

1. Synthesize the following framework containing transition metal aluminophosphate molecular sieves with the $AlPO_4$-5 structure:
   a. CoAPO-5, a known substituted aluminophosphate with little reported characterization.
   b. VAPO-5, a known substituted aluminophosphate with very little reported characterization.
   c. MoAPO-5, an unknown substituted aluminophosphate molecular sieve.

2. Characterize the materials prepared using the following techniques:
   a. X-ray diffraction and adsorption for phase identification, purity, and adsorption capacity.
   b. SEM for morphology determination.
   c. TGA and DTA for determination of % organic and % water
   d. ICP for elemental analysis.
   e. Ion exchange and potentiometric titration for acidity determination.
   f. XPS for surface composition and oxidation state of the elements incorporated.
   g. NMR and UV spectroscopies for element coordination.

3. Determine the redox properties of the synthesized materials.
   a. Calcination in the presence of oxidant, reducing and inert atmospheres
   b. Characterization of calcined materials in different environments by using the

techniques described in objective 2.

4. Study the reactivity of the synthesized materials for methane oxidation.

3.0 EQUIPMENT AND PROCEDURE

3.1 Synthesis of $AlPO_4$-5 and ElAPO-5

$AlPO_4$-5 and ElAPO-5 were prepared using modifications of the procedures described in the literature.[17,22,23] The synthesis of $AlPO_4$-5 involved the following steps:

1. Pseudoboemite alumina was slurried in water.
2. Orthophosphoric acid was dissolved in water.
3. The orthophosphoric acid solution was added to the alumina slurry.
4. The aluminophosphate precursor mixture was aged under ambient conditions.
5. An organic was added to the precursor mixture.
6. The final reaction mixture was charged into autoclaves and statically heated in forced convection ovens.
7. Product crystals were recovered by slurrying the quenched autoclave contents in water, stirring for several minutes, allowing the solids to settle and discarding the supernatant liquid. This procedure was repeated several times until a clear liquid was obtained. Then, the solid was filtered and dried at room temperature.

Reaction mixtures containing transition elements were formed by adding a salt in the case of cobalt and an oxide in the case of vanadium and molybdenum to the synthesis gel after step 4 above. Orthophosphoric acid from Aldrich and pseudoboemite from Vista were used as the phosphorus and aluminum sources. The

most suitable organic bases for the preparation of the substituted aluminophosphates described here were tripropylamine and triethylamine from Aldrich. For comparison, two different preparations for $AlPO_4$-5 using the above templates are given. In addition, CoAPO-5 using tetraethylammonium hydroxide (Alfa products) was prepared as described in example 90 of a Union Carbide Patent[23] but, the product contained some impurities of another phase. Thus, most of the analyses were perfomed on CoAPO-5 synthesized with triethylamine. Cobalt sulphate heptahydrate from Aldrich was used as the cobalt source. Vanadium pentoxide and molybdenum trioxide from Johnson Matthey Inc. and Aldrich respectively were used as vanadium and molybdenum sources. The detailed procedures for the synthesis of $AlPO_4$-5 and ElAPO-5 are given below.

3.1.1 $AlPO_4$-5 using Tripropylamine

A solution of 8.9 g of 85 wt % orthophosphoric acid and 6 ml of de-ionized water was stirred for about 5 min and added to a slurry prepared by stirring 5.3 g of pseudoboemite and 16.9 ml of de-ionized water for about 10 min. A very viscous gel was obtained. After stirring with a magnetic bar and homogenizing by hand at least three times in two hours, the gel became more fluid. Then, 7.5 ml of triproylamine was added. The entire system was stirred and homogenized by hand for 90 min, after which the pH was 4.3. The resulting gel composition was:

$$Pr_3N:Al_2O_3:P_2O_5:40H_2O$$

Portions of the above mixture were transferred to 15 ml teflon lined autoclaves and statically heated in a forced convection oven at 150°C under autogenous pressure. The bombs were removed from the air oven successively after a period

of 2, 4, 8, 16, 24, and 48 h, quenched at room temperature and the pH measured. Product crystals were recovered as previously described in step 7.

3.1.2 $AlPO_4$-5 using Triethylamine

A solution of 8.9 g of 85% orthophosphoric acid and 6 ml of de-ionized water was stirred for 5 min and added to a slurry of 5.3 g of pseudoboemite and 16.9 g of de-ionized water which was previously stirred for 10 min. A very viscous gel was obtained. The gel was blended by stirring with a magnetic bar and homogenizing by hand at least three times in 90 min. Then, 5.86 g of triethylamine were added. The entire mixture was further homogenized for 90 min, after which the pH was 5.5. The gel composition was:

$$1.5Et_3N:Al_2O_3:P_2O_5:40H_2O$$

Portions of the above mixture were transferred to 15 ml teflon lined autoclaves and statically heated in a forced convection oven at 200° C under autogenous pressure. The bombs were removed from the air oven successively after a period of 2, 4, 8, 16, 24, and 48 h, quenched at room temperature and the pH measured. Product crystals were recovered as previously described in step 7.

3.1.3 CoAPO-5

A solution of 8.9 g of 85% orthophosphoric acid and 6 ml of de-ionized water, previously stirred for 5 min, was added to a slurry prepared by stirring 4.25 g of pseudoboemite in 6.0 g. of de-ionized water for about 10 min. A white viscous gel was

formed. The gel was blended by stirring with a magnetic bar and homogenizing by hand at least three times in 90 min. Then, a solution which contained 4.33 g of $CoSO_4.7H_2O$ in 10.35 g of water was added. After homogenizing the resulting red system for 20 min, 5.86 g of triethylamine were added and the system homogenized by hand. At this point the system became violet. The entire gel was further homogenized for 90 min, after which the pH was 4.2. The gel composition was:

$$1.5Et_3N:0.8Al_2O_3:0.2Co_2O_2:P_2O_5:0.4H_2S0_4:40H_2O$$

Portions of the above mixture were transferred to 15 ml teflon lined autoclaves and statically heated in a forced convection oven at 200°C under autogenous pressure. The bombs were removed from the air oven successively after a period of 2, 4, 8, 16, 24, and 48 h, quenched at room temperature and the pH measured. Product crystals were recovered as previously described in step 7.

3.1.4 VAPO-5

A solution of 8.455 g of 85% orthophosphoric acid and 6 ml of de-ionized water, previously stirred for 5 min, was added to a slurry prepared by stirring 5.3 g of pseudoboemite in 16.9 g. of de-ionized water for about 10 min. A white viscous gel is formed. The gel was blended by stirring with a magnetic bar and homogenizing at least three times in 90 min. Then, 0.351 g of V_2O_5 were added. After homogenizing the yellow system for 20 min, 15 ml of tripropylamine were added and the system further homogenized by hand. The entire system was further homogenized for 90 min, after which the pH was 6.9. The gel composition was:

$$2.0Pr_3N:Al_2O_3:0.05V_2O_5:0.95P_2O_5:40H_2O$$

Portions of the above mixture were transferred to 15 ml teflon lined autoclaves

and statically heated in a forced convection oven at 150°C under autogenous pressure. The bombs were removed from the air oven successively after a period of 2, 4, 8, 16, 24, and 48 h, quenched at room temperature and the pH measured. Product crystals were recovered as previously described in step 7.

3.1.5 MoAPO-5

A solution of 8.455 g of 85% orthophosphoric acid and 6 ml of de-ionized water, previously stirred for 5 min, was added to a slurry prepared by stirring 5.3 g of pseudoboemite in 6.0 g. of de-ionized water for about 10 min. A white viscous gel is formed. The gel was blended by stirring with a magnetic bar and homogenizing by hand at least three times in 90 min. Then, 0.556 g of MoO_3 were added. After homogenizing the system for 20 min, 15 ml of tripropylamine were added. The system was further homogenized for 90 min. The resulting gel composition was:

$$2.0Pr_3N:Al_2O_3:0.1MoO_3:0.95P_2O_5:24.23H_2O$$

Portions of the above mixture were transferred to 15 ml teflon lined autoclaves and statically heated in a convection oven at 150°C under autogenous pressure. The bombs were removed from the air oven after a period of 40, 46, 70 and 91 h and quenched at room temperature. Product crystals were recovered as previously described in step 7.

3.2 Crystallization of $AlPO_4$-5 and ElAPO-5

The pH during crystallization was recorded by removing and quenching the teflon lined autoclaves at various times following heat-up. The pH of each liquid phase sample was measured with an Orion Research Ionalizer model 407A with a combined glass electrode. The solid was washed with 500 ml portions of water until a clear supernatant was obtained. Then, the solid was recovered by filtration and dried at room temperature. This solid is called as-synthesized.

3.3 Thermal Treatment

Portions of the as-synthesized material were calcined for 3 hours at 500° C in flowing gas. The gas was selected according to the desired atmosphere. For an oxidizing atmosphere O_2 was used. The reduced materials were obtained by calcining the as-synthesized material in O_2 at 500° C for three hours followed by calcination in H_2 at the same conditions. N_2 and/or a 10% mixture of Ar in He were used as the flowing gases for inert atmospheres.

3.4 X-Ray Powder Diffraction

X-ray powder diffraction data were collected on a Nicolet I2 X-ray diffractometer employing Cu-Kα radiation. Samples were mounted in zero background single crystal

quartz sample holders and scanned 2 sec count time and 0.05° 2θ step size over the 2θ = 3° to 50° region for normal scans.

In order to determine the change in the unit cell volume in CoAPO-5 with respect to $AlPO_4$-5 (Et_3N) and in VAPO-5 with respect to $AlPO_4$-5 (Pr_3N), data were collected on finely ground and homogeneous mixtures of the NaCl exchanged O_2 calcined materials, (CoAPO-5, $AlPO_4$-5 (Et_3N), VAPO-5, and $AlPO_4$-5 (Pr_3N)), with spinel which was used as an internal standard. Slow scans, 25 sec count time and 0.01° 2θ step size, of the peaks with 2θ between 18° and 36° were taken. The two spinel reference lines in the above range occur at 19.00° and 31.272°. Miller indices were assigned to each reflection in the scanned region[9] and the cell parameters determined by a least squares procedure[11] using the subroutine DLSLRG from the IMSL package.

3.5 Thermal Analyses

Thermal analyses were performed in air on the 951 thermogravimetric analyzer (TGA) and on the 1600 differential thermal analyzer (DTA) modules of a Du Pont Thermal Analyst 2100 system. Typically, 10-20 mg of sample were placed into a platinum sample pan and heated at 20° C/min from room temperature to 800° C.

3.6 Pore Volume Analyses

Argon adsorption isotherms for $AlPO_4$-5 (Pr_3N), $AlPO_4$-5 (Et_3N), CoAPO-5, and VAPO-5 were obtained using an Omnisorp 100 analyzer.

Oxygen adsorption on a McBain-Bakr balance was used to determine the pore volume of the unidimensional channels of various $AlPO_4$-5 and ElAPO-5 samples. A schematic representation of the McBain-Bakr balance is shown in Figure 2.

Unit A is an oil diffusion pump. It is controlled by a variac set at 67.5 and 140 V. Unit B is a cold trap. Cooling is supplied by liquid nitrogen which is placed in a dewar surrounding the trap. The manifold is divided into two halves (C and D) for independent operation. Unit E is the pressure gauge, which is connected to a pressure transducer. The pressure gauge reads from 10^{-4} torr to atmospheric. Unit F is the adsorption chamber. It is connected to the top by a ground glass joint. The chamber is approximately 1.75 inches in diameter. The hook at the top of the chamber extends just below the ground glass joint. The hook is connected to a quartz spring (500 mg maximum load, 400 mm maximum extension, spring constant 1.25 mg/mm). The spring is attached to a 10 cm quartz extension wire. The extension wire is then attached to a sample holder. Units G and H are U-tube manometers, each connected to unit J which is a mercury trap. The trap is filled with sulfur to adsorb mercury vapor.

The manifold is designed to simultaneously perform adsorption on four separate samples. Its use was limited to only one sample at a time. Adsorption work presented here was performed in unit F.

The usual start-up procedure is as follows: Initially, valves 1, 3, 6, 7, 9, 10 and 13 are closed, with the remaining valves open. The mechanical pump as well as the heaters to the diffusion pump are switched on. A dewar surrounding the cold trap (B) is filled with liquid nitrogen. The nitrogen level in the trap needs to be adjusted at least twice a day. After 10 min, valve 2 is closed and valves 1 and 3 opened. At this point the diffusion pump is in operation. This pump is capable of providing a vacuum of 10^{-4} torr. The steps involved in measuring oxygen adsorption include :

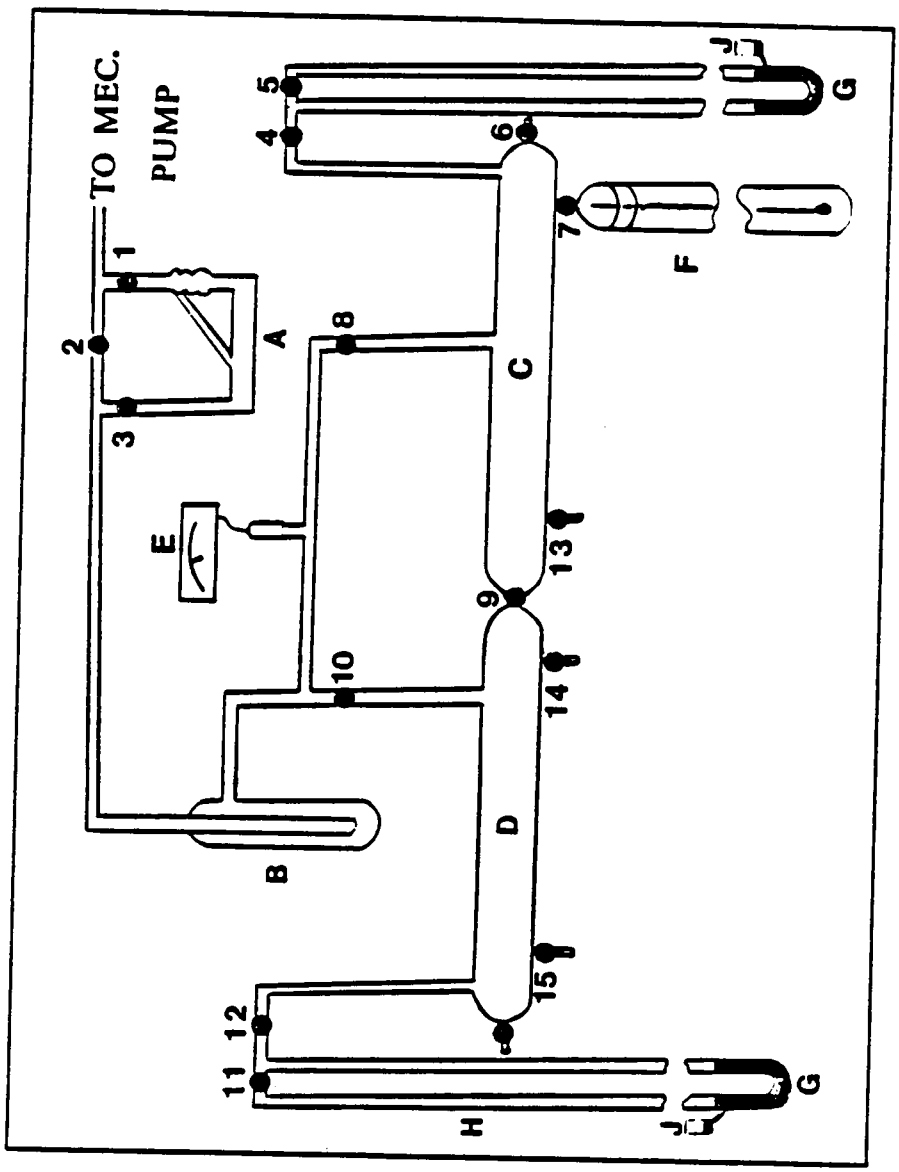

Figure 2. Schematic Diagram of Vacuum Manifold. All letters and numbers are referred to in text.

1. *The weighing of about 80 to 130 mg of the sample* in the sample holder and placing it in the adsorption chamber. At the base of the quartz spring there is an indicator bar. This bar is lined up with the site on a cathetometer and the reading recorded in mm. This reading corresponds to reading #1.

2. *The evacuation of the adsorption chamber* by carefully opening valve 7.

3. *The activation of the sample* by heating it with a variac controlled tube furnace placed around the adsorption chamber. The temperature is adjusted to approximately 350°C by setting the variac to 100. After about 4 hours when no change in the indicator bar is observed in the cathetometer, the furnace is turned off, removed, and the adsorption chamber allowed to cool. Then, a second reading is obtained from the cathetometer. The difference between the two readings is used to determine the mass of the dry sample as follows: mass of the dry sample = mass of the wet sample - (reading #2 - reading #1)(1.25 mg/mm).

4. *The immersion of the sample bulb in liquid nitrogen* by placing a dewar around the adsorption chamber and filling it with nitrogen.

5. *The introduction of oxygen*. Valve 6, connected to an oxygen cylinder, is opened slowly to fill the adsorption chamber with 100 torr of oxygen measured in the Hg manometer. Once the sample is at equilibrium, a third reading is obtained from the cathetometer. Sample pore volume is obtained as follows: Volume of oxygen adsorbed = (reading #2 - reading #3)(1.25)/(mass of dry sample)(density of liquid O_2). This volume is converted to cm^3 per 100 g of sample.

The system is shut down by closing valves 1 and 3 and switching off the diffusion

pump. Valve 2 is then opened and the mechanical pump turned off.

3.7 Scanning Electron Microscopy

Scanning electron micrographs were obtained for various samples of $AlPO_4$-5 and ElAPO-5 synthesized as described in section 1.1 using a Cambridge Instruments Stereoscan 200 scanning electron microscope. Magnifications employed typically ranged from 1000X to 3000X.

3.8 Chemical Analysis

Chemical analysis was performed using an Inductively Coupled Plasma (ICP) spectrometer system. The ICP system consists of a simultaneous spectrometer (Jarrell-Ash ICAP 9000) and a sequential (scanning) spectrometer (Jarrel-Ash Atomscan 2400). The Al and P from all samples were determined using the simultaneous spectrometer. The sequential spectrometer, which scans the spectrum from 190 to 535 nm, stopping at specified wavelengths to register the individual elemental concentrations, was used to analyse Co, V, Mo for the substituted aluminophosphates, and Na for the ion exchanged substituted aluminophosphates.

Standard solutions containing about 1000 μg/ml of the desired element were purchased from Aldrich and diluted to obtain the element in a 3.2 N solution with HCl used as a matrix. Samples to be analyzed were prepared by dissolving 60 mg of aluminophosphate material in about 3 ml of 12N HCL in a glass vessel. The vessel

was then heated to 80° C until 1 ml of concentrated solution was obtained. This solution was diluted to obtain the extracted elements in a 100 ml solution of 3.2N HCL. Analysis was performed on both the calcined and as-synthesized samples.

3.9 X-Ray Photoelectron Spectroscopy

X-Ray Photoelectron Spectroscopy (XPS) was performed on as-synthesized $AlPO_4$-5 and MoAPO-5 and on as-synthesized and calcined CoAPO-5 and VAPO-5 using a Perkin Elmer PHI 5300 ESCA system employing either MgKα or AlKα X-rays.

The number of scans varied between 2 and 10 for the different elements in both instruments. Binding energies are referenced to the carbon 1s transition at 284.6 eV for as-synthesized $AlPO_4$-5 and MoAPO-5. For CoAPO-5 and VAPO-5 materials, gold was sputtered onto a small spot prior to analysis. Thus, binding energies for these samples are referenced to the gold $4f_{7/2}$ transition at 83.8 eV.

When analyzing VAPO-5 overlap between the oxygen satellite and the V(2p) photoelectron peak was present. To provide an accurate quantitative representation of superficial V, the area of the oxygen satellite was estimated and substracted from the sum of the V(2p) photoelecton peak and the oxygen satellite following integration.

3.10 Ion Exchange and Potentiometric Titration

Acidity measurements were obtained from the resulting filtrate of the calcined ElAPOs treated in a 0.1N NaCl solution. Approximately 120 mg of the calcined

materials were treated in 50 ml of 0.1N NaCl solution during 20 hours after which the solid was filtered. Then, 1 ml of the resulting filtrate solution was diluted to 25 ml and titrated with a 0.01N NaOH solution in about 0.1 cm^3 increments to a pH of about 10. All the treated materials were further analyzed by X-ray powder diffraction and the chemical composition of the solid as well as of the filtrate solution before titration, were determined by ICP.

3.11 Magic Angle Spinning NMR

Magic angle spinning ^{27}Al and ^{31}P NMR spectra were recorded on Bruker spectrometers for some synthesized and calcined materials. The ^{27}Al spectra for as-synthesized and calcined $AlPO_4$-5 were obtained at a frequency of 52.15 MHz and a rotation rate of 4.6kHz. The ^{27}Al spectra for as-synthesized VAPO-5 were obtained at a frequency of 52.15 MHz and at rotation rates of 3.6 and 4.2kHz. The ^{27}Al chemical shifts are reported relative to $[Al(H_2O)_6]^{+3}$ and are not corrected for second-order quadrupole effects. The ^{31}P spectra were taken at a frequency of 81.0 MHz and at spinning rates between 3.5 and 4.7 kHz. Chemical shifts are reported relative to 85% H_3PO_4.

3.12 Diffuse UV-VIS Reflectance Spectroscopy

Diffuse reflectance UV-VIS spectra, in the range from 200 to 700 nm, were obtained using a Shimadzu Cs - 9000 spectrometer. In obtaining the spectra, all

samples were placed side by side on a quartz plate and the source was focused as a spot on the samples.

3.13 Reactor System

The reactor assembly for partial oxidation of methane to methanol and formaldehyde is shown schematically in Figure 3. It consists of two sections. The first section includes the reactor and reactant flow delivery. The second is the analytical section concerned with reactant and product analysis.

3.13.1 Reactor and reactant flow delivery

In a typical experiment the reacting gas mixture which includes CH_4 and N_2O or O_2, with 10% Ar in He as diluent, was introduced at flow rates of about 80 ml/min into a vaporizer-mixer into which water was admitted from a syringe pump.

The flow rate of each gas was measured by a rotameter. The vaporizer-mixer consists of a 3.5 inch stainless steel tube filled with glass beads and wrapped with heating tape to maintain a temperature of 165°C. Once flow had passed to the vaporizer-mixer, it was sent either to the analytical system through a bypass or to the reactor.

The reactor consisted of a vycor tube (14 mm o.d. x 60 mm) containing a quartz frit to hold the catalyst. This tube was connected at the inlet and outlet to two 6 mm o.d. vycor tubes of 200 mm and 130 mm respectively. The reactor was housed in a 1″ diameter stainless steel tube. The dead space between the tube and the reactor

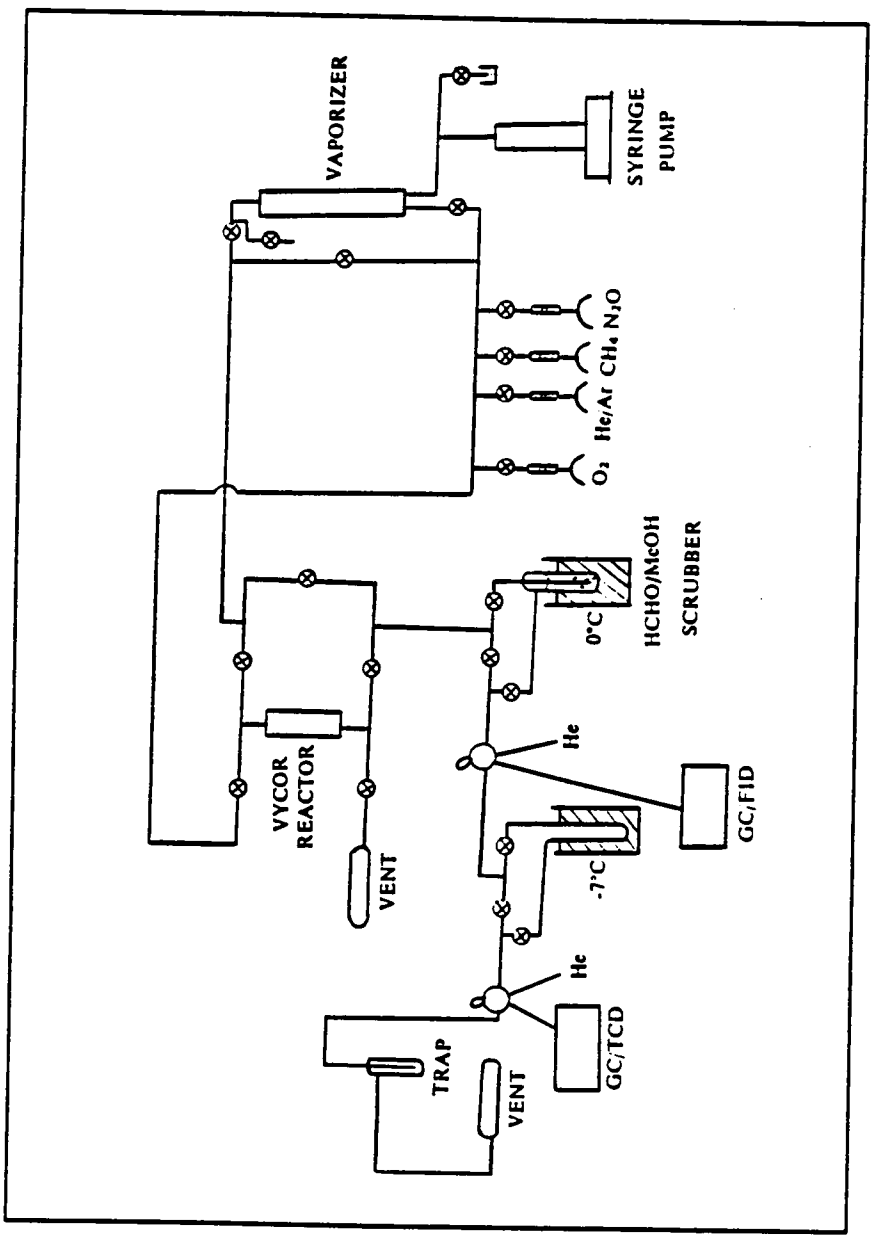

Figure 3. Schematic Diagram of Chemical Reactor System

was filled with glass wool. A type K thermocouple was placed between this tube and the reactor at approximately the middle of the catalyst bed. This thermocouple was used for digital readout of the reactor temperature. The reactor was heated by a tube furnace rated to 1100°C. Temperature control was maintained by an Omega Model CN2011K temperature controller.

All quarter inch copper tubing inlet and outlet lines were maintained at approximately 150° C by variac powered heating tapes in order to avoid liquid condensation. The reactor contained about 1 g of catalyst pressed at 5000-6000 psi and sieved to 35/65 mesh (Tyler). Prior to reaction the catalyst was calcined in situ for 3 hours at 500° C with O_2 flowing through an independent line that went directly to the reactor and from the reactor to a vent.

The effluent from the reactor could either be diverted through the analytical system or through a water scrubber to collect formaldehyde and methanol.

3.13.2 Analytical system

All reactants and products except formaldehyde were analyzed with a TCD and a FID gas chromatograph each using a 6-port automatic sampling valve. Table 5 shows the operating conditions for both TCD and FID chromatographs. A diagram of the 6-port sampling valves is shown in Figure 4. In both valves two positions, called 'sample', corresponding to the active position, and 'load', corresponding to the inactive position, were activated by air pressure and an electric switch. In the 'sample' position, carrier flow (helium) was sent through port #1 and into the TCD or FID column which was connected to port #2. The product gas entered through port #3 and circulated through the sample loop connected to ports #4 and #5. The product

then exited via port #6 where it was exhausted to the vent. In the 'load' position, carrier flushed the product gas from the sample loop onto the TCD or FID column. Product gas was passed through port #3 and exhausted through port #6.

The thermal conductivity detector (TCD) gas chromatograph contained a dual Alltech CTR1 column. It consisted of two concentric, inner and outer, columns. The inner column, (6'x 1/8 ") ss, contained Porapak Q for the separation of CH_4, CO_2 and N_2O. The outer column, (6'x 1/4 ") ss, contained an activated molecular sieve for the separation of Ar, N_2, CH_4, and CO. Since H_2O interferes with CO peak and also adsorbs in the molecular sieve packing of the outer column a cold trap froze out water without restricting flow. The flame ionization detector (FID) gas chromatograph, contained an Alltech column, (8'x 1/8 ") ss, packed with Unibeads A (spherical activated alumina). This column was used to detect methanol, methane, and higher hydrocarbons such as ethane, and ethylene, but formaldehyde was not detected. In order to determine formaldehyde, the effluent from the reactor was sent to a water scrubber cooled in an ice bath and samples were collected at regular intervals. Under this condition, both methanol and formaldehyde were condensed. Methanol was determined by adding a known amount of isopropanol, as an internal standard, to the product from the scrubber and injecting samples of 2 μl into the FID. Formaldehyde was analyzed by means of an iodometric titration[34] substracting off interferences due to the presence of isopropanol. Integrated recordings of the FID and TCD signal were obtained using Hewlett-Packard 3390A integrating-recorders.

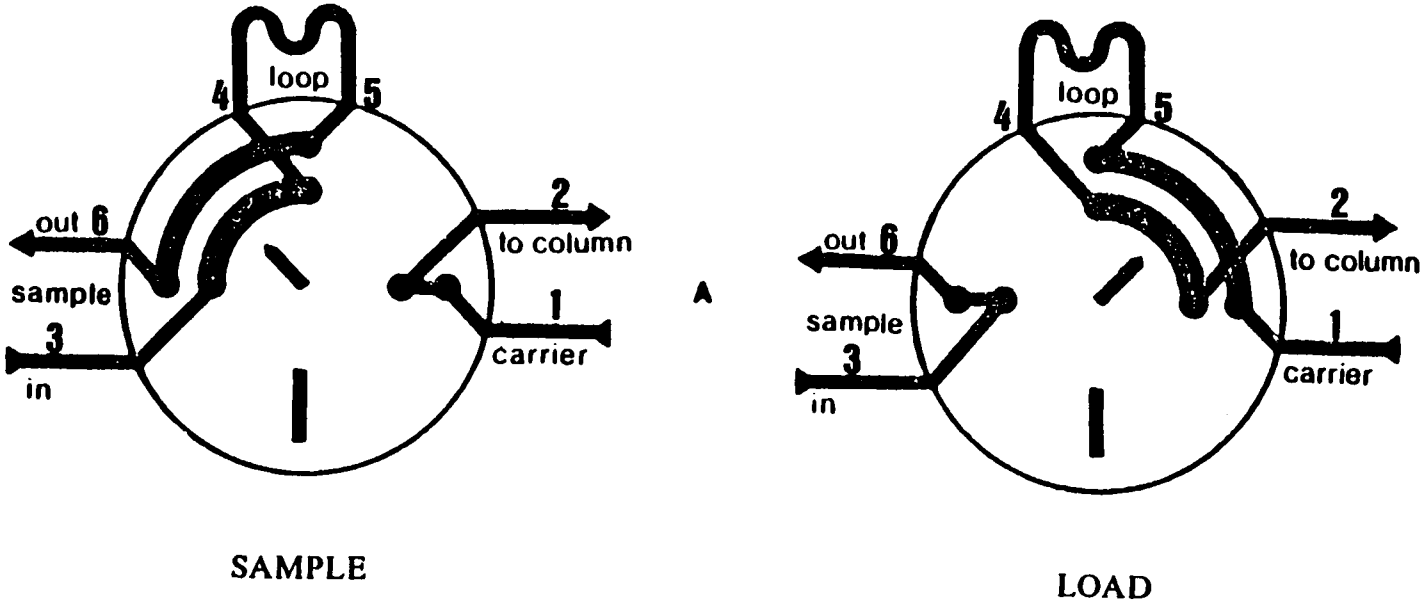

Figure 4. Diagram of Automatic Sample Valve

Table 5. FID and TCD Gas Chromatograph Operating Conditions

Description	FID	TCD
Column temperature, °C	70	20
Cell temperature, °C	-	20
Oven temperature, °C	150	-
Injection temperature, °C	100	-
He carrier gas flow, ml/min	34	80
He carrier gas pressure, psig	40	20
Hydrogen cylinder pressure, psig	40	-
Hydrogen detector pressure, psig	25	-
Air cylinder pressure, psig	60	-
Air detector pressure, psig	35	-

4.0 RESULTS

4.1 $AlPO_4$-5 Synthesis and Characterization

Figure 5 and Figure 6 show the X-ray diffraction patterns of $AlPO_4$-5 samples obtained during crystallization using tripropylamine (Pr_3N) and triethylamine (Et_3N) as the organic. In both cases, comparison of the XRD patterns reveals that the formation of the $AlPO_4$-5 phase occurs at a crystallization period of about 2 hours. However, it is interesting to observe that the intensity of the peak at $2\theta \sim 21$ is lower when triethylamine is used as the organic. Table 6 and Table 7 show d-spacings, 2θ values and relative intensities for typical samples of $AlPO_4$-5 using the above templates.

pH data during crystallization of $AlPO_4$-5 synthesized with tripropylamine and triethylamine are shown in Figure 7. With tripropylamine the pH rises to 8.5 after 8 hours and no significant variation is observed from 8 to 48 hours. Although the background is lower for the product obtained after 16 hours, the x ray diffraction patterns indicate that the product has good crystallinity from 2 to 48 hours and no other phases are observed during this crystallization period. With triethylamine a maximun pH of 9.7 is obtained at 16 hours of heating after which the pH starts to decrease. A small amount of impurity from a second phase appears at about 24 hours. After 48 hours of heating, the pH is almost the same with both organics.

SEMs of the crystals produced with the above templates are shown in Figure 8, and Figure 9 respectively. These figures show the influence of the organic on the

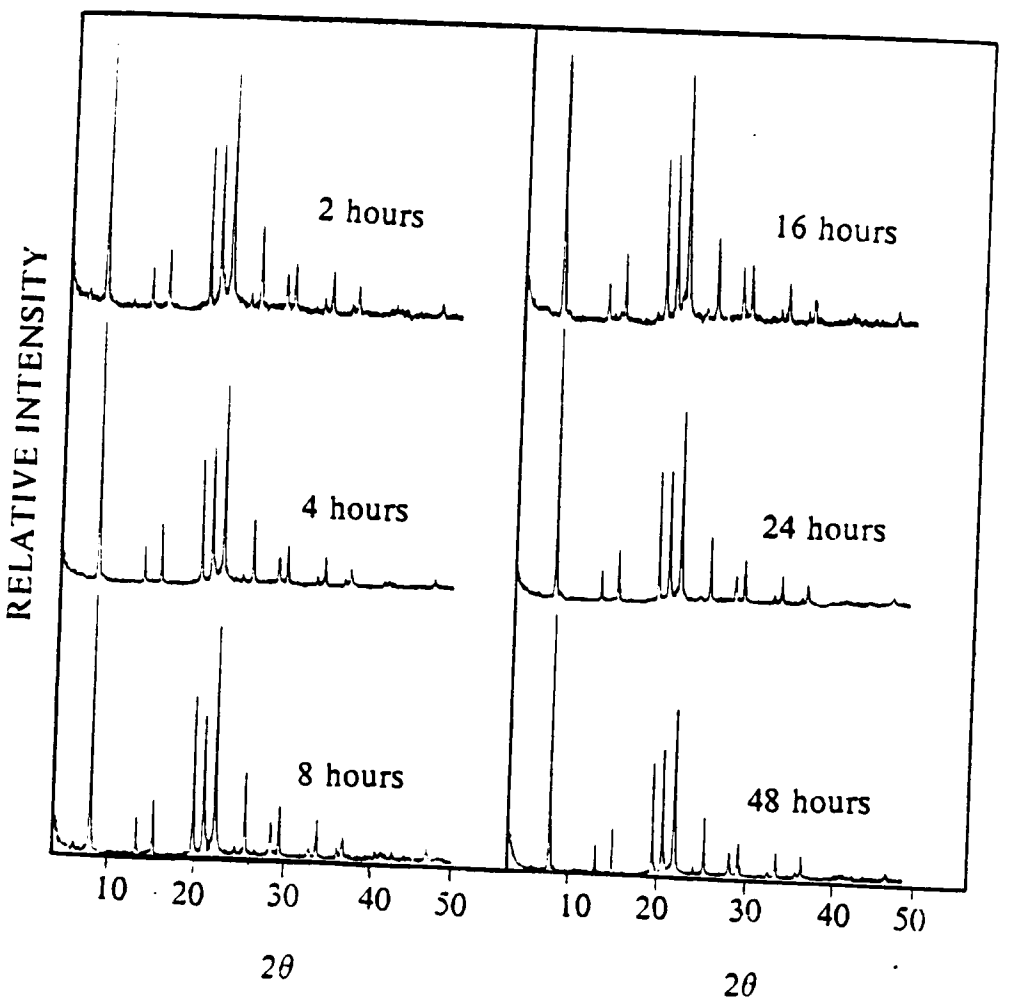

Figure 5. XRD of $AlPO_4$-5 synthesized using tripropylamine

Table 6. d-Spacings, 2θ, and Relative Intensities for $AlPO_4$-5 Synthesized with PR_3N (24 hours)

d-space	2θ	I/I max
11.88160	7.440	100
6.85634	12.912	11.7
5.93231	14.934	19.0
4.48470	19.797	46.6
4.22239	21.040	52.0
4.06012	21.891	2.4
3.96190	22.441	67.6
3.42568	26.011	25.2
3.27965	27.190	1.5
3.16798	28.168	1.0
3.06997	29.087	10.9
2.96528	30.138	14.5
2.66162	33.673	2.9
2.62158	34.203	1.2
2.58931	34.643	9.3
2.44527	36.754	0.9
2.42615	37.054	2.9
2.38490	37.719	7.0
2.22476	40.549	0.7
2.20787	40.873	0.8
2.10442	42.979	0.5
2.03062	44.624	0.6
2.01186	45.063	1.7
1.99398	45.489	0.3
1.97749	45.890	1.4
1.93173	47.042	0.2
1.92370	47.250	0.4
1.90108	47.847	4.0

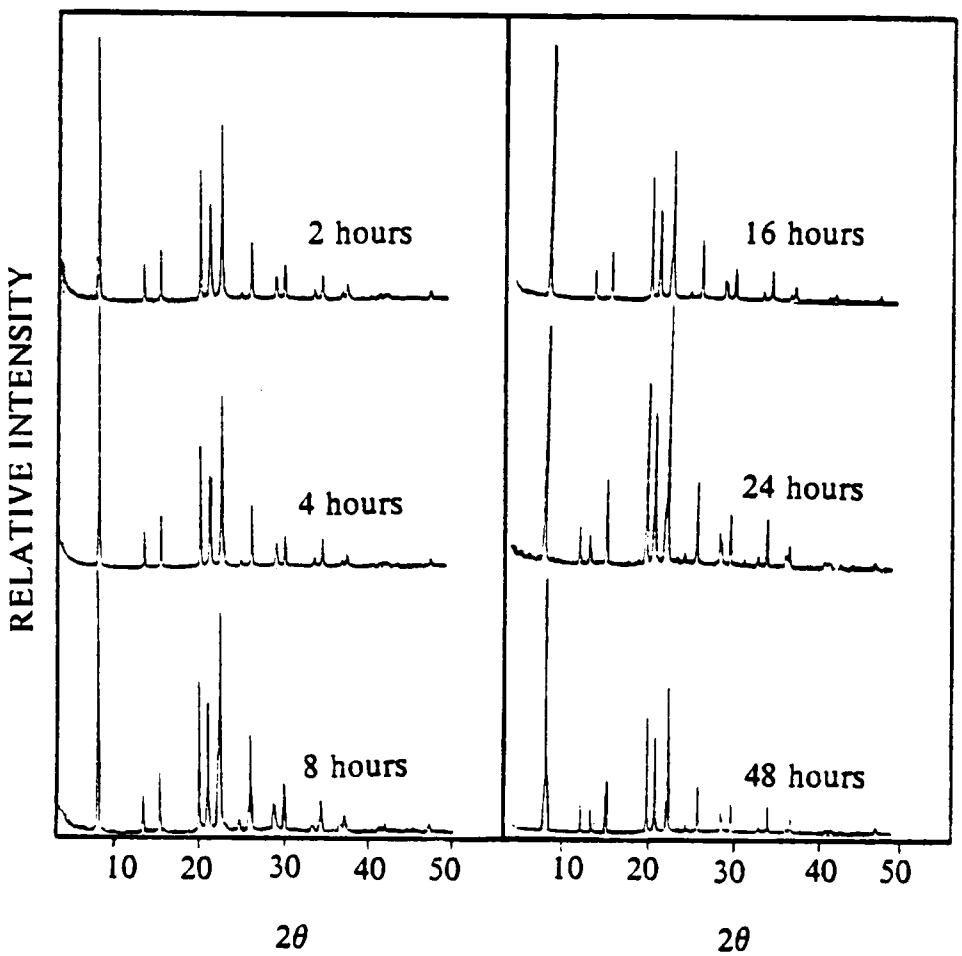

Figure 6. XRD of $AlPO_4$-5 synthesized using triethylamine

Table 7. d-Spacings, 2θ, and Relative Intensities for $AlPO_4$-5 Synthesized with Et_3N (4 hours)

d-space	2θ	I/I max.
11.93191	7.409	100
6.85817	12.908	13.5
5.93787	14.920	19.1
4.48245	19.807	46.2
4.23494	20.977	33.6
3.96086	22.447	62.8
3.60310	24.709	2.5
3.42018	26.053	22.1
3.06877	29.099	8.7
2.96050	30.188	11.6
2.65654	33.739	2.7
2.58458	34.708	9.1
2.42356	37.095	2.2
2.38653	37.692	4.5
2.24811	40.110	0.4
2.16598	41.700	1.6
2.14470	42.133	1.2
2.12626	42.516	1.5
1.89742	47.945	2.0
1.89458	48.021	2.3
1.84515	49.392	0.1
1.83694	49.628	0.5

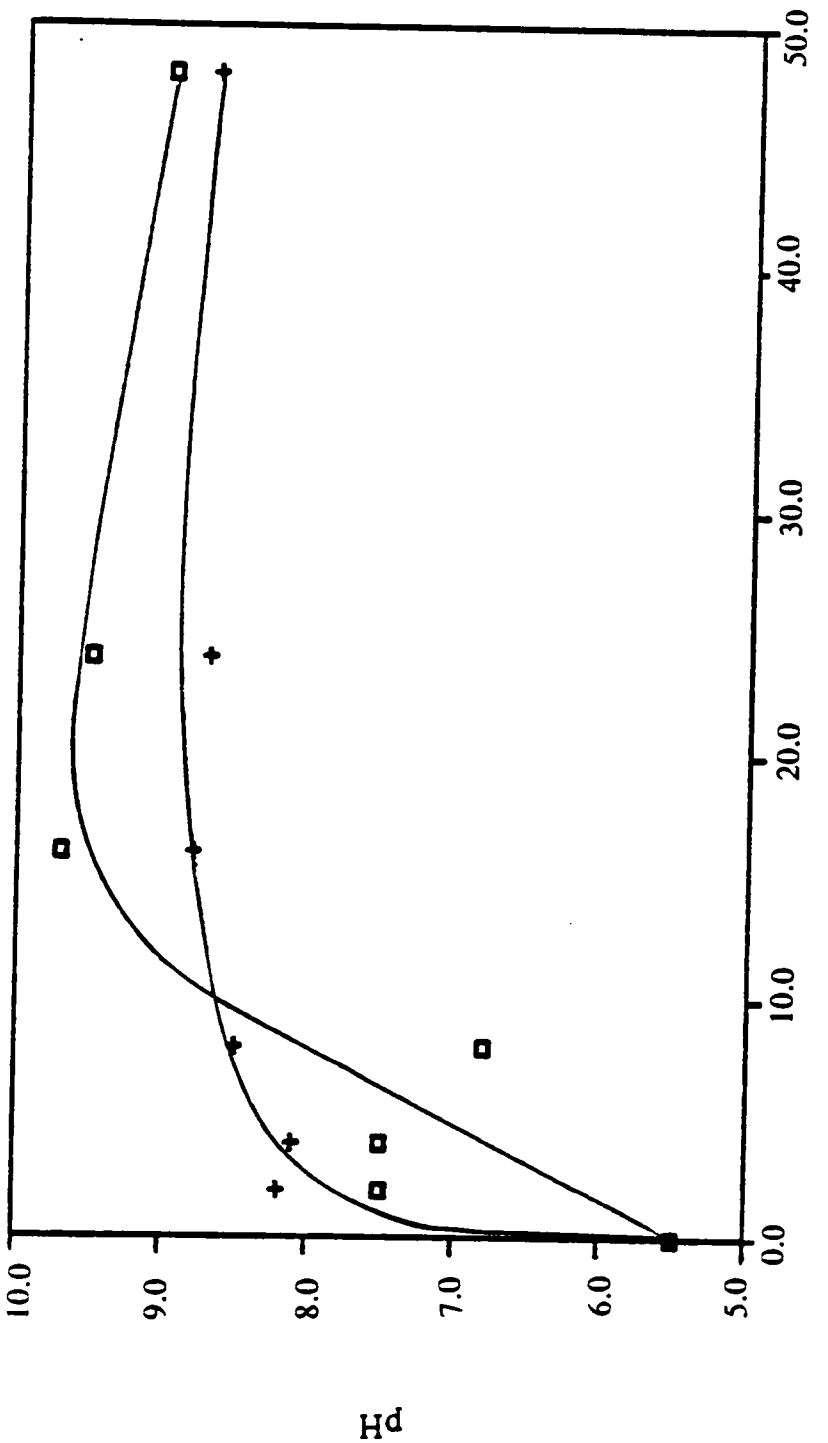

Figure 7. pH during crystallization of $AlPO_4$-5.+ using triproylamine.□ using triethylamine.

crystal morphology.

Figure 10, and Figure 11 show TGA and DTA curves for $AlPO_4$-5 obtained using tripropylamine and triethylamine respectively. $AlPO_4$-5 synthesized with tripropylamine shows four distinct weight losses: two of them, endothermic, in the 25-110°C and 110-150°C ranges. The first endothermic weight loss is assigned to desorption of water and the second to desorption of both water and tripropylamine occluded in the cylindrical channels. The two exothermic weight losses in the 150-460°C, and 460-620°C ranges correspond to decomposition of tripropylamine[38] $AlPO_4$-5 synthesized with triethylamine shows two distinct weight losses: 25-300° and 400-700°. The endothermic loss corresponds to desorption of water, the subsequent exothermic loss corresponds to decomposition of the amine.

Table 8 shows binding energies referenced to the C1s level at 284.6 eV of the electron energy levels used to characterize $AlPO_4$-5 crystals together with superficial and elemental composition determined by XPS and chemical analysis (CA) respectively. XPS/CA ratios are used to obtain qualitative indications of the proportion of elements near the external surface.

From TGA, DTA and chemical analysis the empirical formula of the products obtained with tripropylamine (Pr_3N) and triethylamine (Et_3N) are respectively:

$$0.045Pr_3N.(Al_{0.5}.P_{0.5})O_2.0.19H_2O$$

$$0.06Et_3N.(Al_{0.5}.P_{0.5})O_2.0.09H_2O$$

Figure 12 and Figure 13 illustrate the ^{27}Al and ^{31}P NMR spectra of both synthesized and calcined $AlPO_4$-5 (Pr_3N).

The ^{27}Al spectrum for the as-synthesized material gives resonance maxima at 39.84 ppm and 31.96 ppm. Another upfield line is observed at -9.97 ppm. The calcined material, shows resonance maxima at 37.11 ppm and 26.50 ppm and an upfield component -15.627 ppm. The ^{31}P spectra for the as-synthesized material show a

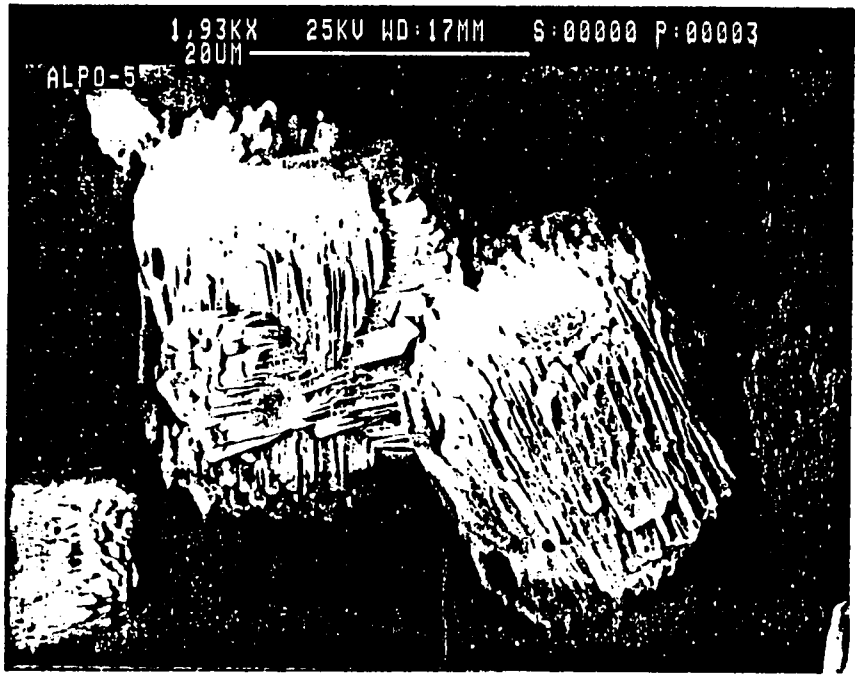

Figure 8. SEM of $AlPO_4$-5 synthesized using tripropylamine

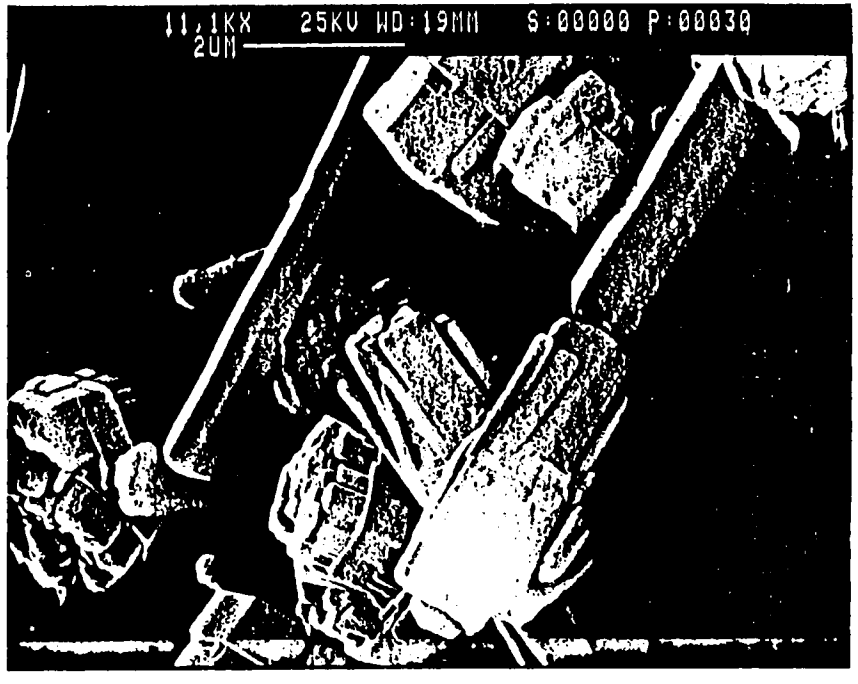

Figure 9. SEM of $AlPO_4$-5 synthesized using triethylamine

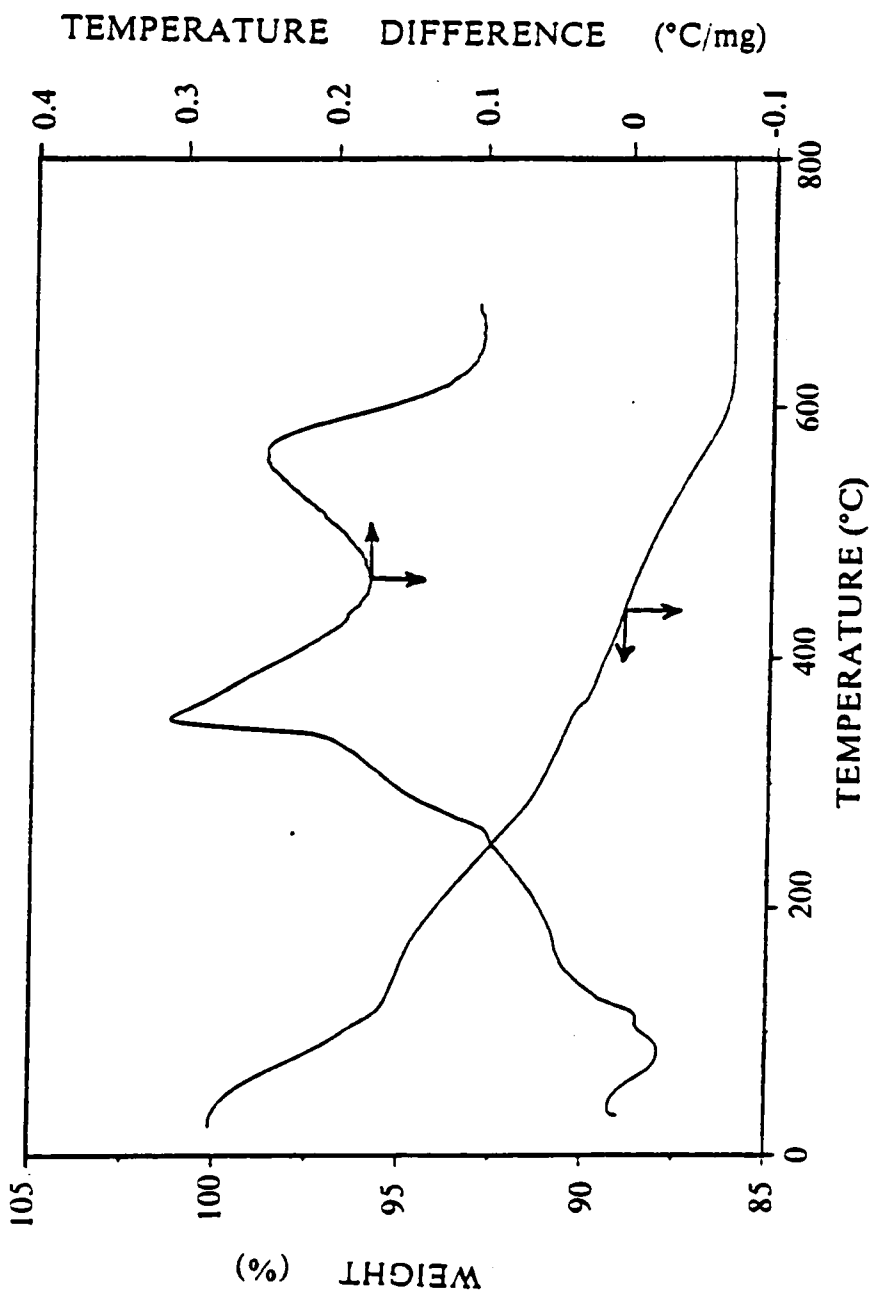

Figure 10. TGA and DTA of $AlPO_4$-5 synthesized using tripropylamine

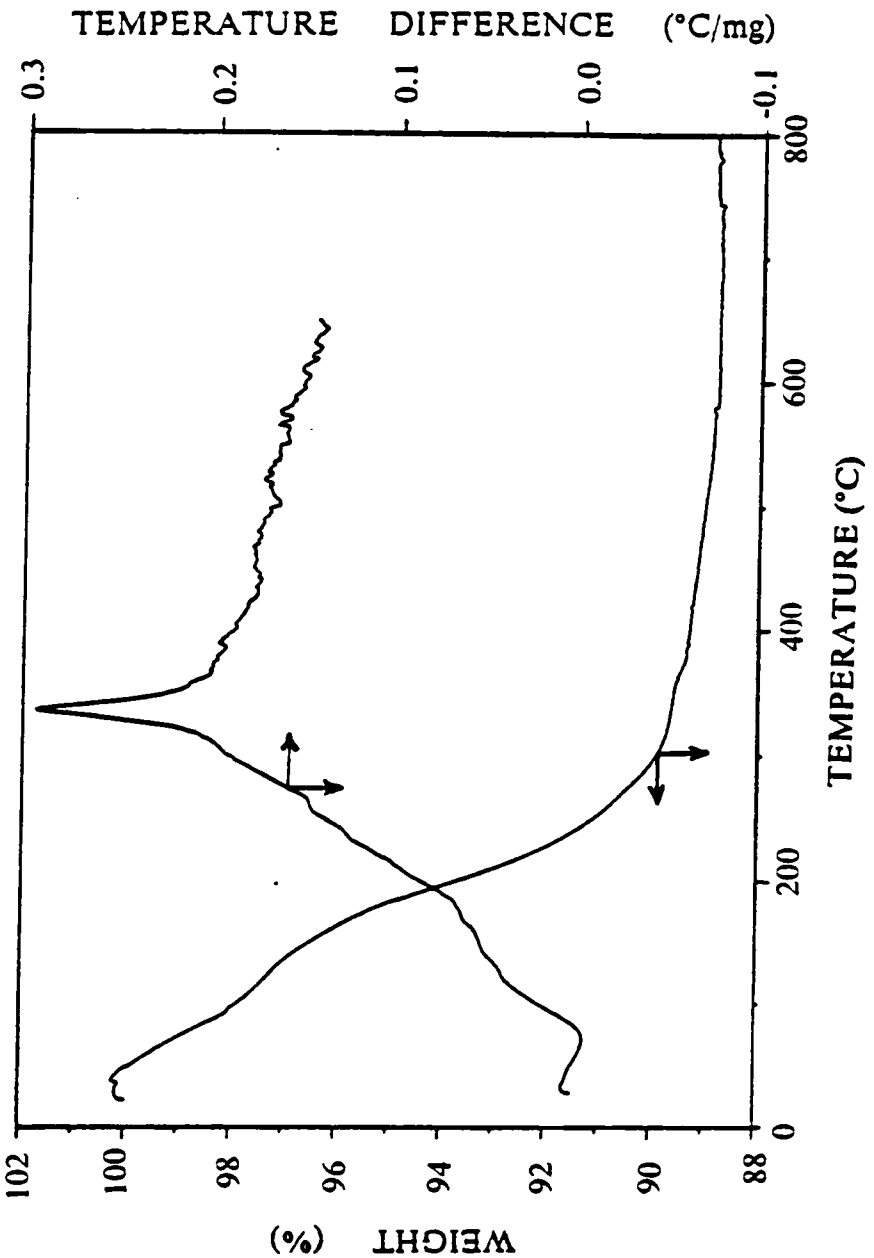

Figure 11. TGA and DTA of $AlPO_4$-5 synthesized using triethylamine

Table 8. Binding Energies, XPS and Chemical Analysis of Elements in $AlPO_4$-5

(Referenced to C1s at 284.6 eV)

Element	Binding energy (eV)	XPS†	CA†	XPS/CA
O(1s)	532.5	3.34	-	-
Al(2p)	75.5	0.521	0.506	1.03
P(2p)	134.7	0.479	0.494	0.970

† Expressed in terms of $(Al_xP_y)O_z$

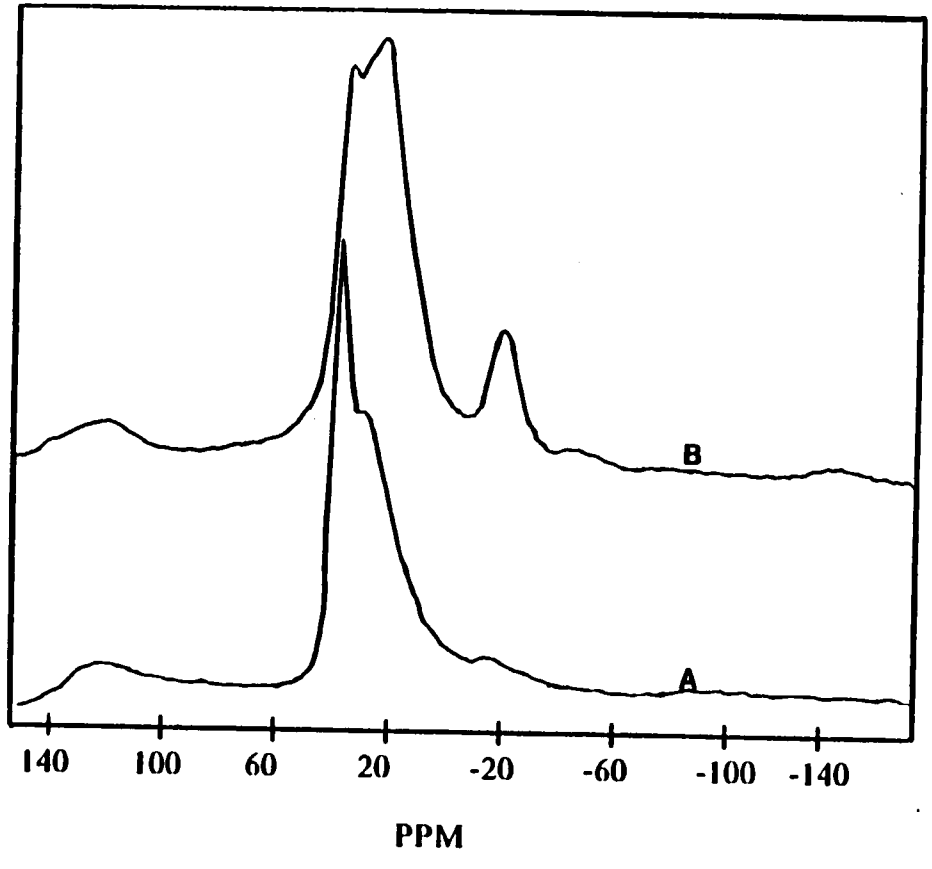

Figure 12.^{27}Al NMR spectrum of (A) as-synthesized and (B) calcined $AlPO_4$-5 using tripropylamine

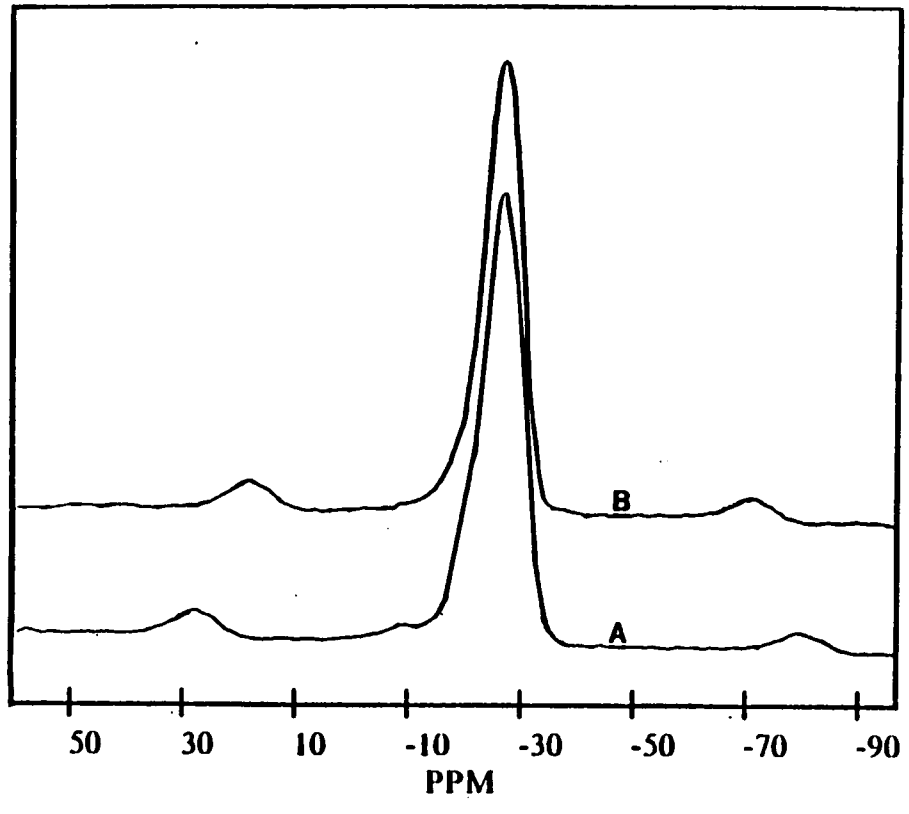

Figure 13. ^{31}P NMR spectrum of (A) as-synthesized and (B) calcined $AlPO_4$-5 using tripropylamine

symmetrical line at -28.60 ppm and a small peak at -11.0 ppm. Spinning side-bands are observed at -80 ppm upfield, and 35 ppm downfield. For the calcined material, a symmetrical line at -29.40 ppm is observed together with upfield and downfield spinning side-bands at -75 ppm, and about 18 ppm respectively.

4.2 CoAPO-5 Synthesis and Characterization

As mentioned in section 3, description of equipment and procedure, a pure CoAPO-5 product was synthesized using triethylamine as the organic. In addition, a different sample of CoAPO-5 having the following water and organic free composition, assuming all Co, Al, and P in the framework:

$$(Co_{0.04}Al_{0.46}P_{0.5}).O_2$$

was obtained using tetraethylammonium hydroxide as described in example 90 of a Union Carbide Patent[23]. This sample contained some impurities from another phase, most likely CoAPO-44. The analyses described below for CoAPO-5 refer to the pure product obtained with triethylamine unless specification of the organic is given in order to distinguish between CoAPO-5 (Et_3N) obtained with triethylamine and CoAPO-5 (TEA) obtained with tetraethylammonium hydroxide.

Figure 14 shows the X-ray diffraction patterns during crystallization of CoAPO-5. The pure phase $AlPO_4$-5 like material is obtained at 2 and 4 hours of heating and the relative intensities of all peaks are comparable to those of $AlPO_4$-5 synthesized using triethylamine as the organic. From 8 to 48 hours, the presence of small amount of CoAPO-47 is observed. During this period of time the intensity of the peak at $2\theta \sim 21$ is larger compared to the intensity of the same peak at 2 and 4 hours. Table 9 show a list of d-spacings, 2θ values and relative intensities for a typical sample of CoAPO-5.

The pH profile of CoAPO-5 is compared with the pH profile of $AlPO_4$-5 synthesized with triethylamine in Figure 15. The presence of $CoSO_4.7H_2O$ lowers the pH of the gel. However, the addition of $CoSO_4.7H_2O$ does not appear to hinder the nucleation time since the $AlPO_4$-5 like phase appears at about 2 hours of heating which is the same

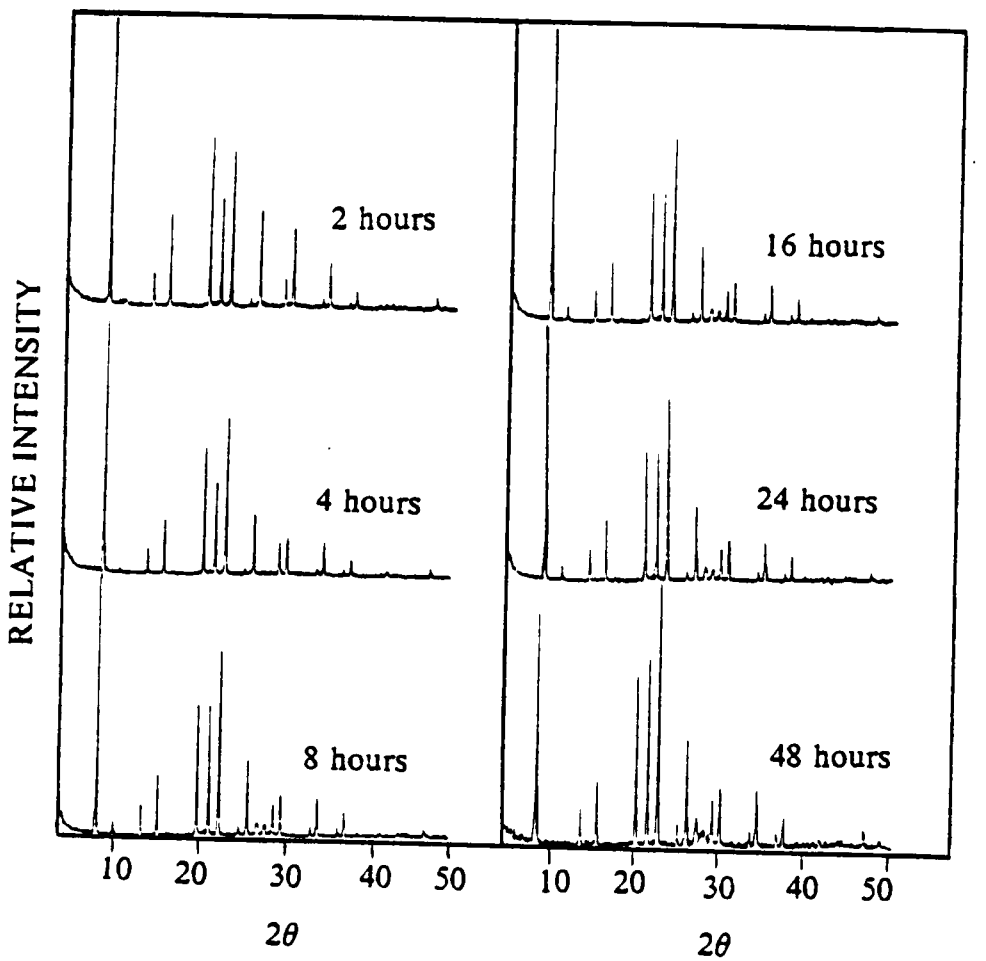

Figure 14. XRD patterns during crystallization of CoAPO-5

Table 9. d-Spacings, 2θ, and Relative Intensities for CoAPO-5 (4 hours)

d-space	2θ	I/I max
11.94885	7.398	100.0
6.88978	12.849	10.2
5.96592	14.849	20.8
4.50832	19.692	50.8
4.20772	21.114	36.7
3.97218	22.382	61.2
3.59458	24.769	2.7
3.44409	25.869	22.8
3.07852	29.005	11.1
2.98257	29.959	14.6
2.63302	34.050	0.8
2.60339	34.450	12.4
2.43508	36.913	2.3
2.38176	37.771	6.1
1.91167	47.565	3.3

time as pure $AlPO_4$-5 phase crystallizes in the absence of the salt.

Argon adsorption isotherms measured at liquid argon temperatures for CoAPO-5 are compared to $AlPO_4$-5 in Figure 16 and Figure 17. From Figure 16 the argon adsorption capacity at P/Po = 0.43 is 0.121 cm^3/g solid, compared to 0.146 cm^3/g solid for $AlPO_4$-5 under the same conditions. The oxygen adsorption capacity of CoAPO-5 measured in a McBain-Bakr apparatus at 100 mm Hg and at liquid N_2 temperatures is 0.11 cm^3/g solid. This value is lower than the value obtained for the pure $AlPO_4$-5 phase (0.1749 cm^3/g solid) measured at the same conditions. The isotherms shown in Figure 17 compare the argon isotherm at low P/Po for CoAPO-5 and $AlPO_4$-5 and indicate that the pore size of CoAPO-5 is slightly smaller than that of $AlPO_4$-5.

Figure 18 shows a SEM of CoAPO-5 (4 hours). Here, the morphology of CoAPO-5 is similar to the morphology of $AlPO_4$-5 (Pr_3N) instead of $AlPO_4$-5 (Et_3N). In addition, small particles are observed on the crystals.

Figure 19 shows TGA and DTA curves for CoAPO-5. It is worth nothing the difference between these curves and the corresponding curves for $AlPO_4$-5 synthesized with triethylamine shown in Figure 11. CoAPO-5 shows four distinct weight losses: 25-250°C, 250-400°C, 400-500°C, 500-700°C. Each range has a characteristic pattern in the DTA. The first endothermic loss is due to desorption of water, the second endothermic loss is most probably due to desorption of both water and the organic. The third loss, exothermic, corresponds to decomposition of the organic and the fourth loss, exothermic may be due to a Hoffman-type degradation of the protonated amine associated with the acid sites.[35]

XPS and chemical analysis were performed on as-synthesized and calcined samples of CoAPO-5. The samples exhibit different colors depending on the treatment. The as-synthesized sample is blue, the O_2 calcined is yellow-green, the

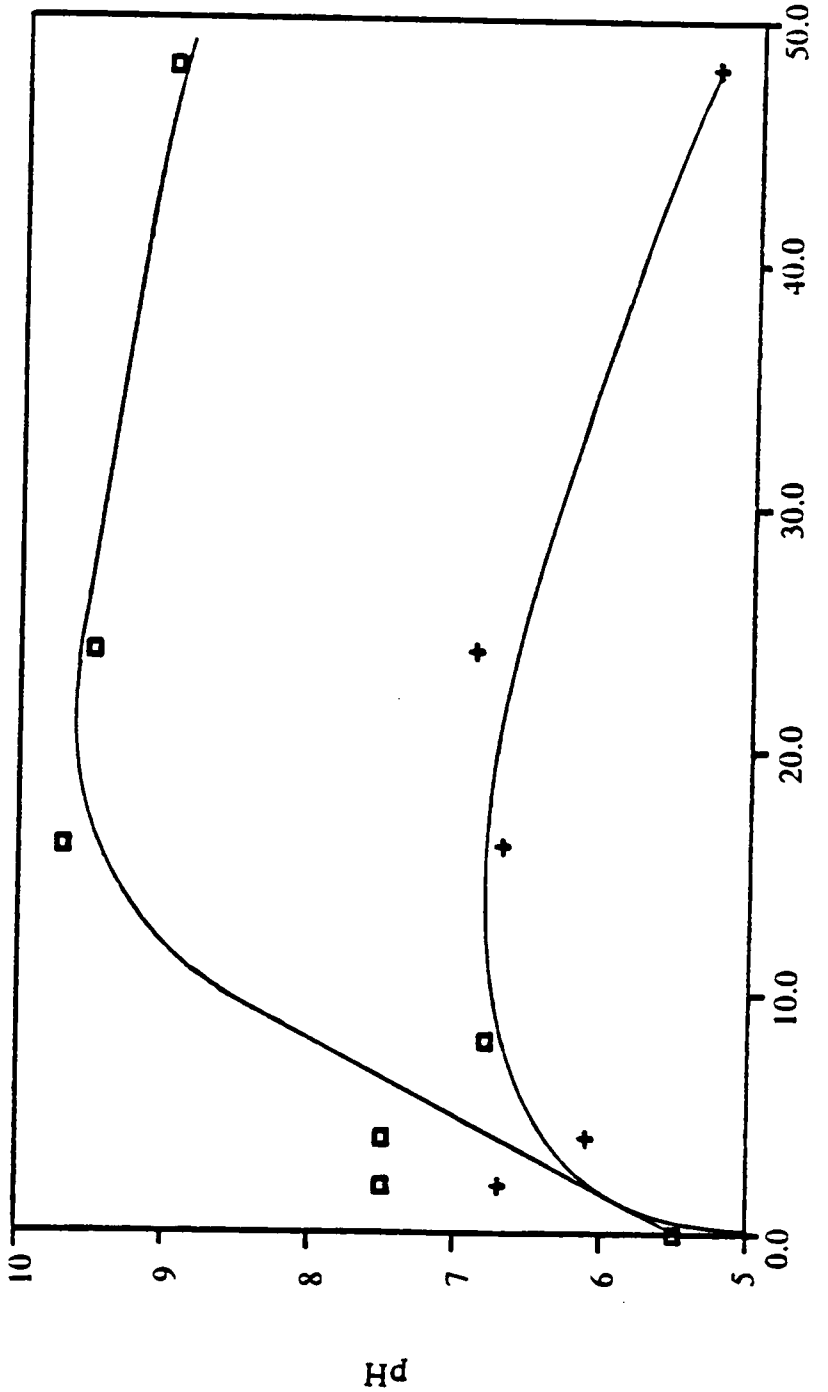

Figure 15. pH profile of + CoAPO-5 and □ $AlPO_4$-5 synthesized with triethylamine

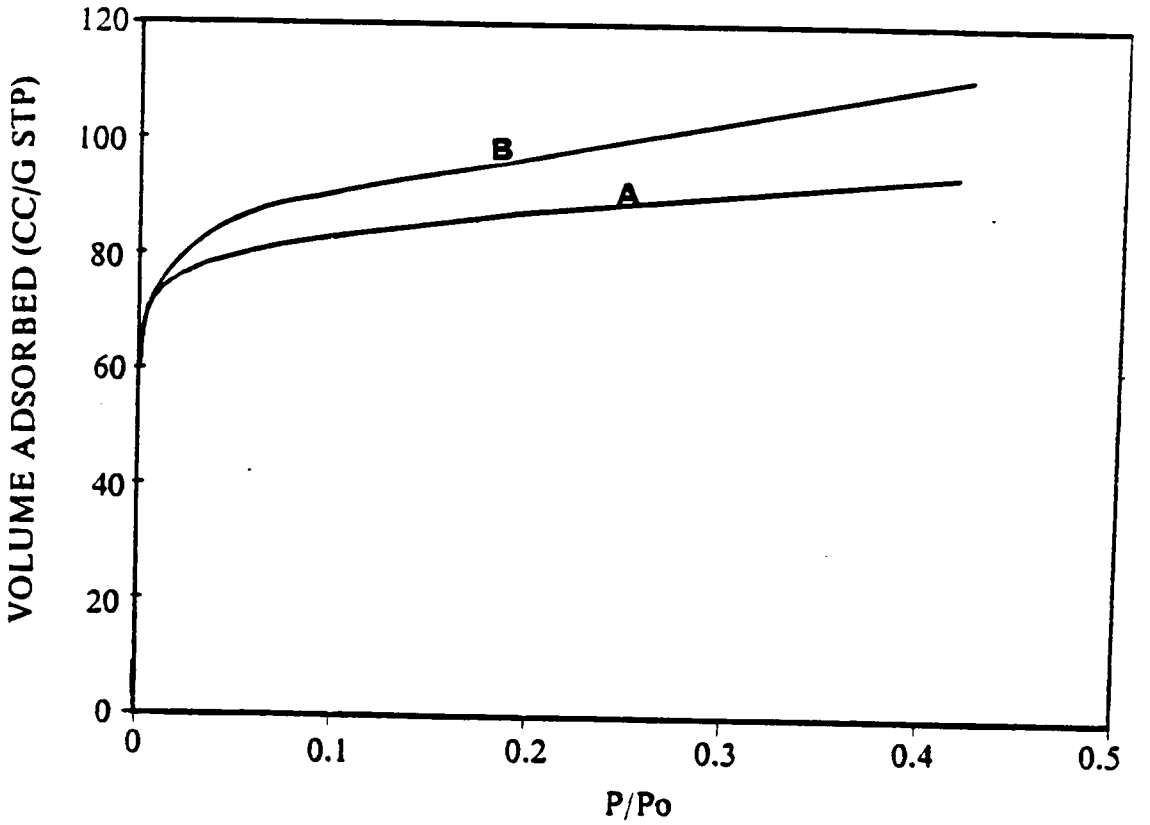

Figure 16. Argon Adsorption Isotherm of (A) CoAPO-5, (B) $AlPO_4$-5

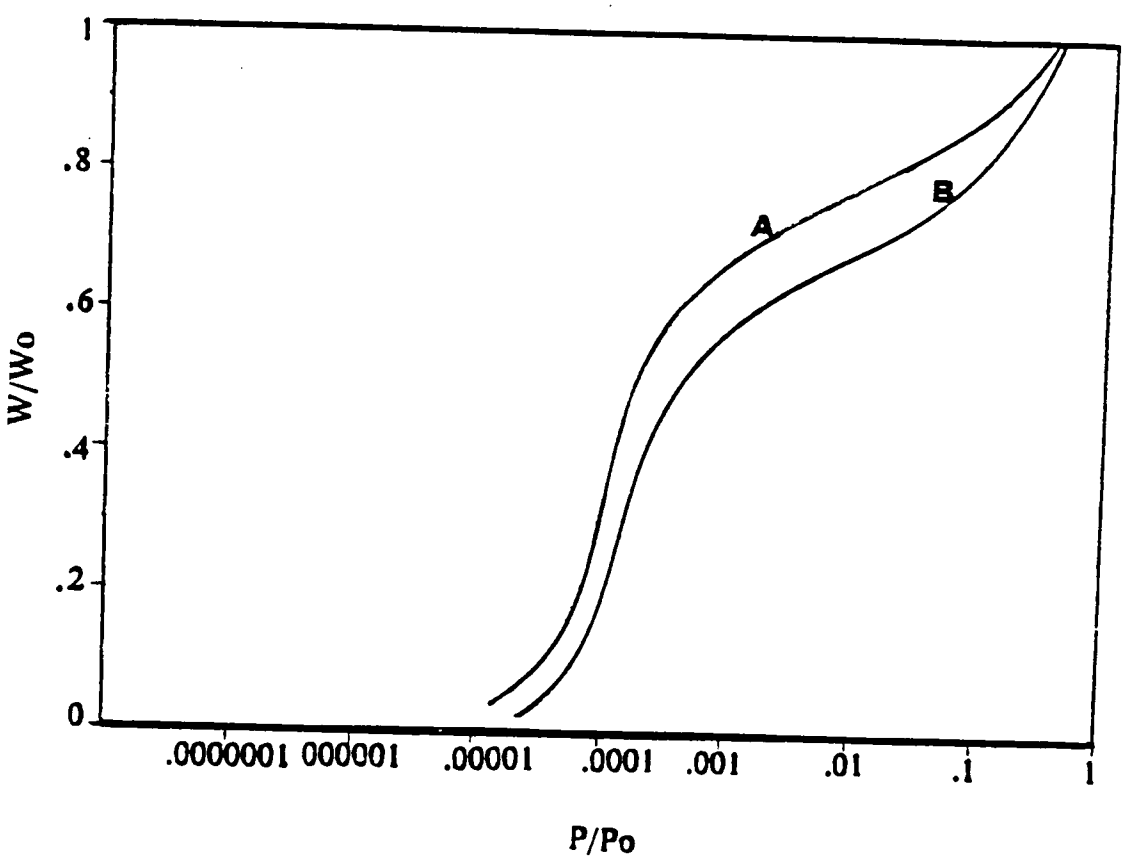

Figure 17. Argon Adsorption Isotherm of (A) CoAPO-5, (B) $AlPO_4$-5

Figure 18. SEM of CoAPO-5

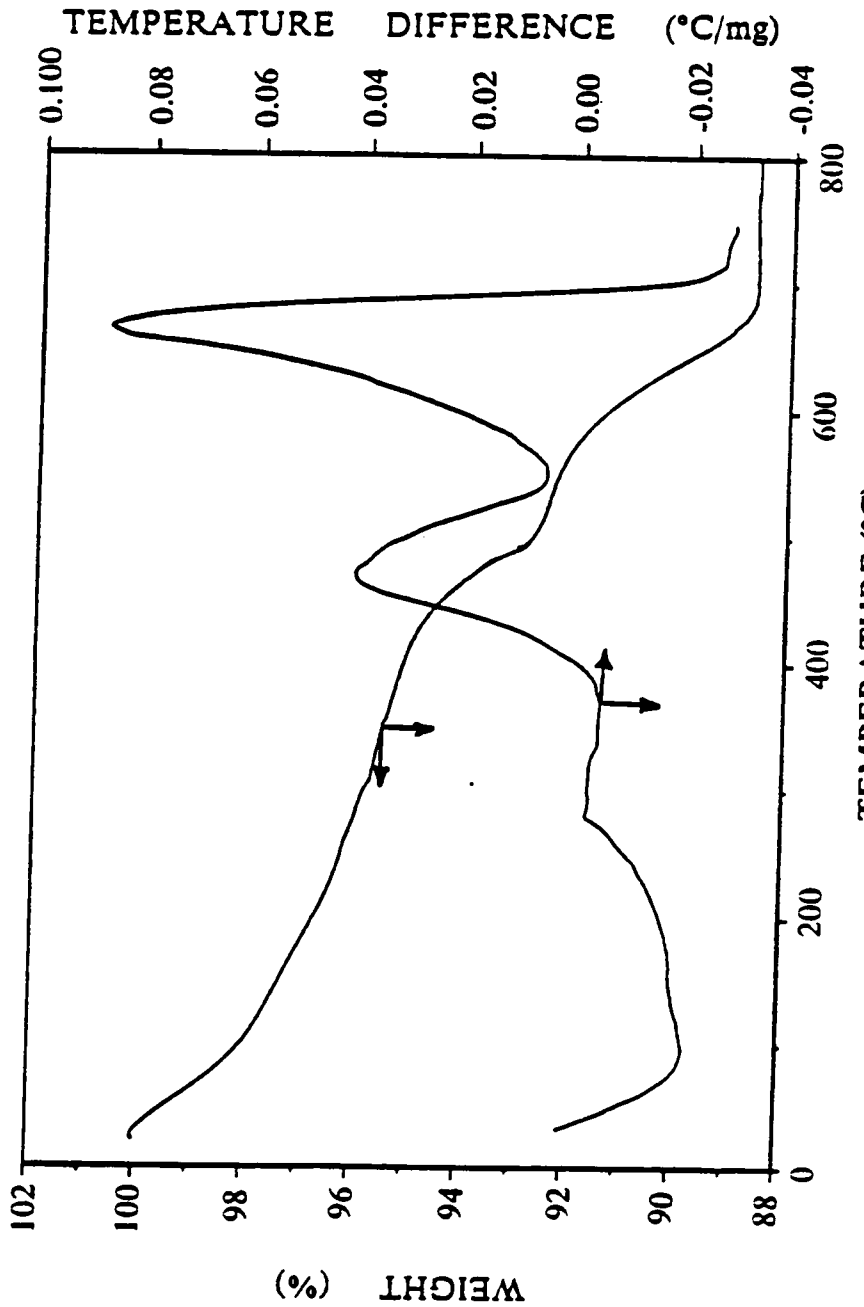

Figure 19. TGA and DTA curves for CoAPO-5

N_2 calcined is dark blue, and the O_2/H_2 calcined is blue. Table 10 shows the binding energies of the elements of different as-synthesized and calcined samples of CoAPO-5. The binding energies of oxygen (1s), aluminum (2p) and phosphorus (2p) are typical of those reported elsewhere.[43] Figure 20 shows the spectra of Co 2p of as-synthesized and calcined samples of CoAPO-5. It is observed that, accompanying the principal core line, satellite structures are also present at about 5 eV higher binding energy. This structure has been assigned to a shake-up process from $O_{2p} - Co_{3d}$ and is characteristic of photoionization of cobaltous ions, Co(II).[51] In addition, spin-orbit splitting of the Co $2p_{3/2}$ and $2p_{1/2}$ levels is observed with a ΔE of about 16 eV typical of paramagnetic Co(II).[51]

Table 11 reports the XPS and chemical analysis (CA) data for the framework elements in CoAPO-5 as-synthesized and after different treatments. The ratio XPS/CA gives the elemental surface composition of Co relative to the bulk. From TGA, DTA, and chemical analysis the empirical formula of as-synthesized CoAPO-5, assuming all the elements are in the framework, is:

$$0.053Et_3N.(Co_{0.101}Al_{0.399}P_{0.499}).O_2.0.158H_2O$$

Titration curves for CoAPO-5 after different treatments, obtained by neutralization of the resulting filtrate solution after NaCl exchange, appear in Figure 21. Very subtle acidity differences are observed for as-synthesized CoAPO-5 and for the material after different treatments.

Table 12 gives chemical composition of as-synthesized and calcined CoAPO-5 after exchange. Table 13 gives the chemical composition of the filtrate solution after exchange. It is interesting to point out that Co, P and relatively a very small amount of Al is dissolved from the O_2 and O_2/H_2 calcined solids during exchange while the filtrate of the N_2 calcined sample contains Co, Al and relatively a small amount of P.

Figure 22 compares the diffuse reflectance in the visible region, obtained from

Table 10. Binding Energies of elements in CoAPO-5

Referenced to Au $4f_{7/2}$ at 83.8 eV

Sample	Color	Binding Energy (eV)			
		$Co2p_{3/2}$	P2p	Al2p	O1s
As synt.	royal-blue	782.5	134.2	75.2	532.3
O_2calc.	yellow-green	782.7	134.3	75.0	532.4
O_2/H_2 calc.	royal-blue	783.1	134.9	75.4	532.9
N2 calc.	dark blue	782.2	134.7	75.3	532.7

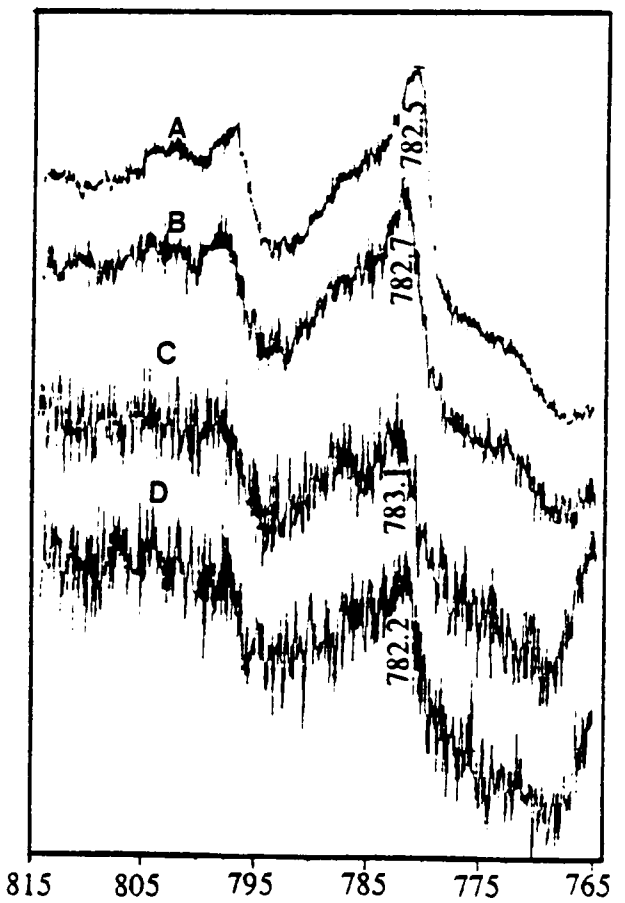

Figure 20. ESCA spectra of Co2p core level of (A) as-synthesized, (B) O_2 calc., (C) O_2/H_2 calc., (D)N_2 calc. CoAPO-5

Table 11. XPS and Chemical Analysis of Elements in CoAPO-5

Sample	XPS		CA		XPS/CA
	Al/P	Co/P	Al/P	Co/P	Co
As-synt.	0.6398	0.4303	0.7984	0.2024	2.126
O_2 calc.	0.9712	0.2261	0.8296	0.1709	1.3230
O_2/H_2 calc.	0.7403	0.0648	0.8060	0.1943	0.3335
N_2 calc.	0.9970	0.0611	0.8030	0.1822	0.3352

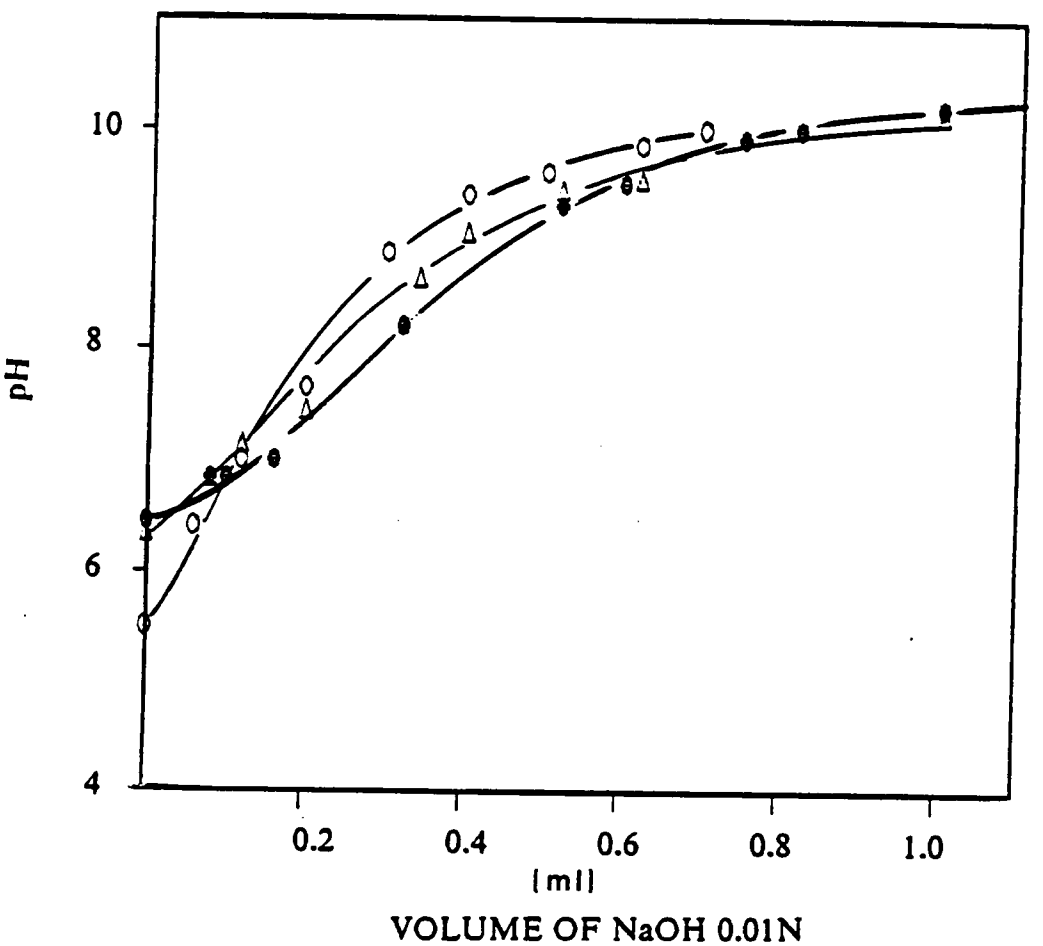

Figure 21. Titration curves for △ O_2/H_2, ○ O_2, • N_2 calcined exchanged CoAPO-5.

Table 12. Elemental Concentration of Na, Co, P, and Al in CoAPO-5 after NaCl exchange

Sample	Na/P	Co/P	Al/P
As-synt.	0.0133	0.1681	0.8171
O_2/H_2 calc.	0.0486	0.1450	0.8365
N_2 cal.	0.0437	0.1612	0.8394
O_2 calc.	0.0471	0.1121	0.8630

Table 13. Elemental Concentration of Filtrate Solution (μmol/ml) after NaCl Exchange of CoAPO-5

Sample	Na	Co	Al	P
As-synt.	15.3677	0.0051	0.0074	0.0161
O_2/H_2 calc.	14.3238	0.1042	0.0074	0.0678
N_2 cal.	14.4586	0.0745	0.0581	0.0111
O_2 calc.	16.1159	0.1900	0.0074	0.1453

calcined samples of CoAPO-5 (TEA). The O_2/H_2 calcined material absorbs in the 505-660 region, the O_2 calcined material shows absorption bands from 350 to 480 nm and from 480 to 680 nm. The N_2 calcined material shows an absorption band from 500 to 700 nm. Figure 23 compares the diffuse reflectance spectra in the visible region, for as-synthesized and calcined samples of CoAPO-5 (Et_3N). Absorption bands in the 400-700 nm are observed for the as-synthesized material. The O_2 calcined material absorbs in two regions: 350-480 nm and 480-700 nm. The O_2/H_2 calcined material absorbs in the 400 to 700 nm region. Figure 24 compares the diffuse reflectance spectra of the calcined samples of CoAPO-5 (Et_3N). Again, absorption bands in almost the same regions specified above are observed. Figure 25 compares the visible spectra of the O_2 CoAPO-5 (TEA) calcined material before and after exposure to methanol at room temperature. In these spectra the absorption band in the 350 to 480 nm region observed for the O_2 calcined material is not longer observed after the sample is exposed to methanol.

Figure 26 shows the solid-state ^{31}P NMR spectrum of CoAPO-5. Resonance maximum at -27.294 ppm is consistent with tetrahedral phosphorus. Spinning side bands at 127.939, 75.560, 24.202, -8.656, -130.160, -181.222 are also observed.

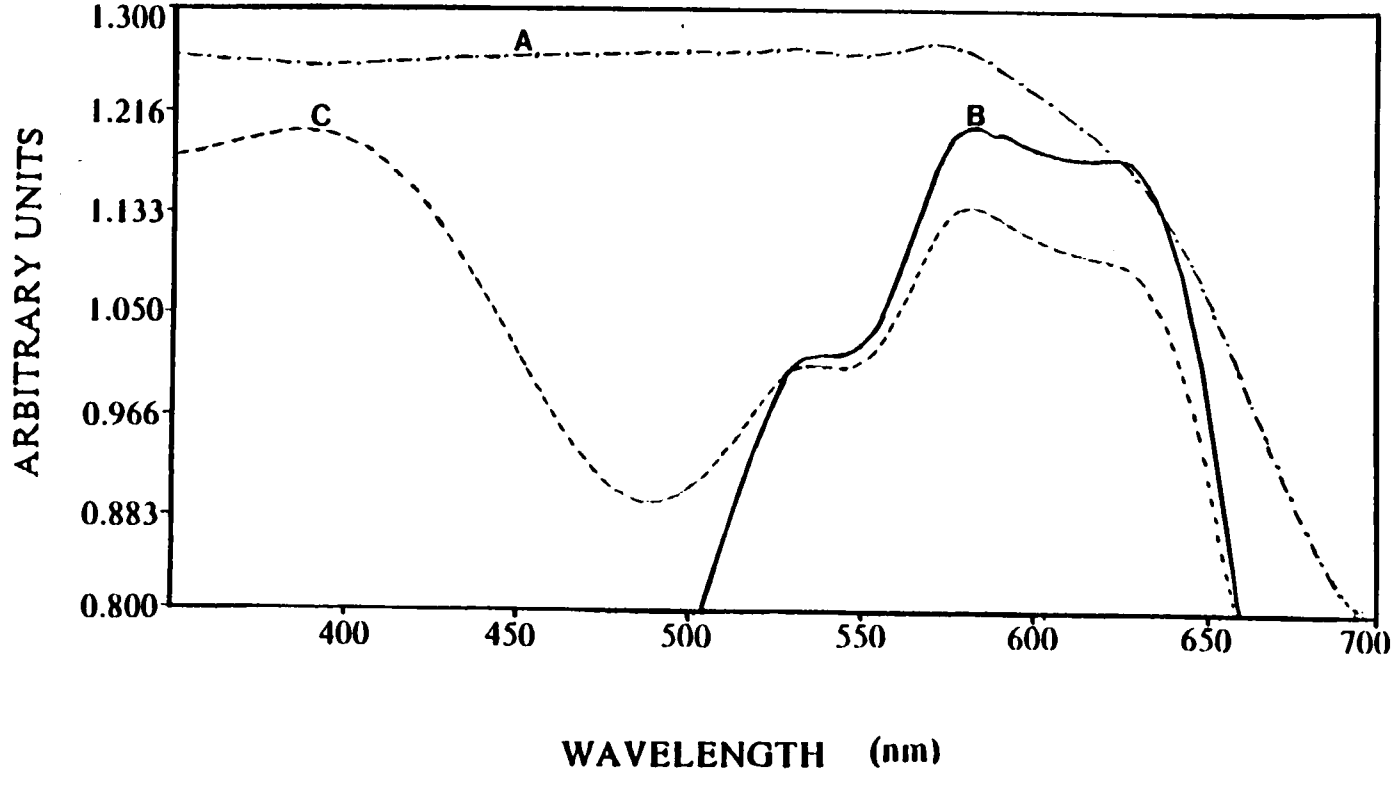

Figure 22. Visible diffuse reflectance spectra of (A) Vaccum calc. (dark-blue) (B) O_2/H_2 calc.(royal-blue) (C) O_2 calc. (yellow-green) CoAPO-5(TEA)

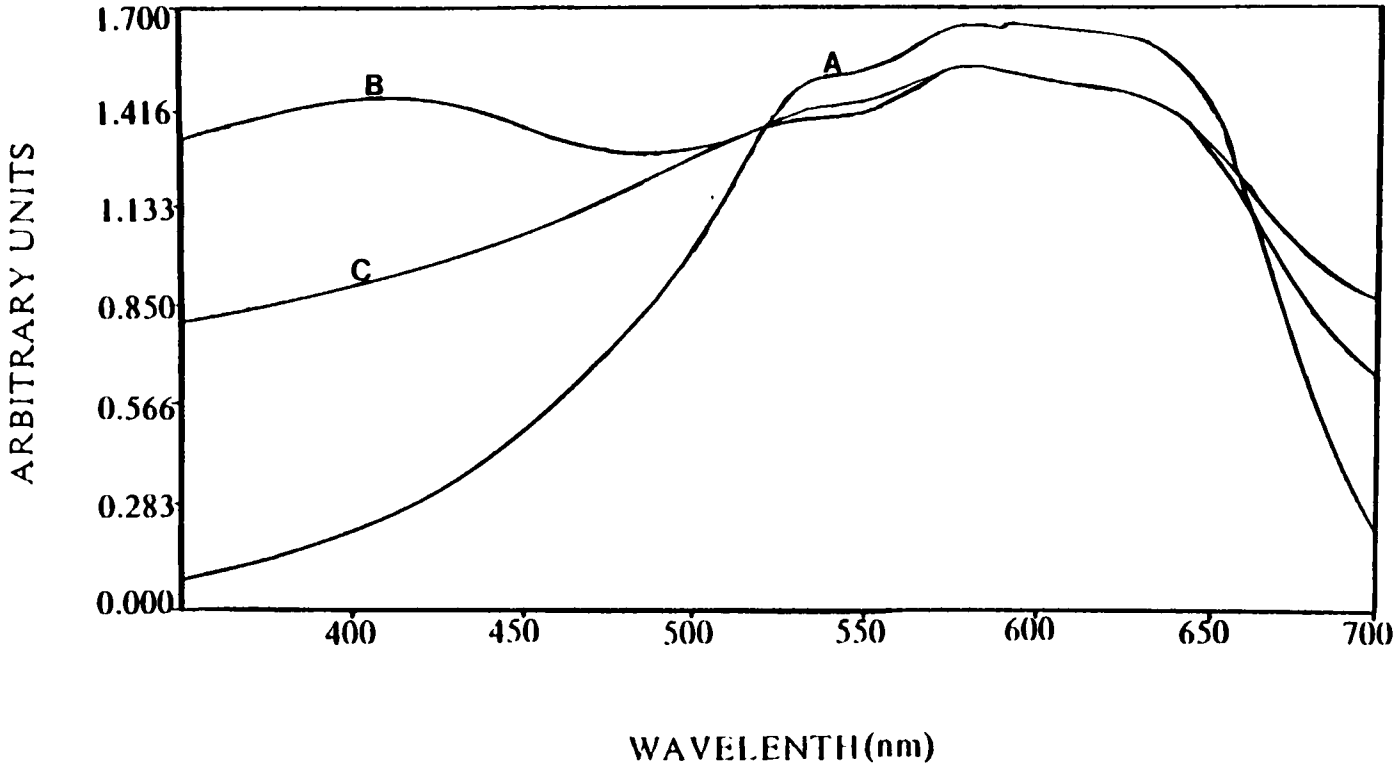

Figure 23. **Visible diffuse reflectance spectra of (A) As synt. (royal-blue) (B) O_2 calc. (yellow-green) (C) O_2/H_2 calc. (royal-blue) CoAPO-5(Et_3N)**

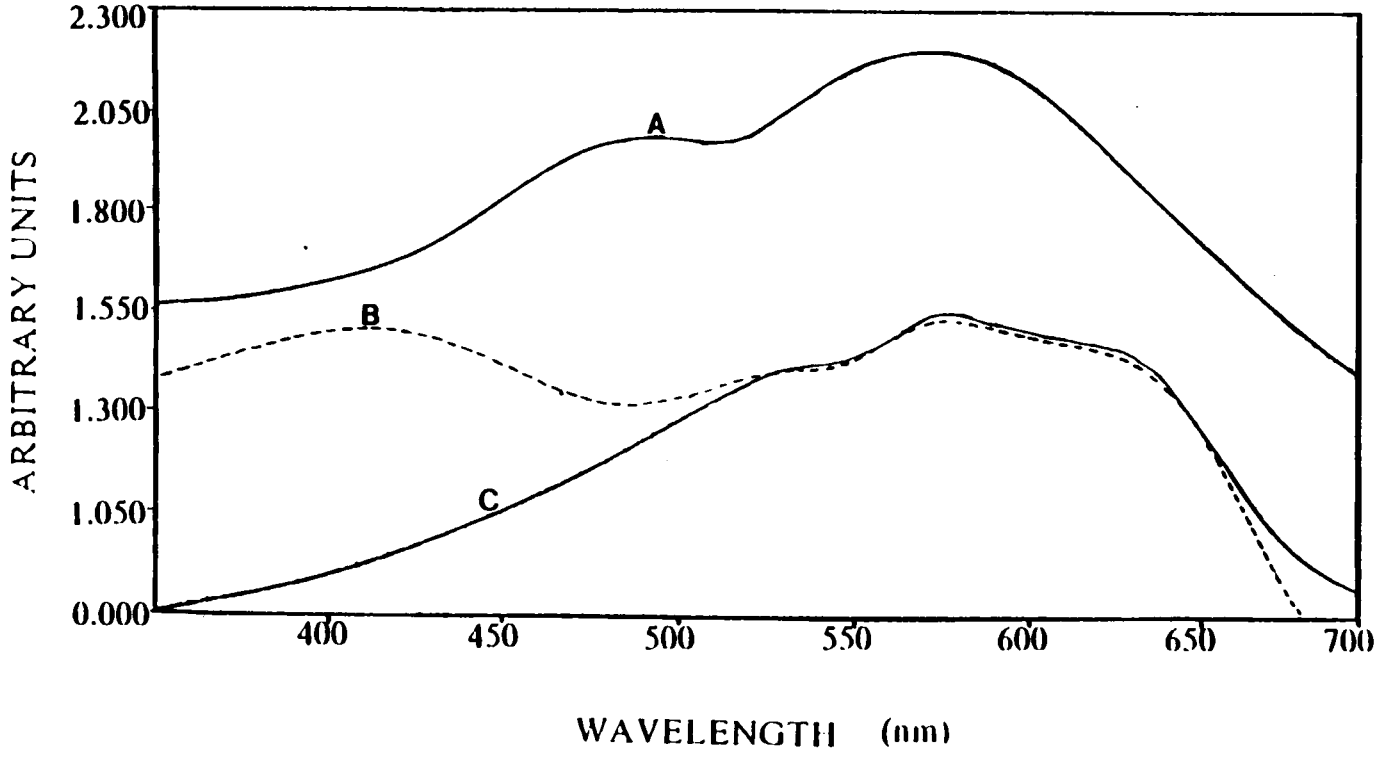

Figure 24. **Visible diffuse reflectance spectra of (A) N_2 calc. (dark-blue) (B) O_2 calc. (yellow-green) (C) O_2/H_2 calc. (royal-blue) CoAPO-5(Et_3N)**

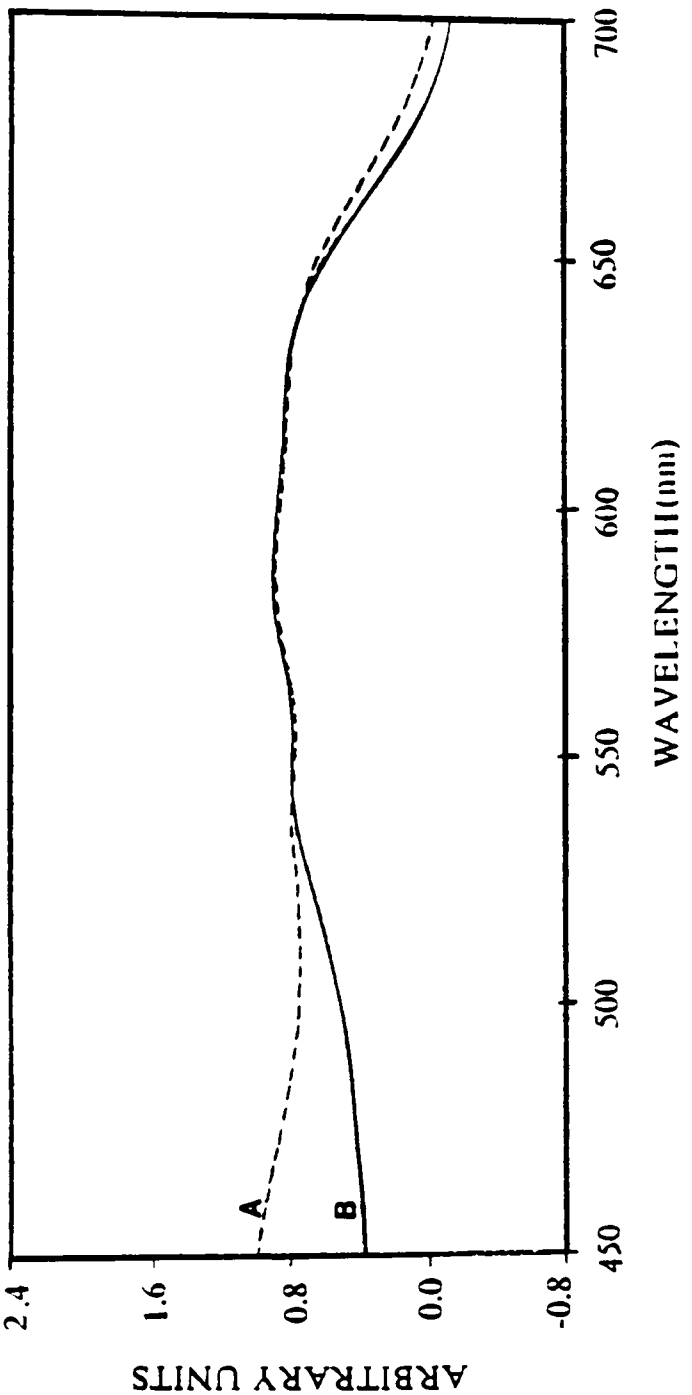

Figure 25. Visible diffuse reflectance spectra of O_2 calc. CoAPO-5 (TEA) (A) before, (yellow-green) (B) after, (blue) methanol exposure

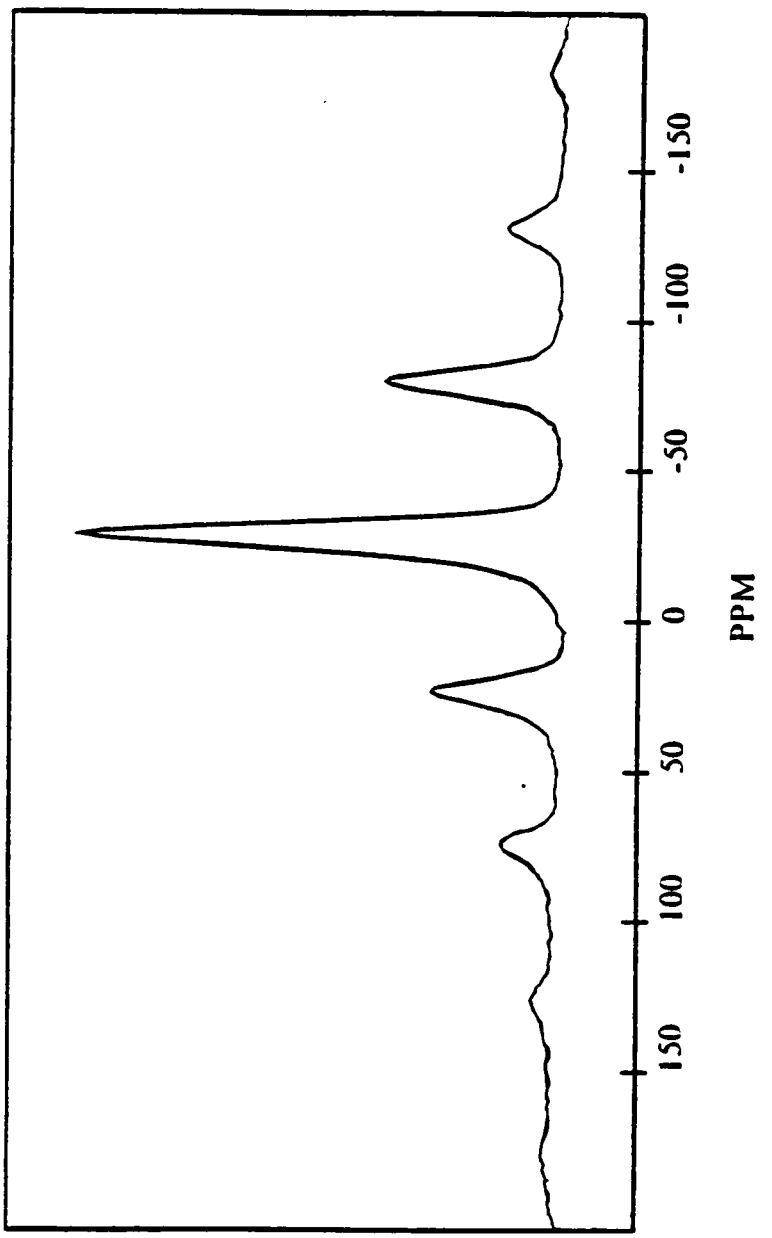

Figure 26. Solid-State ^{31}P NMR spectrum of CoAPO-5

4.3 VAPO-5 Synthesis and Characterization

Figure 27 shows the different X-ray diffraction patterns obtained during crystallization of VAPO-5 and Table 14 lists d-spacings, 2θ values and relative intensities for a typical sample of VAPO-5.

pH during crystallization of VAPO-5 compared with pH during crystallization of $AlPO_4$-5 synthesized with tripropylamine is shown in Figure 28. Compared with the $AlPO_4$-5 gel containing tripropylamine, the presence of V_2O_5 delays the formation of $AlPO_4$-5 like crystals beyond two hours. After 4 hours the product looks crystalline and no other phases are observed during the crystallization period studied.

Figure 29 and Figure 30 show complete argon adsorption isotherms for VAPO-5 and $AlPO_4$-5 measured at liquid argon temperature. From Figure 29 the argon adsorption capacity at P/Po = 0.43 is 0.15 cm^3/g. The oxygen adsorption capacity for VAPO-5 meausured in a McBain-Bakr balance, at 100 torr O_2 pressure and at liquid N_2 temperatures, is 0.17 cm^3/g solid which compares relatively well with the value for the pure $AlPO_4$-5 phase (0.1749 cm^3/g solid).

Figure 31 shows a SEM of VAPO-5. As can be observed, the morphology of VAPO-5 is similar to the morphology of $AlPO_4$-5 synthesized with tripropylamine.

Figure 32 show TGA and DTA curves for VAPO-5. In contrast with the corresponding curves for $AlPO_4$-5 synthesized using tripropylamine as the organic, it appears that the presence of V_2O_5 in the gel affects the interactions of the organic with the framework elements in VAPO-5. In VAPO-5 the three first weight losses are comparable to those observed in $AlPO_4$-5. However, the fourth exothermic weight loss observed in $AlPO_4$-5 synthesized with tripropylamine is not observed here.

Table 15 shows the binding energies of the framework atoms of different

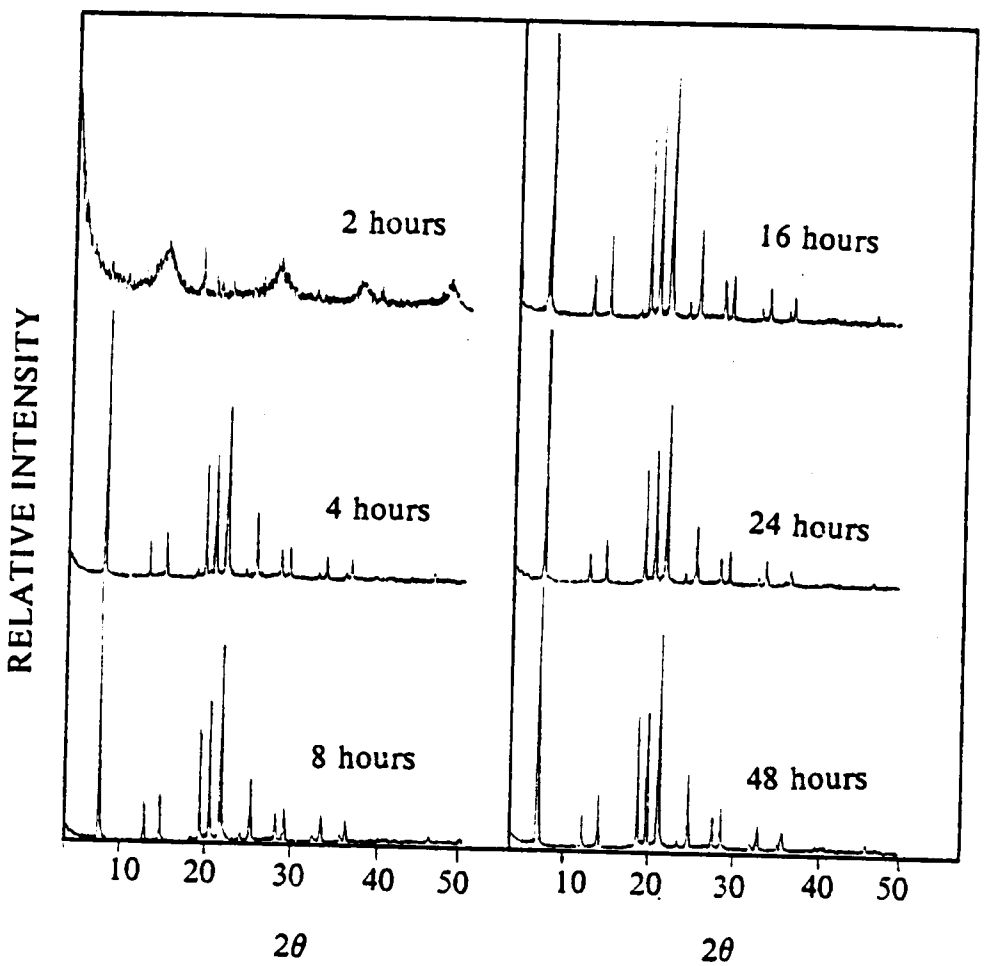

Figure 27. XRD patterns during crystallization of VAPO-5

Table 14. d-Spacings 2θ, and Relative Intensities for VAPO-5 (24 hours)

d-space	2θ	I/I max
11.94580	7.406	100.0
6.86817	12.890	13.6
5.94720	14.896	18.4
4.49419	19.754	47.9
4.22990	21.002	52.4
3.96963	22.396	79.2
3.59801	24.745	4.0
3.42963	25.980	24.8
3.07508	29.038	11.5
2.98916	29.892	2.5
2.97107	30.078	14.2
2.78022	32.197	0.6
2.66172	33.672	4.5
2.62927	34.100	1.2
2.59262	34.597	9.8
2.42979	36.997	3.0
2.38684	37.687	6.6
2.21165	40.800	0.5
2.17058	41.607	1.5
2.13955	42.240	1.7
2.11289	42.799	1.5
2.02757	44.694	0.6
1.98947	45.598	0.5

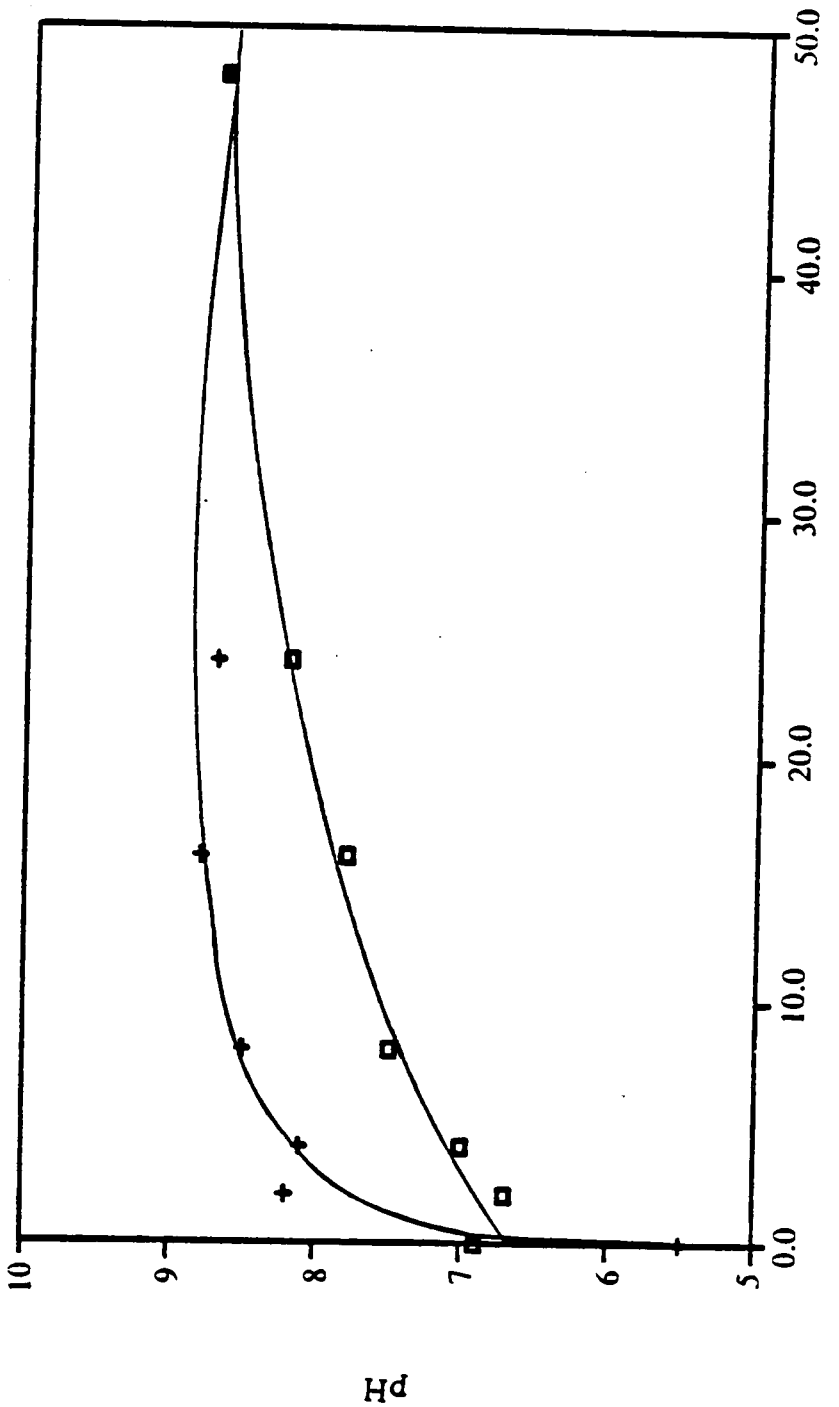

Figure 28. pH during crystallization of □ VAPO-5 and + $AlPO_4$-5 synthesized with tripropylamine

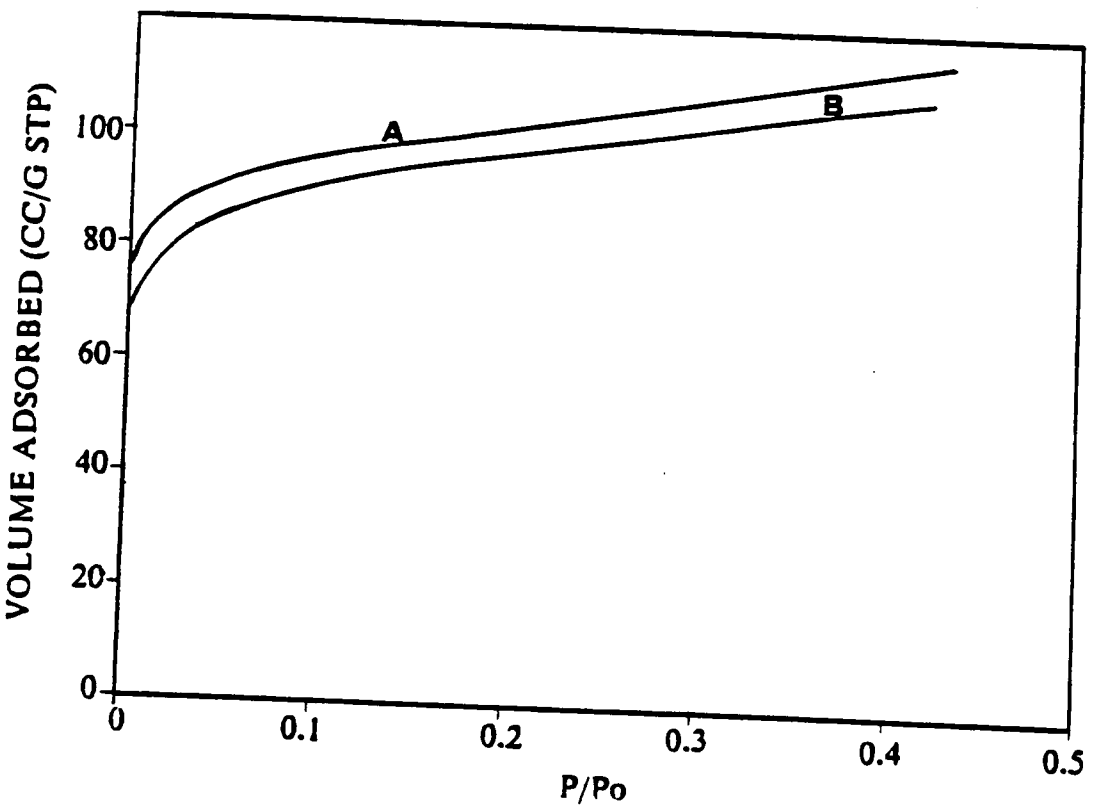

Figure 29. Argon adsorption isotherm of (A) VAPO-5 (B) $AlPO_4$-5

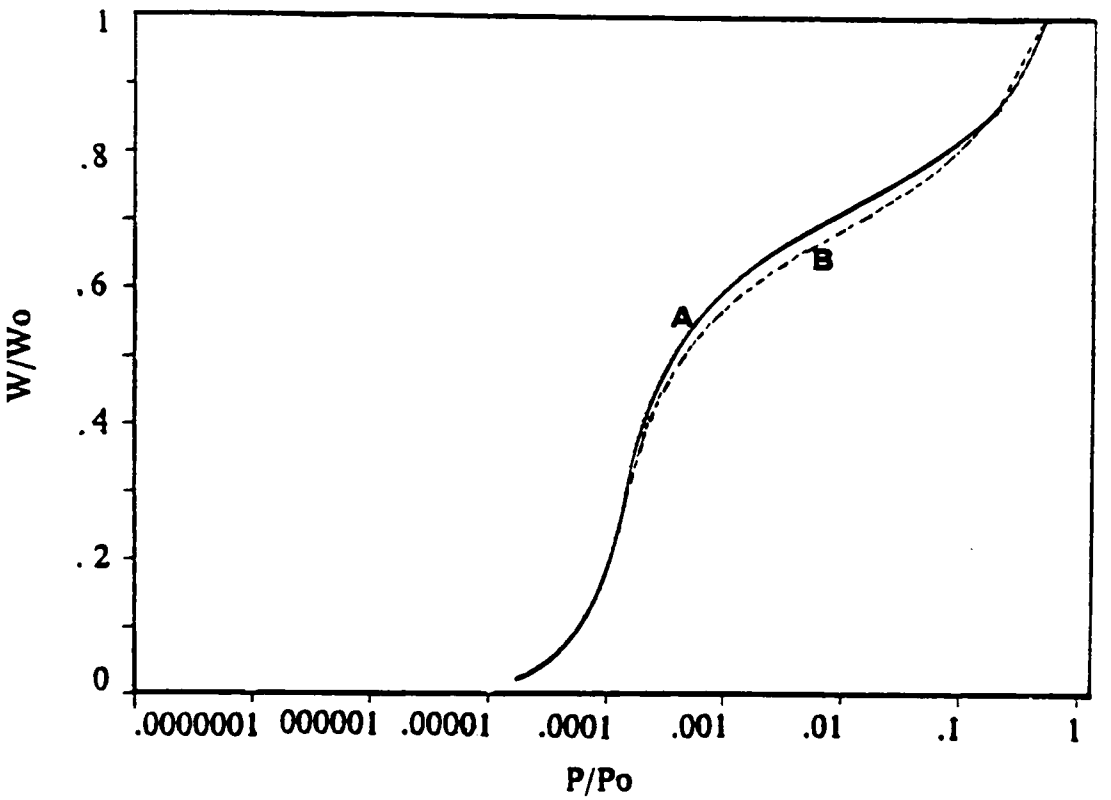

Figure 30. Argon adsorption isotherm of (A) VAPO-5 (B) $AlPO_4$-5

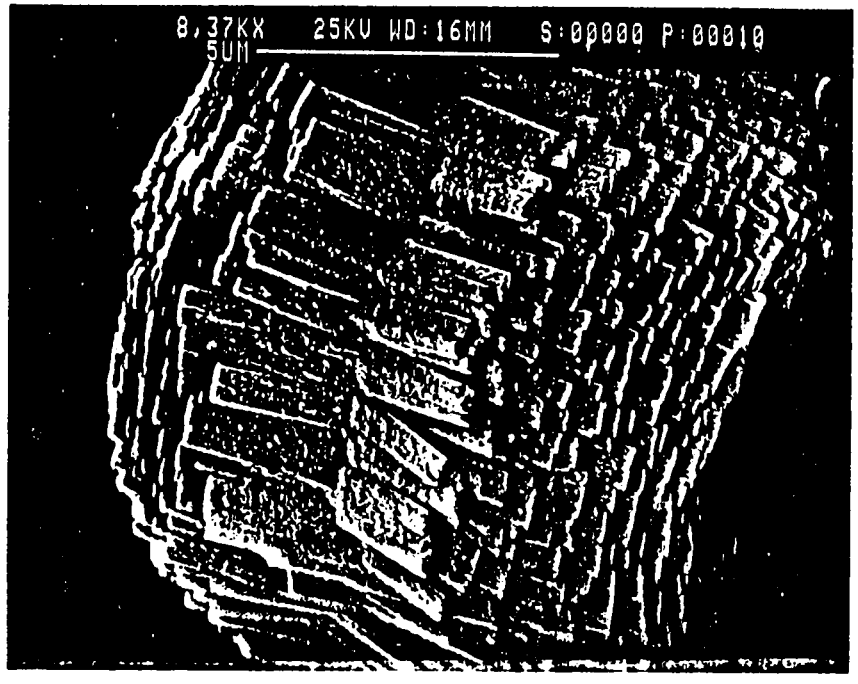

Figure 31. SEM of VAPO-5

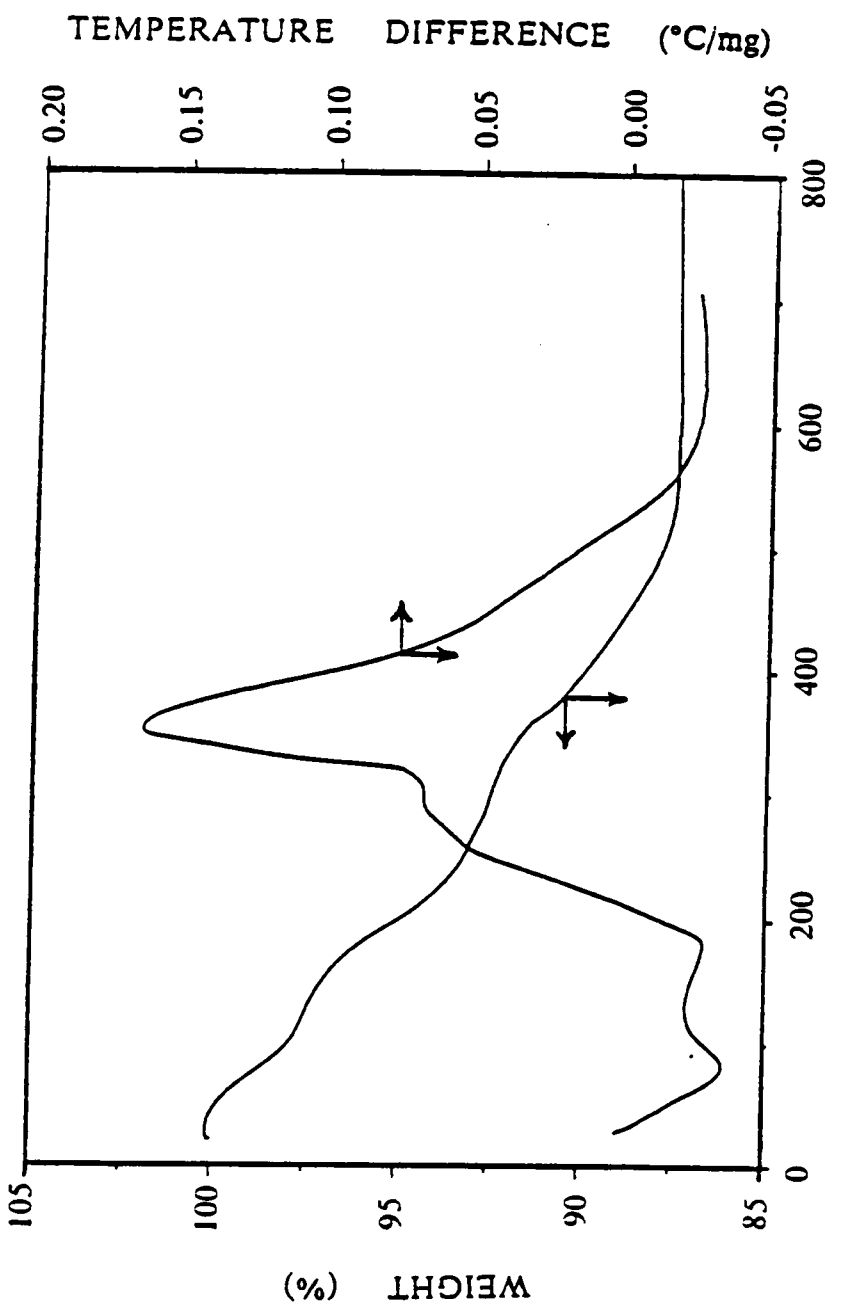

Figure 32. TGA and DTA curves for VAPO-5

samples of VAPO-5 and Figure 33 shows the ESCA spectra of the V(2p) core level of VAPO-5. Two as-synthesized samples of VAPO-5 differing only on the preparation date show a 0.5 eV binding energy difference. For the calcined materials it is evident that within experimental error the binding energy of the $V(2p_{3/2})$ lines are essentially equal. These values correspond closely to those of V_2O_5. [60] However, these materials exhibit different colors depending on the treatment. The as-synthesized product looks light blue and becomes apple-green while sitting in the lab for about 6 months. The O_2 calcined material looks yellow. The N_2 or Ar/He calcined material looks light brown and the O_2/H_2 calcined material looks apple-green.

Table 16 reports XPS and elemental chemical analysis (CA) for VAPO-5 as-synthesized and after different treatments. The ratio XPS/CA gives the elemental surface composition of V relative to the bulk. From TGA, DTA, and chemical analysis, the empirical formula of as-synthesized VAPO-5, assuming framework siting of all the elements, is:

$$0.02Pr_3N.(Al_{0.5}V_{0.007}P_{0.493}).O_2.0.23H_2O$$

Figure 34 illustrates the potentiometric titration curves of VAPO-5 obtained with the filtrates following NaCl treatment. Characteristic curves for each material are observed. The curve corresponding to the O_2/H_2 calcined VAPO-5 appears to indicate more acidity than the curves corresponding to the O_2 and the Ar/He calcined VAPO-5. From these curves the amount of NaOH consumed to neutralize the protons released by the samples gives an idea of the ion exchange capacity of the treated materials. The values obtained are: 0.03083 meq/g for the O_2/H_2 calcined sample and approximately 0.01542 meq/g for the O_2 and Ar/He calcined sample which is half of the value for the O_2/H_2 calcined sample.

Table 17 gives the chemical composition of the solid for the calcined VAPO-5 materials after NaCl exchange. The data obtained for O_2 calcined $AlPO_4$-5 (Pr_3N) is

Table 15. Binding Energies of Elements in VAPO-5 †

Referenced to Au $4f_{7/2}$ at 83.8 eV

Sample	Color	Binding Energy (eV) V2p$_{3/2}$	P2p	Al2p	O1s
As synt. (7-15-88)	apple green	517.1	134.9	74.5	532.3
As synt. (11-11-88)	light blue	516.6	134.7	74.7	532.3
O_2calc. (11-11-88)	yellow	517.1	135.0	75.2	532.7
O_2/H_2 calc. (11-11-88)	apple green	516.9	134.8	74.7	532.5
Ar/He calc. (11-11-88)	light brown	516.8	135.0	75.0	532.6
N2 calc. (11-11-88)	light brown	517.0	135.1	75.2	532.8

†Data taken during February 1989.
The numbers inside the parenthesis indicate the synthesis date.

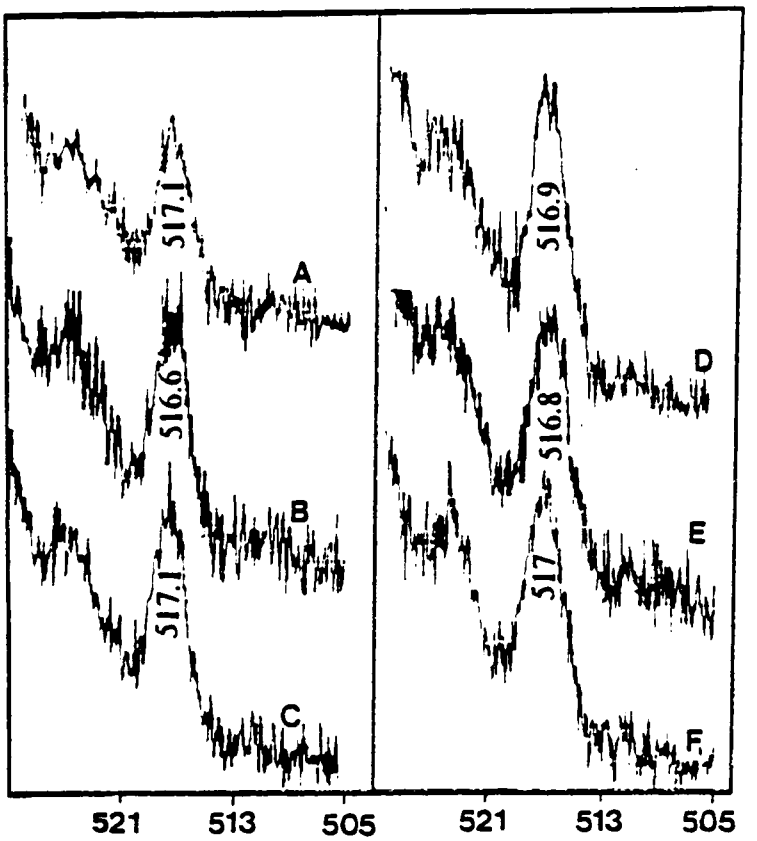

Figure 33. ESCA spectra of V(2p) core level of: (A) as-synthesized (7-15-88), (B) as-synthesized (11-11-88) (C) O_2 calc., (D) O_2/H_2 calc., (E) Ar/He calc.,(F)N_2calc.VAPO-5

Table 16. XPS and Chemical Analysis of Elements in VAPO-5 †

Sample	XPS		CA		XPS/CA
	V/Al	P/Al	V/Al	P/Al	V
As-synt. (7-15-88)	0.0187	0.6526	0.0136	0.9838	1.3750
As-synt. (11-11-88)	0.0254	0.9351	0.0154	0.9658	1.6494
O_2 calc. (11-11-88)	0.0209	0.8431	0.0155	0.9953	1.3453
O_2/H_2 calc. (11-11-88)	0.0148	0.6371	0.0152	0.9892	0.9737
N_2 calc. (11-11-88)	0.0188	0.7727	0.0147	0.9938	1.2781
Ar/He calc. (11-11-88)	0.0165	0.7618	0.0151	0.9970	1.0936

†The numbers inside the parenthesis indicate the synthesis date.

shown for comparison. The first column was obtained by substrating the amount of Na contained in O_2 calcined $AlPO_4$-5 (Pr_3N) from the Na content of the calcined materials and ratioing this value with the respective V content. These values give an idea of the number of protons exchanged for sodium ions. Table 18 give chemical composition of the filtrate solution following NaCl exchange. Also for comparison, the data obtained for a sample of O_2 calcined $AlPO_4$-5 (Pr_3N) is included.

Figure 35 and Figure 36 show the ^{27}Al and the ^{31}P NMR spectra of as-synthesized VAPO-5. Sharp resonances at 32.624 and -29.3018 ppm for ^{27}Al and ^{31}P respectively are consistent with aluminum and phosphorus in tetrahedral coordination.

Figure 37 compares the diffuse reflectance UV difference spectra relative to $AlPO_4$-5 obtained from as-synthesized and calcined VAPO-5. For all of these materials an absorption band between 200-400 nm is observed, which suggests the presence of vanadium in tetrahedral geometry.[44,45]

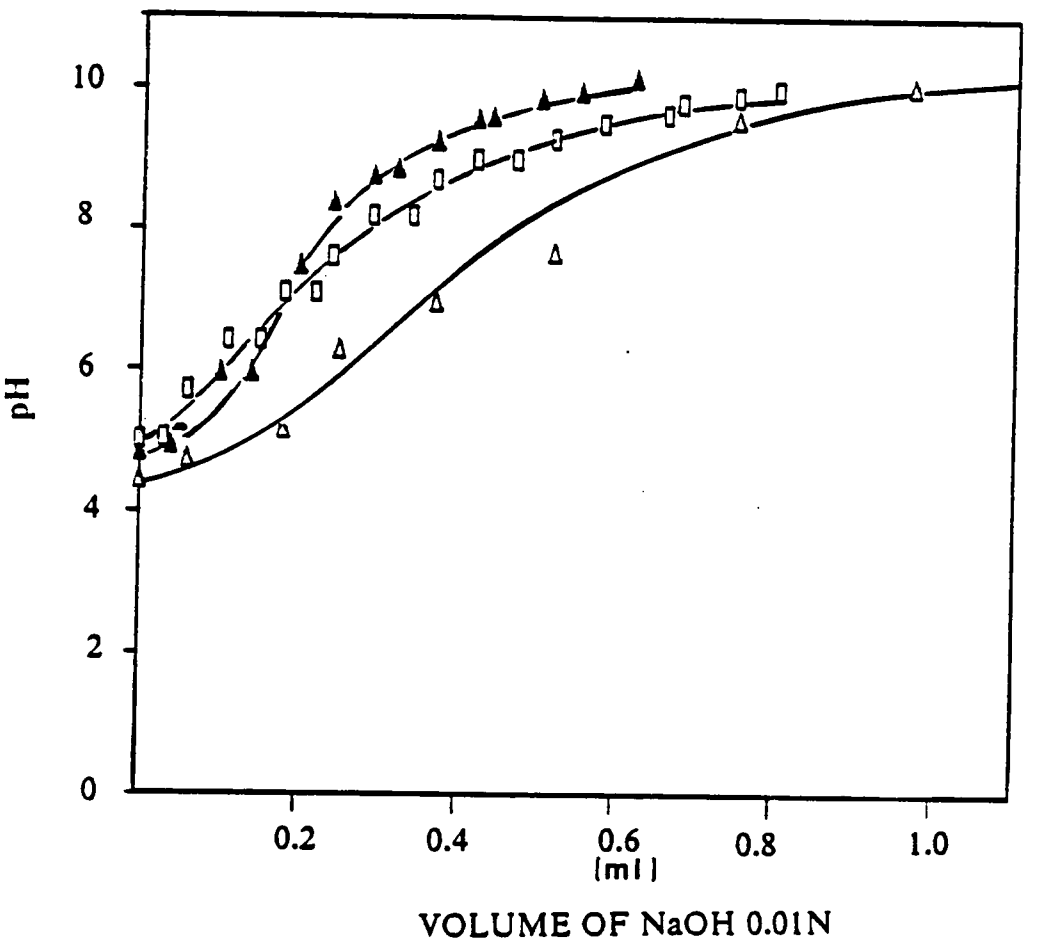

Figure 34. Titration curves for □ Ar/He, ▲ O_2, △ O_2/H_2 calcined-exchanged VAPO-5.

Table 17. Elemental Concentration of Na, V, Al, and P in VAPO-5 after NaCl exchange

Sample	Na/V†	Na/Al	V/Al	P/Al
O_2/H_2 calc. (11-11-88)	4.2199	0.0978	0.0141	0.9932
Ar/He cal. (11-11-88)	2.2331	0.0680	0.0133	1.0036
O_2 calc. (11-11-88)	2.3188	0.0697	0.0136	0.9936
$AlPO_4$-5 O_2 calc.	-	0.0383	-	1.0288

† Referenced to the ratio Na/Al for $AlPO_4$-5 O_2 calc.
The numbers inside the parenthesis indicate the synthesis date.

Table 18. Elemental Concentration of Filtrate Solution (μmol/ml) after NaCl Exchange of VAPO-5 †

Sample	Na	V	Al	P
O_2/H_2 calc. (11-11-88)	15.1372	0.0032	0.1038	0.0807
Ar/He cal. (11-11-88)	17.3294	0.0071	0.0815	0.0775
O_2 calc. (11-11-88)	16.4508	0.0037	0.0852	0.0775
$AlPO_4$-5 O_2 calc.	16.0419	-	0.0741	0.0872

†The numbers inside the parenthesis indicate the synthesis date.

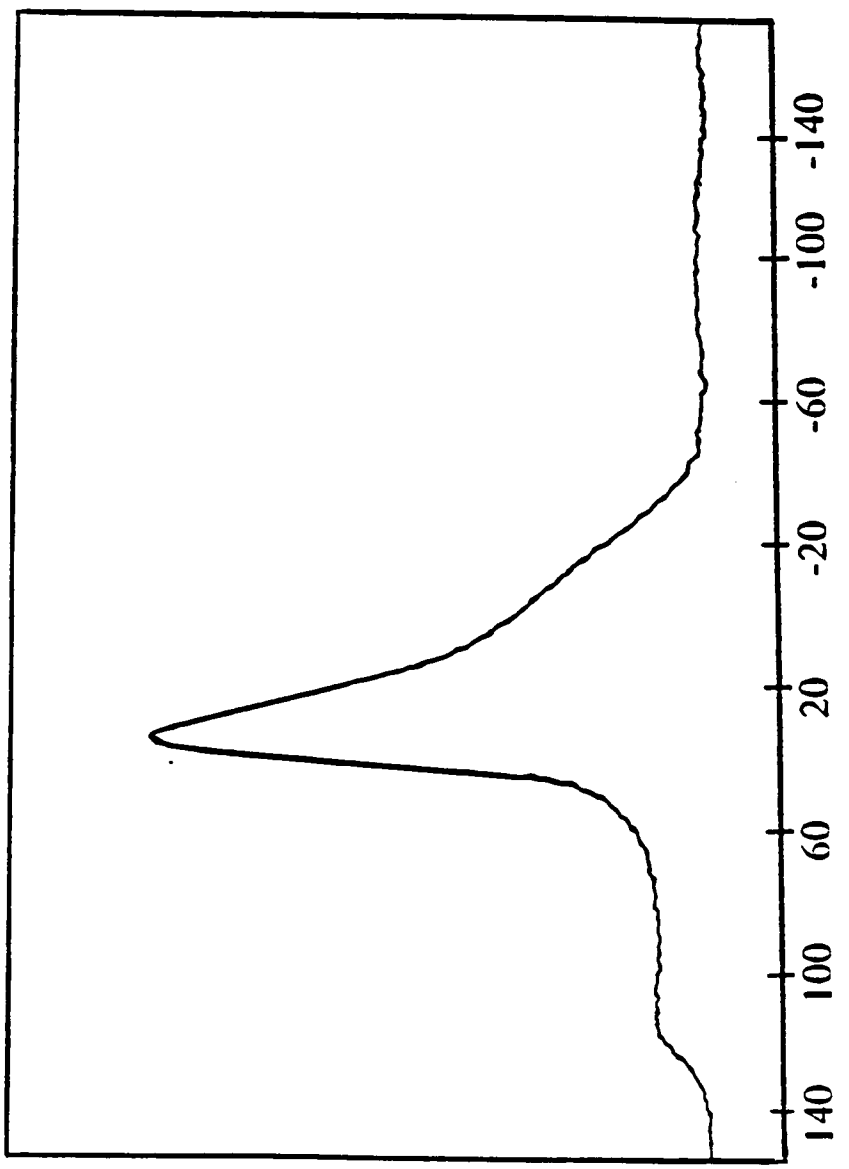

Figure 35. Solid-state ^{27}Al NMR spectrum of VAPO-5

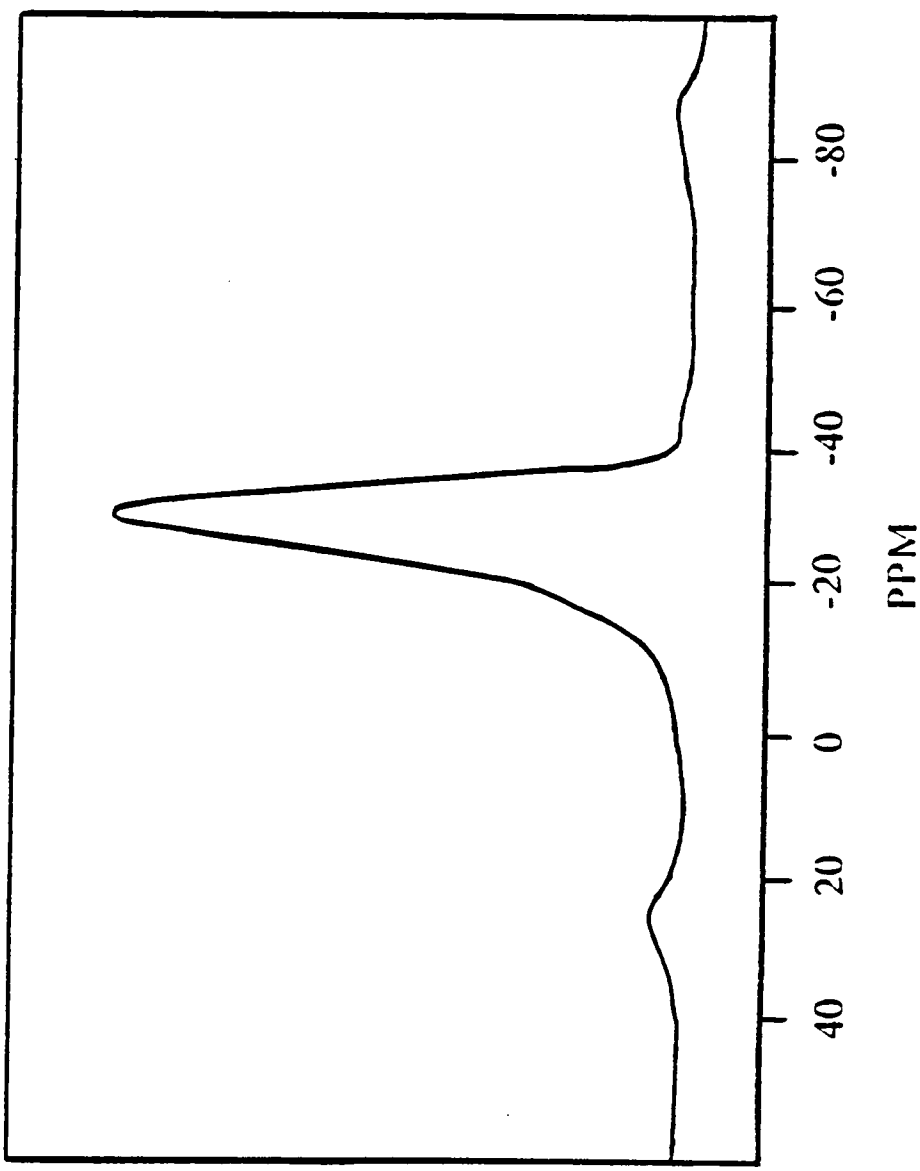

Figure 36. Solid-State ^{31}P NMR spectrum of VAPO-5

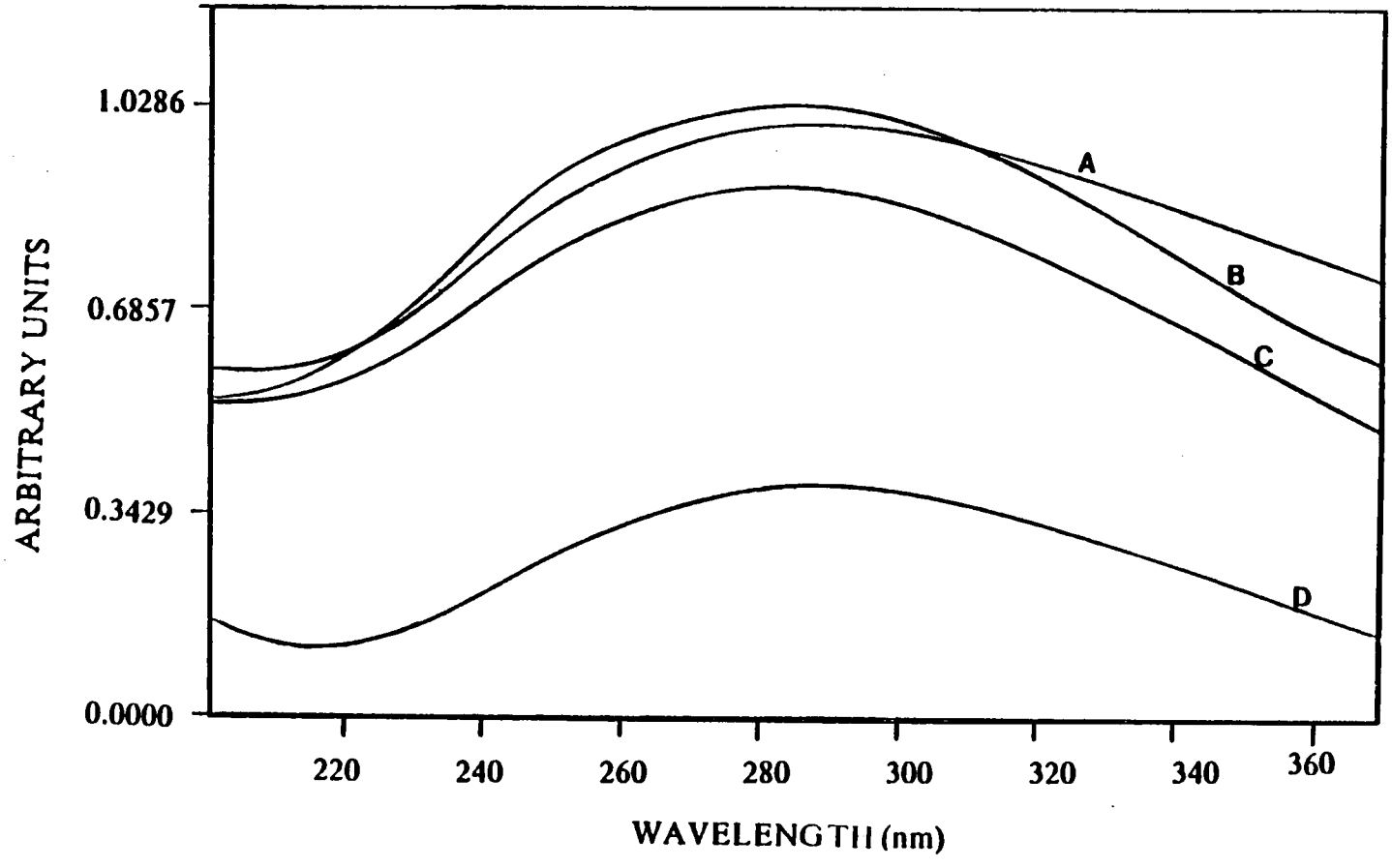

Figure 37. UV difference spectra of (A) N_2 calc. (brown) (B) O_2 calc.(yellow) (C) O_2 /H_2 cal. (apple-green) (D) As synthesized (light blue) VAPO-5

4.4 MoAPO-5 Synthesis

A light blue molybdenum containing $AlPO_4$-5 material, which becomes white after calcination in O_2, was obtained. Its x-ray diffraction pattern and argon and oxygen adsorption capacities were identical to those of the pure $AlPO_4$-5 phase. It was not possible to determine the oxidation state of molybdenum by XPS because the amount of molybdenum contained in the samples was below detection limits. Table 19 gives the chemical composition of typical samples.

As observed, the amount of molybdenum incorporated in the as-synthesized material is about 0.1%, and after exchange the remaining molybdenum drops to 0.07%.

When using aluminum isopropoxide as the aluminum source, the pH of the synthesis gel was about 8 and the blue color of the solid obtained looks more intense than the color of the solid obtained using Catapal alumina. Bulk chemical analysis of Mo, Al and P showed that these samples contained about 0.9% Mo, 51.23% Al and 47.8% P. This analysis shows that Mo may substitute for P but the ratio (Mo + P)/Al is less than 1. In addition, no molybdenum was detected by XPS in these samples.

For the above reasons further characterization of the molybdenum containing materials was not pursued.

Table 19. Elemental Concentration of Na, Mo, P, and Al in MoAPO-5

Sample	Na	Mo	P	Al
As synt. (6-5-88)	-	0.001173	0.4888	0.5100
NaCl exch. (6-5-88)	0.0122	0.0007	0.4907	0.5086

4.5 Catalytic Activity

Table 20 and Table 21 report the activity of CoAPO-5 (TEA) and VAPO-5 for the partial oxidation of methane to methanol and formaldehyde. These reactions were carried out in the flow reactor system described in section 3 at a total flow rate of gases (F) of 1.2 ml/sec and partial pressures of 90, 300, and 100 torr for CH_4, N_2O and H_2O respectively. Several temperatures and pseudocontact times (W/F) were used. Here W is the mass of catalyst and F is the flow rate, evaluated at 25°C. In these experiments the value of W/F was varied by changing the mass of catalyst and holding the flow rate constant.

For CoAPO-5 (TEA), Table 20 shows that at very low conversions formaldehyde is obtained, and at high conversions most of the products are oxides of carbon. No methanol was observed under the conditions studied. The use of the same catalyst in various runs leads to the formation of small quantities of formaldehyde indicating catalyst deactivation. Additionally, the X ray diffraction of the material used after four runs shows catalyst transformation to tridymite. Using O_2 as oxidant the conversion of CH_4 is very low and only traces of CO_2 are produced.

For VAPO-5, Table 21 shows that no products were obtained at temperatures below 400°C. At temperatures over 500°C mainly CO and CO_2 are produced at low conversions. The selectivity toward formaldehyde is very low and no methanol was observed under the conditions studied.

Using O_2 as oxidant in the 300-400°C range, no products were detected. A small decrease in the crystallinity of the product after two runs was observed, but the VAPO-5 structure of the catalyst remained the same.

Table 20. OXIDATION OF CH_4 BY NITROUS OXIDE OVER CoAPO-5(TEA)

Run	W/F g.sec/ml	T°C	% CH_4 Conversion	Selectivity		
				CO_2	CO	HCHO
9-10-88	0.07	300	-	-	-	-
9-12-88	0.07	400	-	-	-	-
	0.07	500	0.4	28.15	-	71.84
9-22-88	1.08	500	84.53	83.33	16.55	0.13
9-23-88	1.08	300	-	-	-	-
	1.08	400	0.84	92.34	-	7.66
	1.08	500	3.11	47.38	49.33	3.29
9-24-88	1.08	450	5.69	49.74	49.30	-
	1.08	460	8.36	33.51	66.08	.4
	1.08	470	15.80	42.81	57.83	-
	1.08	480	76.21	81.07	18.86	0.06
9-27-88	0.45	500	65.33	78.42	21.58	-

Table 21. OXIDATION OF CH_4 BY NITROUS OXIDE OVER VAPO-5

Run	W/F. g.sec/ml	T°C	% CH_4 Conversion	Selectivity		
				CO_2	CO	HCHO
10-04-88	0.68	300	-	-	-	-
	0.68	350	-	-	-	-
	0.68	400	-	-	-	-
10-29-88	0.41	500	0.18	100	-	-
	0.41	550	1.6	74.37	17.75	7.89
	0.41	560	4.85	44.33	51.02	4.65
	0.41	570	4.81	55.47	39.63	5.66
	0.41	580	8.50	47.88	48.99	3.13

5.0 DISCUSSION

5.1 $AlPO_4$-5 Synthesis and Characterization

$AlPO_4$-5 was synthesized with two different organics and used for comparison to CoAPO-5 and VAPO-5. In general, the results obtained for $AlPO_4$-5 in this study are consistent with those reported elsewhere.[9,38]

From the X-ray diffraction patterns shown in Figure 5 it is observed, that using tripropylamine as the organic the best product is obtained between 24 and 48 hours of crystallization. Using triethylamine, the best product is obtained between 4 and 16 hours of crystallization (Figure 6).

The pH profile for $AlPO_4$-5 (Et_3N) is above that of the corresponding pH profile for $AlPO_4$-5 (Pr_3N), (Figure 7). This may be due to the higher amount of Et_3N (1.5 moles) in the initial gel compared to Pr_3N (1.0 mol). The morphology of the resulting product is also influenced by the type of amine used. With Pr_3N (Figure 8), the product consists of spheres composed of hexagonal rods wrapped around a central cavity. When using Et_3N (Figure 9), most of the crystals appear as individual hexagonal rods.

The DTA of $AlPO_4$-5 (Pr_3N) in Figure 10 shows two exothermic weight losses corresponding to decomposition of tripropylamine. The DTA pattern for this material has been reported elsewhere,[38] and is the same as observed here. Also similar behaviour has been observed in temperature programmed desorption experiments of tripropylamine from calcined $AlPO_4$-5.[39] In agreement with the value reported elsewhere,[9] the total content of Pr_3N obtained from DTA corresponds to one molecule

per unit cell. The size of Pr_3N is about 8.5Å similar to the size of the unidimensional pores in $AlPO_4$-5. Thus, the decomposition of the amine is expected to involve thermal cracking of the occluded tripropylamine, followed by oxidation of the cracking products in the intra- and inter-crystalline spaces, and also oxidation of tripropylamine within the channels. The delay in the removal of tripropylamine from $AlPO_4$-5 has been reported to be due to the presence of heavy, complex oxygenates in the channels formed under oxygen deficient conditions. This oxygenates have low diffusivity and are difficult to remove. Further oxidation of this oxygenates to simpler products facilitates their removal.[38] Only one exotherm is observed in Figure 11 for $AlPO_4$-5 (Et_3N). From TGA it can be determined that there are approximately 1.41 molecules per unit cell. A value reported elsewhere[8] is 1.2 molecules per unit cell. Since Et_3N is smaller than Pr_3N it can diffuse out of the pores of $AlPO_4$-5 much easier. This speculation is consistent with the difference in the DTA pattern observed for $AlPO_4$-5 (Pr_3N) and $AlPO_4$-5 (Et_3N).

Although samples of $AlPO_4$-5 (Et_3N) and $AlPO_4$-5 (Pr_3N) were treated the same way before unit cell determination as described in equipment and procedure, their unit cell dimensions are sligthly different. The unit cell size of $AlPO_4$-5 (Et_3N), $a = 13.61$ Å and $c = 8.47$ Å gives a volume of 1359 $Å^3$ while the unit cell size of $AlPO_4$-5 (Pr_3N), $a = 13.67$ Å and $c = 8.44$ Å, gives a volume of 1357 $Å^3$. Changes in the unit cell size of different preparations of the same aluminophosphate structure have been reported.[6] However, the reason for these differences is not clear at this time.

As expected, the Al and P binding energies shown in Table 8 correspond[42] to Al^{+3} and P^{+5}. The XPS/CA ratio for both elements is close to 1 indicating no zoning.

The ^{27}Al NMR spectra in Figure 12 show all the major resonance maxima in the tetrahedral region with four phosphorus atoms in the second coordination sphere (40-29 ppm). The resulting line-shapes with two resonance maxima, at 39.84 and

31.96 ppm in the as-synthesized material and at 37.11 and 26.50 ppm in the calcined material, are characteristic of dominant second order quadrupole effects. The high field components at -9.97 ppm in the as-synthesized material, and at -15.627 ppm in the calcined material may be due to impurities, slight structure degradation, or some secondary interaction of certain framework Al sites with the organic (tripropylamine) and/or H_2O molecules entrapped within the channel system.[36,40,41] The NMR spectra shown in Figure 13 are consistent with phosphorus in tetrahedral coordination with four aluminum atoms in the second coordination sphere.[18,36,37,40]

5.2 CoAPO-5 Synthesis and Characterization

During the crystallization of CoAPO-5, changes in crystallinity followed by X-ray diffraction (Figure 14) are correlated to the pH variation of the reaction mixture (Figure 15). The reaction mixture is acidic before crystallization begins, and a marked increase in pH is noted to accompany crystal formation. Also, the formation of a second phase is accompanied by a pH decrease. The X-ray diffraction patterns indicate that the CoAPO-5 phase is metastable in the synthesis gel and pure product is obtained during times no longer than 4 hours of heating. The above changes are similar to those observed for $AlPO_4$-5 (Et_3N) but at lower pH values. The decrease in the pH values observed in CoAPO-5 with respect to $AlPO_4$-5 (Et_3N) are most probably due to the formation of H_2SO_4 from the $CoSO_4.7H_2O$ salt present in the synthesis gel.

The argon adsorption capacity for CoAPO-5, (Figure 16), as well as the oxygen adsorption capacity are lower than those of $AlPO_4$-5. Since no amorphous or other crystalline phases are observed in this sample from x-ray diffraction, this result is

ascribed to the presence of occluded or dispersed cobalt within the pores of the calcined material. The isotherm shown in Figure 17 supports the above assumption. The relative pressure required to adsorb the same relative weight of argon in CoAPO-5 is lower than in $AlPO_4$-5 (Et_3N) indicating a smaller pore size in CoAPO-5. This could be explained by assuming that some cobalt is not within the framework but rather occluded in the channels. Two extraframework cobalt possibilities, neither of which can be identified by X-ray diffraction, have been reported for CoAPO-5:[20] a submicroscopic intergrowth of a separate Co phase within the $AlPO_4$ crystals or a Co-rich phase to occupy some of the channel system.

By comparison of the DTA from CoAPO-5 shown in Figure 19 and $AlPO_4$-5 shown in Figure 11, an extra-exotherm between 500-700°C is observed in CoAPO-5 which is probably indicative of protonated amine balancing framework charge. Thus, in CoAPO-5 some Et_3N species are most likely occluded as the free amine and some are protonated. The total content of organic material corresponds to 1.27 molecules per unit cell. The corresponding value for $AlPO_4$-5 (Et_3N) is 1.41 molecules per unit cell.

It can be observed in Table 10 that the binding energy of the $Co2p_{3/2}$ energy level in the as-synthesized and treated materials is 782.5 ± 0.6 eV, which is higher than the values expected for CoO, Co_2O_3 or Co_3O_4.[48] Binding energies as high as 783.42 eV for the $Co2p_{3/2}$ photoelectron peak in Co-exchanged ZSM-5 have been reported.[43,49] The high binding energy reported was interpreted as an indication of Co present in a highly oxidized environment resulting from the interaction between Co and the ZSM-5 support. Increases in the $Co2p_{3/2}$ binding energy of highly dispersed cobalt supported on γ-alumina have also been reported.[50] Furthermore, the same authors[51] have been able to distinguish between Co^{+2} and Co^{+3} by whether or not the satellite structure, at about 5 eV higher binding energy from the $Co2p_{3/2}$ core level, appears. Since

binding energy values as high as those observed have been reported for Co^{+2} and because the satellite structure is present in the spectra of the as-synthesized and calcined CoAPO-5 materials, as shown in Figure 20, divalent cobalt appears to be the predominant species in the superficial region of CoAPO-5.

Chemical analyses of CoAPO-5 materials give an indication of the kind of substitution mechanism that has taken place. The data in Table 11 reflects that the dominant substitution mechanism is mainly replacement of Al by Co. The ratio XPS/CA for the as-synthesized and O_2 calcined material indicates, within experimental error, that the composition is uniform. For the N_2 calcined material the low ratio XPS/CA is most probably due to the presence of residual carbon from the organic amine. However, for the O_2/H_2 calcined material the low ratio XPS/CA is unnexplainable at this time.

From the ion exchange chemical analysis results shown in Table 12, it can be observed, that the amount of Co relative to P decreased after exchange in the as-synthesized and treated materials compared to the same materials before exchange (Table 11). The decreases observed appear to be related to the amount of Na exchanged: in the O_2 and O_2/H_2 calcined materials the decrease is (within experimental error) equal to the amount of Na^+ exchanged. In the N_2 calcined sample, the decrease observed is half of the amount of Na^+ exchanged.

Chemical analysis of the filtrate solution obtained after exchange of the calcined materials (Table 13) indicates that some Co, P, and relatively a small amount of Al are present in the exchange solution of the O_2 and O_2/H_2 calcined materials while the exchange solution of the N_2 calcined material contains Co, Al and relatively a small amount of P. From the above results it can be inferred that in the O_2 and O_2/H_2 calcined materials Na^+ is being exchanged for monovalent species which contain Co and P; in the N_2 calcined material two Na^+ species appear to be exchanged by Co^{+2}.

The ion exchange capacity differences among the calcined materials are very small. These results are in agreement with the potentiometric titration curves of the filtrate following exchange shown in Figure 21.

The above results make it difficult to attempt to quantify the amount of cobalt present as cations, and to draw conclusions related to the changes in ion exchange capacity of the calcined materials due to the possibly changes in the cobalt oxidation state. One reason could be that the equilibrium between the different species in solution and in the solid was reached during the time allowed for exchange and not all of the cobalt containing species balancing the framework charge were exchanged. Probably further exchange using fresh NaCl solutions would have shown further differences. However, the ion exchange results can qualitatively support the idea of having occluded or dispersed Co within the channels of CoAPO-5 and this thought is also consistent with the decrease in O_2 and Ar adsorption capacities and in the lower P/Po required for argon adsorption.

The diffuse reflectance spectra in the visible region for the as-synthesized as well as for the O_2/H_2 calcined materials show absorption bands from 400 to 700 nm typical of Co(II) species in tetrahedral coordination.[52] Another indication of tetrahedral cobalt is the royal blue color of these samples.

The color of the N_2 calcined sample is dark blue (almost black), but after TGA in air the sample presents the royal blue color characteristic of tetrahedral Co(II). Although the presence of some cobalt oxide can not be discarded, the dark color of the calcined sample may be due to residual carbon. The diffuse reflectance spectrum of this sample presents absorption bands from 500 to 650 nm.

The diffuse reflectance spectrum of the yellow-green O_2 calcined version of CoAPO-5 shows an absorption band at the same position and almost the same intensity as in the O_2/H_2 calcined sample. In addition to this band, another band from

350 to 480 nm is observed which has been assigned to Co(III) in tetrahedral coordination.[52] This band disappears after exposure of the sample to methanol at room temperature, and the sample becomes blue. The O_2 calcined CoAPO-5 material also turns blue when exposed to ethanol and acetone. However, subsequent calcination in O_2 leads to a return of the yellow-green color and the corresponding Co(III) band.

The above results suggest that there is a portion of the cobalt present in CoAPO-5 that can undergo changes in oxidation state and remain tetrahedral. The other portion appears to be tetrahedral divalent cobalt. Some of the divalent cobalt may be balancing framework charge, and some occluded and balanced by occluded phosphate species. Since only Co(II) was detected by XPS even in the O_2 calcined samples, it seems that most of the Co present in CoAPO-5 corresponds to the last portion mentioned above. Most known discrete Co(III) complexes are octahedral.[53] Tetrahedral Co(III) has been observed only in a few solid state situations.[54,55] Therefore, it is very likely that the portion of Co present in CoAPO-5 that can switch oxidation states and remain tetrahedral is occupying framework positions. However, this postulate cannot yet be regarded as conclusive.

The identification of a unit cell volume expansion (or contraction) has provided confirmation on incorporation of other elements into the structural framework sites.[47] The unit cell of CoAPO-5 is $a = 13.70$ Å, $c = 8.44$ Å and gives a unit cell volume of 1372 Å^3 compared to the unit cell size of $AlPO_4$-5 (Et_3N) where $a = 13.61$ Å and $c = 8.47$ Å which gives a unit cell volume of 1359 Å^3. The expansion of about 13 Å^3 in the unit cell volume of CoAPO-5 is an indication of framework siting of cobalt. The divalent cobalt ion (0.72 Å)[25] is larger than the trivalent aluminum ion (0.52 Å).[25] It is worth noting that the expansion in volume is due only to a larger a-axis in CoAPO-5 compared to $AlPO_4$-5(Et_3N) while the c-axis is smaller. This may indicate preferential

siting of cobalt in the framework.

5.3 VAPO-5 Synthesis and characterization

The pH values of reaction vessel contents taken after different heating times were obtained for the purpose of examining the effects of V_2O_5 upon the crystallization process. From Figure 27 it can be observed that the time required for the formation of crystalline product has increased compared to the time required to crystallize pure $AlPO_4$-5. Transformation of VAPO-5 to other phases is not observed at prolonged heating times. It is interesting to note that the initial pH of the VAPO-5 gel is 6.9 and increases moderately after heating to reach a value of 8.7 at 48 hours. For $AlPO_4$-5 (Pr_3N) the initial pH is 4.3 and is observed to increase very rapidly to 8.2 at 2 hours. After that point, the pH increases very slowly and at 48 hours the pH is the same as in VAPO-5.

It is well known[58] that V_2O_5 dissolves in acids as well as in bases. According to the available data on the pH ranges and existence of various species at different vanadium concentrations,[57] the vanadium species present during the synthesis of VAPO-5 gel are speculated as follows. A pH value of 2.3 is recorded for the white aluminophosphate gel before the addition of the organic. After V_2O_5 is added the pH is 2.5 and the gel becomes orange yellow; the most probable species present in solution taking a vanadium concentration of 0.0001 atom-g/ml is the $[VO_2]^+$ ion.[57] The addition of the organic brings the pH to about 6.9. The original yellow color of the gel looks less intense and the most probable species is $[H_2VO_4]^-$.[57]

From visual observations of the X-ray diffraction patterns, the VAPO-5 product

appears to be the most crystalline after 24 hours of heating at 150°C. For this sample, the pH of the autoclave contents is 8.2 and the system, (solid and solution), looks blue or blue-green indicating that vanadium may be V(IV). Most oxovanadium (IV) compounds are blue.[61]

It has been observed that the color of the as-synthesized material becomes apple-green after sitting in the lab for about six months. This may be an indication of vanadium oxidation and/or that an equilibrium between V(IV) and V(V) exists. In fact, a difference of 0.5 eV for the binding energy of the V($2p_{3/2}$) photoelectron peak is observed in Figure 33 and in Table 15 for the as-synthesized materials, VAPO (11-11-88) and VAPO (7-15-88), differing only on the date of preparation. The binding energy of the older material corresponds to V(V)[60] while the binding energy of the more recently prepared material is intermediate between V(IV) and V(V). For the calcined samples the binding energy corresponds also to V(V). Very small differences in binding energy are observed for the O_2/H_2 and Ar/He calcined samples with respect to the O_2 and N_2 calcined samples.

It has been reported[59] that the species $[VO_4]^{3-}$, $[HVO_4]^{2-}$, $[H_2VO_4]^-$ and H_3VO_4 contain a tetrahedrally coordinated vanadium atom. The evidence comes from Infrared and Raman studies that indicate that $[VO_4]^{3-}$ is tetrahedral in solution as it is in the solid state. This is supported by ^{51}V n.m.r. work,[59] although some distortion therefrom may occur. The V-O bond lengths range[58] from 1.64 to 1.74 Å. For the other ions, the tetrahedral coordination is supported by EMF(pH) measurements performed under equilibrium or rapid flow.[59] Because species of these types are expected at the vanadium concentration used in the synthesis gel, it is very likely that V(IV)/V(V) species substitute for P(V) in the $AlPO_4$ framework of VAPO-5.

Substitution of vanadium for phosphorus is observed in various naturally occurring minerals. Examples of materials showing this type of substitution are:

- Schoderite, $2Al_2O_3.V_2O_5.P_2O_5.16H_2O$, a phosphovanadate mineral found in Nevada[63] and in Arkansas.[64,65]
- Sincosite[66], $CaV_2O_2(PO_4)_2.5H_2O$.
- Rusakovite[67], $(Fe,Al)_5[(V,P)O_4]_2(OH)_9.3H_2O$, with Fe:Al = 4:1 and V:P = 2:1.
- A phosphate mineral variscite from Utah, containing up to 0.32% V_2O_3.[68]

Bond strength considerations[62] indicate that V(V) would more readily substitute for P(V) into the $AlPO_4$ framework. In this case no change in the net charge and consequently no acid sites will be expected. The DTA curve in Figure 32 is consistent with the proposed substitution. It shows only one exotherm due to decomposition of the amine but, Hoffman type degradation is not observed at higher temperatures. It is interesting to point out that from TGA a value of 0.44 molecules of Pr_3N per unit cell is obtained for VAPO-5 in contrast to 1 molecule of Pr_3N per unit cell in $AlPO_4$-5 (Pr_3N).

The oxygen adsorption capacity as well as the argon adsorption capacity of VAPO-5 obtained from Figure 30 are slightly higher than the corresponding values for $AlPO_4$-5 (Pr_3N). The X-ray diffraction patterns shown in Figure 27and the SEM shown in Figure 31 indicate the absence of any amorphous material or a second crystalline phase. In addition, from the normalized argon adsorption isotherms of VAPO-5 and $AlPO_4$-5 shown in Figure 29 the pore size of VAPO-5 is the same as $AlPO_4$-5. Thus, there is not extraneous material within the pores of VAPO-5

The chemical analyses of the as-synthesized and calcined materials listed in Table 16 indicate that V is substituting for phosphorus. It is worth noting that except for the O_2/H_2 calcined sample, V/Al ratios are higher from XPS experiments that from chemical analysis, but the XPS/CA ratios are all well within experimental error to say that the composition is uniform.

The change in the unit cell volume of VAPO-5 compared to $AlPO_4$-5 is an indication of framework content in V(V). The pentavalent vanadium ion (0.60 Å)[25] is larger than the pentavalent phosphorus ion (0.305 Å).[25] Thus, a lattice expansion would be expected upon substitution of V(V) for P(V). Indexing of the X-ray diffraction lines of a O_2 calcined VAPO-5 sample after NaCl exchange gives a unit cell volume of 1365 $Å^3$ with a = 13.671 Å and c = 8.435 Å. For $AlPO_4$-5 (Pr_3N) an O_2 calcined and NaCl exchanged sample gives a unit cell volume of 1357 $Å^3$ with a and c sizes of 13.639 and 8.427 Å respectively. Therefore, the unit cell volume expansion of VAPO-5 is 8 $Å^3$.

From the NMR results for VAPO-5, shown in Figure 35 and Figure 36, both Al and P are tetrahedral. Broadening of the ^{27}Al NMR spectrum is observed in VAPO-5 compared to $AlPO_4$-5 (Pr_3N) which may suggest the presence of Al-O-V linkages. From UV diffuse reflectance spectra of as-synthesized and calcined samples of VAPO-5, shown in Figure 37, the coordination of vanadium is also tetrahedral.[45]

Although the above data seems to indicate that V(V) substitutes for P(V) in VAPO-5 with no acidity expected, the potentiometric titration curves for the calcined materials shown in Figure 34 indicate ion exchange capacity in the treated materials. The ion exchange capacity in the O_2/H_2 calcined material is twice the ion exchange capacity of the O_2 and Ar/He calcined materials. In agreement with these values the sodium exchange data in the first column of Table 17 show that the number of moles of Na^+ exchanged per mole of V in the O_2/H_2 calcined sample is twice the value obtained for the Ar/He and for the O_2 calcined samples. The Al, P, and V content of the filtrate solution following exchange, shown in Table 18, is very small. Thus, it can be assumed that the acidity comes from only one type of species in solution. The potentiometric titration curves in Figure 34 confirm this assumption since only one end point is observed for each curve. An explanation for the acidity observed in

VAPO-5 can be given in terms of the local structural defects created assuming that the tetrahedral unit VO_4^{3-} is present in $AlPO_4$ framework sites with two terminal oxygens and two bridging oxygens. The following simple representation of the sites where the substitution has occurred reflects the various pieces of experimental evidence in this study.

1. For the substitution of P(V) for V(V) as in the O_2 and Ar/He calcined samples:

2. For the reduced material as in the O_2/H_2 calcined sample after exposure to air at room temperature.

It is important to point out that the reduced sample had a light violet color during exposure in H_2. Once the sample was taken from the calcination tube and exposed to air the color changed inmediately to apple-green. The XPS analysis of this sample indicates the presence of V(V). Thus, the question whether or not V can switch oxidation state and remain in the structure is probably affirmative under controled reducing conditions. All the analyses taken on the VAPO-5 samples are consistent with the postulated scheme, however further study is needed to conclusively prove this picture.

5.4 Catalytic Activity

The results shown in Table 20 and Table 21 for partial oxidation of methane in the presence of CoAPO-5 and VAPO-5 respectively indicate very low selectivities toward formaldehyde with no production of methanol, and the major products being oxides of carbon. Similar results have been reported for zeolites.[69]

So far, no satisfactory solution has been found to the kinetic problem involved in the partial oxidation of methane since from a thermodynamic point of view the partial oxidation of methane to methanol ($\Delta G_{427°C}$ = -22 kcal/mol) and formaldehyde ($\Delta G_{427°C}$ = -70 kcal/mol) is not favored over the total oxidation of methane to carbon monoxide ($\Delta G_{427°C}$ = -136 kcal/mol) and carbon dioxide ($\Delta G_{427°C}$ = -189 kcal/mol).[30]

6.0 CONCLUSIONS

1. Cobalt can be incorporated into the $AlPO_4$-5 framework. The redox character of the resulting material can be determined by diffuse reflectance spectroscopy and by observing the change in color when the material is consecutively oxidized and reduced. However, the amount of metal incorporated is not readily obtained since a relatively appreciable portion remains as balancing cations, occluded in the pores, and/or dispersed on the surface of the crystals.

2. Pentavalent vanadium substitution for pentavalent phosphorus into the $AlPO_4$-5 framework has been obtained in VAPO-5. Although a neutral framework is expected, increased acidity with respect to $AlPO_4$-5 is observed. This could be explained in terms of the the local structural defects that would be created into the $AlPO_4$ framework if vanadium shares only two of its four oxygens.

3. Incorporation of molybdenum into the $AlPO_4$-5 framework is not obtained by the procedure described.

4. In spite of the redox properties exhibited by CoAPO-5 and VAPO-5, they are not selective catalysts for the partial oxidation of methane to methanol and formaldehyde.

7.0 RECOMENDATIONS

1. Determine the feasibility of removing most of the extraframework cobalt present in CoAPO-5 by exchanging it several times in diluted NH_4Cl solution and study the redox behaviour and thermal stability of the resulting material.
2. Use other techniques, like Raman spectroscopy and EXAFS to obtain more supporting evidence for the proposed vanadium substitution into the $AlPO_4$-5 framework.
3. Determine, by ESR, the valence states of vanadium in oxidized and reduced samples of CoAPO-5 and VAPO-5.
4. Investigate the shape selective properties of CoAPO-5 and VAPO-5 in oxidation of aromatics such as benzene or toluene to phtalic anhydride or maleic anhydride.
5. Determine the maximum amount of Co and V that can be incorporated in the $AlPO_4$-5 framework by introducing regular amounts of the corresponding sources in the synthesis gel and characterizing the resulting materials.
6. Study the effect of other Co and V sources, for example trying to use Co(III) and V(III) as starting materials respectively and determine, by ESR, the valence states of the elements incorporated.
7. Study the effect of different organics on the quantity and quality of the elements incorporated.
8. Study the thermal and hydrothermal stability of the substituted $AlPO_4$s.

REFERENCES CITED

1. Wilson, S. T.; Lok, B. M.; Flanigen, E.M.; *U.S. Patent 4,310,440, (1982)*; Wilson, S. T.; Lok, B. M.; Flanigen, E.M.; *J. Am. Chem. Soc.*, **104**, p. 1146, (1982).

2. Davis, M. E.; Montes, C.; Garcés, J.M.; *Am. Chem. Soc. Symp. Ser.*, (1989), in press.

3. Szostak, R.; *Molecular Sieves Principles of Synthesis and Identification*, Van Nostrand Reinhold, New York, p. 275, (1988).

4. Parise, J. B. and Day, C.S.; *Acta Cryst.*, **C41**, p. 515-520, (1985).

5. Parise, J. B.; *Inorg. Chem.*, **24**, p. 4312-4316, (1985).

6. Bibby, D.M.; Chang, C.D.; Howe, R.F.; Yurchak, S. (eds), *Methane Conversion*, Elsevier, Amsterdan, p. 553, (1988).

7. Flanigen, E. M.; Lok, B. M.; Patton, R. L.; Wilson, S. T.; *Pure & Appl. Chem.*, **10**, (58), p. 1351-1358, (1986).

8. Wilson, S. T.; Lok, B. M.; Messina, C. A.; Cannan, T. R. and Flanigen, E. M., *ACS Symp. Ser.*, **218**, p. 79, (1983)

9. Bennett, J. M.; Cohen, J. P., Flanigen, E. M.; Pluth, J. J. and Smith, J. V.; *ACS Symp. Ser.*, **218**, p. 109, (1983).

10. Davis, M. E.; Montes, C.; Hathaway, P. E.; Arhancet, J. P.; Hasha, D. L.; Garcés, J.; *J. Am. Chem. Soc.*, (1989) in press.

11. Boisen, M.B.; Gibbs, G. V.; in Ribbe, P. H. (Editor), *Reviews in Mineralogy*, **15**, p.325, (1985).

12. Lohse, U.; Noack, M. and Jahn, E.; *Adsorption Science and Technology*, **3**, p. 19-24, (1986).

13. Choudhary, V. R., Akolekar, D.B., Singh, A. P. and Sansare, S.D.; *J. Catal.*, **111**, p. 254-263, (1988).

14. Choudhary, V.R. and Akolekar, D.B.; *J. Catal.*, **103**, p. 115, (1987).

15. Bond, G. C.; Gelsthrope, M. R.; Singh, K.S.W., and Theocharis, C. R., *J. Chem. Soc. Chem. Commun*, **15**, p.1056, (1986).

16. Pike, D. R.; Whitney, P; Houghton, Hilary; *Appl. Cat.*, **18**, 173-190, (1985).

17. Lok, B. M.; Messina, R.L.; Patton; Gajek, R. T.; Cannan, T. R.; Flanigen, E. M.; U. S. Patent 4,440, 871, (1984); *J. Am. Chem. Soc.*, **106**, p. 6092, (1984).

18. Hasha, D.; De Saldarriaga, L.; Saldarriaga, C; Hathaway, P; Cox, D. F.; Davis, M. E.; *J. Am. Chem. Soc.*, **110**, p. 2127, (1988).

19. Hedge, S. G.; Ratnasamy, P.; Kustov, L. M.; Kazansky, V. B.; *Zeolites*, **8**, p. 137-141, (1988).

20. Tapp, N. J.; Milestone, N. B.; Bibby, D. M.; in Grobet, P. J. et al (Editors), *Innovations in Zeolite Materials Science*, Elsevier, Amsterdam, p. 393-402, (1988).

21. Flanigen, E. M.; Look, B. M.; Patton, R. L.; Wilson, S. T.; in Murakami, Y; Iijima, A.; Ward, J. W.; (Editors), *New Developments in Zeolite Science and Technology, Proc. 7th. Internat. Zeolite Conf.*, Elsevier, p. 103, (1986).

22. Tapp, N. J.; Milestone, N. B.; Wright, L. J.; *J. Chem. Soc. Chem. Comm.*, p. 1801-1803, (1985).

23. Wilson, S.T.; Flanigen, E.M.; *U.S. patent* 4,567,029 (1986).

24. Pauling, L.; *The Nature of the Chemical Bond*, Cornell University Press, Ithaca, NY, 3rd. ed., pp. 543ff, (1960).

25. Shannon, R. D.; *Acta Cryst.*, **A32**, p. 751-767, (1976).

26. Bennett, J. M.; Markus, B.K., in Grobet, P. J. et al. (Editors), *Innovation in Zeolite Materials Science*, Elsevier, Amsterdan, p. 269, (1988).

27. Milestone, N. B.; Tapp, N. J. in Bibby, D. M.; Chang, C. D.; Howe, R. F.; Yurchak, S., (Editors), *Methane Conversion*, Elsevier, Amsterdan, p. 553-562, (1988).

28. Godolets, G. L.; *Heterogeneous Catalytic Reactions Involving Molecular Oxygen*, Vol 15 of Studies in Surface Science and Catalysis, Elsevier, Amsterdam, (1983).

29. Foster, N. R.; *Appl. Cata.*, **19**, p. 1, (1985).

30. Pitchai,R and Klier, R; *Catal. Rev. -Sci. Eng.*, **28** (1), p. 13-88, (1986).

31. Pasquon, I. *Catalysis Today*, **1**, p. 297-333, (1987).

32. Moss, R.L.; in Anderson, R.B.; Dawson, P. T.; *Experimental Methods in Catalytic Research*, Vol II, Academic Press, New York, p.43-44, (1976).

33. Garnett, J.L.; Kennedy, E.M.; Long, M. A.; Than, C.; Watson, A.J.;in Bibby, D.M.; Chang, C. D.; Howe, R. F.; Yurchak, S. (Editors), *Methane Conversion*, Elsevier, Amsterdam, p. 389-393, (1988).

34. Walker, J. F., *Formaldehyde*, 2nd ed. (ACS Monograph Series No. 120), Reinhold Publishing, New York, p. 385-386, (1953)

35. Parker,L.M.; Bibby, D.M. and Wright L.J., *J. Chem. Soc., Chem. Commun.*, p. 1801, (1985).

36. Blackwell,C.S. and Patton,R.L., *J. Phys. Chem.*, **88**, p. 6135-6139, (1984).

37. Muller, D; Jahn, E; Fahlke,B; Ladewig, G; Haurbenreisser,U; *Zeolites* , **5**, p.53, (1985).

38. Choudhary,V.R.; Akolekar, D.B.; Sansare, S.D.; *Materials Chemistry and Physics*, **18**, p. 245-254, (1987).

39. Dworezkov, Genadij; Rumplmayr, Gerd; Mayer, Helmut; Lercher, Johannes A; in Che, M.; Bond, G.C. (Editors), *Adsorption and Catalysis on Oxide Surfaces*, Elsevier, Amsterdam, p. 163, (1985).

40. Blackwell, C. S.; Patton, R. L.; *J. Phys. Chem.*, **92**, p. 3965-3970, (1988).

41. Alemany, L.B.; Timken, H. K. C.;; Johnson, I.D.; *Journal of Magnetic Resonance*, **80**, p. 427, (1988).

42. Wagner, C.D.; Riggs, W. M.; Davis, L.E.; Moulder, J.F.; in Muilenberg, G.E. (Editor), *Handbook of X-Ray Photoelectron Spectroscopy*, Perkin Elmer Corporation, Minnesota, p. 50, 54 (1978).

43. Rao, V.U.S.; *Physica Scripta*, **T4**, p. 71, (1983).

44. Praliaud, H.; Michel-Vital, M.; *J. Chim. Phys.*, **73**, p.689-693, (1976).

45. Yoshida, S; Tanaka, T; Nishimura, Y; Mizutani, H; Funabiki, T; in Phillips, M.J.; Ternan, M.(Editors); *Proceedings 9th International Congress on Catalysis*, Calgary, **3**, p. 1473, (1988).

46. Szostak, R. *Molecular Sieves Principles of Synthesis and Identification*, Van Nostrand Reinhold, New York, p.71, (1989).

47. Szostak, R. *Molecular Sieves Principles of Synthesis and Identification*, Van Nostrand Reinhold, New York, p.291, (1989).

48. Wagner, C.D.; Riggs, W. M.; Davis, L.E.; Moulder, J.F.; in Muilenberg, G.E. (Editor), *Handbook of X-Ray Photoelectron Spectroscopy*, Perkin Elmer Corporation, Minnesota, p. 78, (1978).

49. Stencel, J.M.; Rao, V.U.S.; Diehl, J.D.; Rhee,K.H; Dhere, A.G.; DeAngelis, R.J.; *J.*

Catal.,**88**, p. 431, (1984).

50. Chin, R.L.; Hercules, D.M.; *J. Phys. Chem.*, **86**, p. 360, (1982).

51. Chin, R.L.; Hercules, D.M.; *J. Phys. Chem.*, **86**, p. 3079, (1982).

52. Shimura, Yoichi; Tsuchida, Ryutaro; *Bull. Chem. Soc. Jpn.*, **30**, p. 502, (1957).

53. Cotton, F.A.; Wilkinson, G., *Advanced Inorganic Chemistry*, John Wiley & Sons, p. 766, (1979).

54. Wood, D.L.; Remeika, J.P.; *J. Chem. Phys.*, **46**, p. 3595, (1967).

55. Baker, L. C. W.; Simmons, V. E.; *J. Amer. Chem. Soc.*, **81**, 4744, (1959).

56. Cotton, F.A.; Wilkinson, G., *Advanced Inorganic Chemistry*, John Wiley & Sons, p. 712, (1979).

57. Clark, R. J. H.; in Bailar, J. C.; Emelius, H.J.; Nyholm, S R.; Trotman-Dickenson, A.F., (Editors), *Comprehensive Inorganic Chemistry*, Pergamon Press, New York, p. 491, (1973).

58. Clark, R. J. H.; in Bailar, J. C.; Emelius, H.J.; Nyholm, S R.; Trotman-Dickenson, A.F., (Editors), *Comprehensive Inorganic Chemistry*, Pergamon Press, New York, p. 522, (1973).

59. Pope, M. T.; Dale, B.W., *Quart. Rev.*, **22**, p. 527, (1968).

60. Wagner, C.D.; Riggs, W. M.; Davis, L.E.; Moulder, J.F.; in Muilenberg, G.E. (Editor),

Handbook of X-Ray Photoelectron Spectroscopy, Perkin Elmer Corporation, Minnesota, p. 70, (1978).

61. Cotton, F.A.; Wilkinson, G., *Advanced Inorganic Chemistry*, John Wiley & Sons, New York, p. 714, (1979).

62. Shannon, R.D.; Chenavas, J.; Jouber, J.C.; *Journal of Solid State Chemistry*, **13**, p. 16, (1975).

63. Wagner, C.D.; Riggs, W. M.; Davis, L.E.; Moulder, J.F.; in Muilenberg, G.E. (Editor), *Handbook of X-Ray Photoelectron Spectroscopy*, Perkin Elmer Corporation, Minnesota, p. 78, (1978).

64. Hausen, D.M; *The American Mineralogist*, **47**, p. 637, (1962).

65. Pabst,A.; *The American Mineralogist*, **64**, p. 713, (1979).

66. Schaller, W. T. *Am. Jour. Sci.*, **8**, p.462, (1924).

67. Ankinovich, E.A. *Zapiski V ses. Mineralog. Obshch.*, **89**, p. 440, (1960) (in Russian).

68. Schaller, W.T., *U.S. Geol. Survey Bull.*, **509**, p.48, (1912).

69. Kowalak, S; Moffat, J. B. *Appl. Cat.*, **36**, p. 139, (1988).

The vita has been removed from the scanned document